NTNU

Norwegian University of
Science and Technology

New switching pattern for AC/AC converters with RB-IGBTs for offshore wind parks

Anne Berit Mogstad

Master of Science in Energy and Environment
Submission date: June 2008
Supervisor: Marta Molinas, ELKRAFT

Norwegian University of Science and Technology
Department of Electrical Power Engineering

Problem Description

A new DC based offshore wind park topology should be examined and compared to a conventional topology. The losses in the converter topology should be specially considered.

Investigation of RB-IGBTs and bidirectional switches should be carried out and high frequency high power transformers should be examined.

A model in PSCAD should be made for the wind turbine and losses in the converter should be simulated.

Assignment given: 21. January 2008
Supervisor: Marta Molinas, ELKRAFT

Sammendrag

Havvindmøller har fått en økende interesse hos forskere og politikere. Det er derfor viktig å finne en optimal løsning for å møte kravene fra både samfunn og næringsliv. Ved å forske på havenergi, kan havvindmøller gå en lys framtid i møte. Denne masteroppgaven foreslår en ny omformertopologi for havvindturbinparker. Siden den foreslåtte topologien er basert på DC overføring i stedet for AC overføring, er den bedre egnet for bruk i parker langt fra land. Alle omformerne er plassert i vindturbinene og vindturbinene er koblet sammen i serie. Denne seriekoblingen av vindturbiner er koblet direkte til land, uten noen transformeringstrinn.

En-fase AC til tre-phase AC omformeren med det nye svitsjemønsteret er beskrevet og en metode for å finne tapene er forklart. Methoden er basert på bryterens karakteristiske data som er beskrevet i databladet. I dette tilfellet blir det databladet til en bakoversperrende IGBT. Ledetapene, sperreforsinkelsestapene, innkoblings- og utkoblingstapene beregnes for hver bryter og multipliseres med antall brytere i omformeren. En likning for det totale tapet i en bryter er gitt og simuleringer er utført i PSCAD, med gode resultater.

Omformeren består av bidireksjonale brytere. I dette tilfellet er det to bakoversperrende IGBTer som er brukt og disse to er sammenlignet med andre typer bidireksjonale brytere bestående av IGBT og diode i antiparallell. Tapene ved ledetilstand er redusert pga at en bakoversperrende IGBT har like stort spenningsfall i ledetilstand som en vanlig IGBT. Dette fører til en halvering av spenningsfallet i bryteren pga at det ikke er noen diode. Oppbyggingen av en bakoversperrende IGBT er lik en vanlig IGBT med untak av at p^+ laget har blitt strukket opp til gateisolasjonen for å hindre lekkstrømmer på kantene av chipen. Det aktive området av chipen bli dermed separert fra sidene.

En design av en høyfrekvens, høyeffekts transformator er foreslått. Det er brukt en kjent metode for å komme fram til designen og et program som utfører beregninger er laget. Resultatet er en transformator med en dobbel E-kjerne. Det er en ferrittkjerne med en bredde på midterste bein på 4,5 cm. Både primær og sekundær viklingene er viklet rundt det midterste beinet ved hjelp av en spoleform. Viklingene består av kobber og er folieformet. Primærviklingene er delt i to deler med sekundærviklingen i mellom. De består begge av lag med to folieledere. Mens primærdelene har 12 lag hver, har sekundærviklingen 24 lag. Hver folieleder har en høyde på 4,5 cm og en tykkelse på 0.3165 mm.

Den nye omformertopologien reduserer omformertapene på grunn av færre omformertrinn, den nye bakoversperrende IGBT bryteren og det nye svitsjingsmønsteret. Topologien reduserer også vekten av omformersystemet på grunn av at det ikke er noen kondensator og en lettere transformator. Dette er viktig for flytende vindturbiner.

For å underbygge resultatene fra denne rapporten må en prototype av omformertopologien bygges og testes. Det må utføres simuleringer hvor en hel vindmøllepark er modellert både ved vanlig drift og ved feil.

Abstract

Offshore wind power has an increasing interest in the research community and among the politicians. Therefore it is important to find the right solutions to meet the environmental and commercial requirements to give offshore wind power a promising future. This thesis are proposing a new converter topology for offshore wind parks. Since the topology is based on DC transmission in stead of AC transmission it is better suited for use in this type of parks. All the converters are located in the wind turbines and the turbines are connected in series directly connected to shore without any transformation stages.

The one-phase AC to three-phase AC converter with the new switching pattern is explained and a method to calculate the losses in the converter is given. The loss calculation method is based on the characteristics of the switch found in the data sheet, which in this case is a RB-IGBT. The conduction losses, turn-on, turn-off and recovery losses for one switch are calculated and multiplied with the number of switches in the converter. An equation of the total losses per switch is given and there are performed loss simulations for the converter in PSCAD with good results.

In the AC-AC converter there are bidirectional switches, in this case two reverse-blocking IGBTs. The RB-IGBT is compared to other types of bidirectional switches which is made of IGBTs and diodes in anti parallel. The comparison shows that with the RB-IGBTs the on-state voltage drop is halved since a RB-IGBT has the same on-state voltage drop as a normal IGBT. This also reduces the on-state losses. The architecture of the RB-IGBT is almost the same as the IGBT but with an extension of the p^+ layer on the edges up to the gate isolation. This separates the sides from the active region of the chip so the leakage currents from the side surfaces of the device are blocked.

A design of a high power high frequency transformer for the converter topology in the nacelle of the wind turbine is proposed. A design method is used and a program to calculate the necessary values is made. The transformer should be a double E-core with a centre leg of 4.5 cm made of the ferrite material N27. Both primary and secondary windings, which will be copper foils, should be wound on the centre leg of the core using a bobbin. The primary windings will be separated in two sections each section having 12 layers with two turns per layer. The secondary windings will be sandwiched between the primary sections and will consist of 24 layers with two turns per layers. Each foil conductor has a height of 4.5 cm and a thickness of 0.3165 mm.

The new converter topology reduces the converter losses due to fewer converter stages, a new type of reverse-blocking IGBT and a new switching pattern. It also reduces the weight of the converter system because of no capacitors and a lighter transformer. This is important for floating wind turbines.

A prototype of the converter topology with protection should be made to verify the results of this thesis. Simulation studies for the whole park during operation and faults should also be carried out to see if the topology fits the harsh conditions offshore.

Preface

This is my Masterthesis in Electric Power Engineering carried out at the Faculty of Information Technology, Mathematics and Electrical Engineering at the Norwegian University of Science and Technology(NTNU). The thesis is a part of an extensive study of offshore wind power that has just started at the university.

First, I would like to thank my supervisor Marta Molinas for her kindness and helpfulness. I would also like to thank her for giving me the opportunity to go to Japan to learn more about parts of my study and to get to know the friendly Japanese culture.

Secondly, I will thank Ms Kikuchi and Mr Takaku at Fuji Electric for their helpfulness and informative visits at Fuji Electric in Japan. I would also like to thank Mr Itoh at Nagaoka University of Technology for letting me take part in their studies. And of course thanks to all the students at the laboratory for their helpfulness, for telling me about their studies and for the parties. A special thanks to Mr Kato for the information on the converter losses.

I will also like to thank Professor Arne Nysveen at NTNU and Magne Hernes at SINTEF for the help with the transformer design. A thank to Jon Are Suul, Ibrahim Abuishmais and Arkadiusz Kulka for the answers to all my questions and a thank to Giuseppe Guidi for helping me with the loss simulation.

Finally, I would like to thank my friends and family. You have all made the hard days easier.

Anne Berit Mogstad
Trondheim, Norway
13th June 2008

Contents

List of Figures

List of Tables

CHAPTER 1

INTRODUCTION

1.1 Offshore wind parks

The last twenty years there have been an increasing interest in offshore wind power due to the large available areas and the need for renewable energy sources. Both noise and visual impacts are less for offshore wind parks than for onshore parks. The wind speed is also higher and has less turbulence and lower wind shear[7]. Because of the topography and the small variations in wind speed offshore, it is possible to design the park as a regular array, which maximizes the energy capture [8].

1.2 Transmission system

The distance to shore has a huge influence on the decision of what kind of transmission system to use. The options are AC and DC transmission. According to [9] HVAC systems lead to the lowest transmission losses for distances up to 55-70 km depending on the size of the wind parks. For longer distances high voltage DC (HVDC) transmission has the lowest losses. HVDC also gives the lowest year zero total costs for distances above 90 km, as can be seen in Figure 1.1 on the next page [1]. Figure 1.1 on the following page shows the year zero total cost of AC and DC transmission for different transmission lengths. The costs considered in [1] are the cost of cable installation and protection, the cost of converter stations and the losses in the converter stations.

Today the parks are not located far from shore and the maximum size is 166 MW [10]. Therefore the transmission systems are AC systems. In the future the parks will consist of more turbines and be located far from shore. In that case DC transmission will be a good option. Since the operating wind parks today are close to shore, they are placed in shallow water, up to 20 meters, and the foundations are placed on the seabed using monopole structure, gravity base structure or tripod structures. In the future the turbines will be placed in deeper water and floating turbines might be the only option. Some wind park layout might require offshore substations like Horns Rev (2002), Nysted (2004) and Barrow (2006) have today [1]. For the future parks, the substations will most likely have to float like the rest of the park and the foundation and construction will be expensive and complex. Therefore it might be convenient to have a wind park topology without offshore substations.

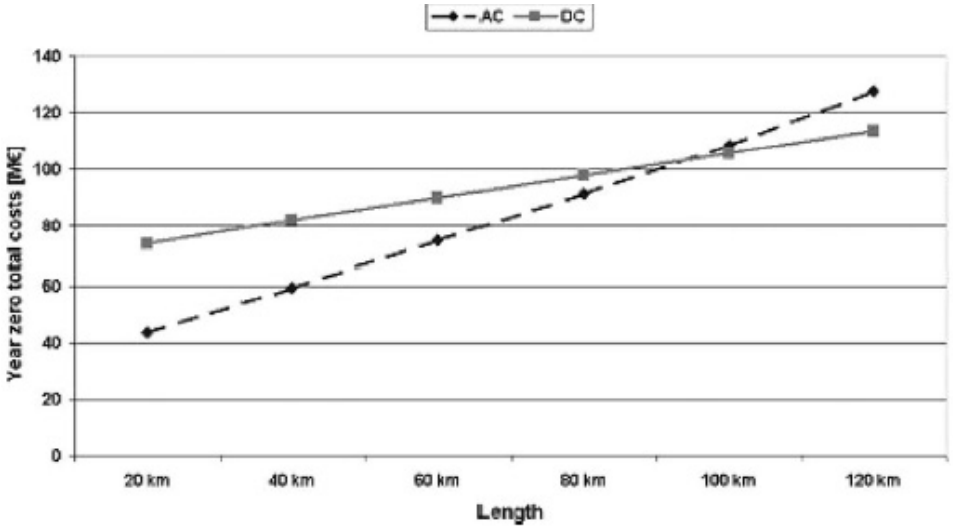

Figure 1.1: Economic results of sensitivity analysis for different transmission lengths of AC and DC transmission [1]

1.3 The report

The purpose of this report is to describe a new wind park layout for the future offshore wind parks. The wind park is based on DC transmission and series connected wind turbines. According to [11] the DC based offshore wind parks where the wind turbines are connected in series give better energy production cost than if they are connected in clusters in parallel. The energy production cost is strongly dependent on the average wind speed and decreases with increasing power of the wind park. Since the turbines are connected in series, the desired transmission voltage is achieved and the park has no need for offshore substations, as shown in Figure 1.2 on the next page. The wind park is further explained in Chapter 2 on page 5.

In Chapter 3 on page 11 a new type of semiconductor devices to reduce the converter losses is explained and a bidirectional switch consisting of the device is compared to other bidirectional switches. A thorough investigation of the losses in the AC-AC converter is carried out in Chapter 4 on page 19. The study results in an equation for the total losses. The wind park uses high frequency high power transformers and a design is proposed in Chapter 5 on page 27. In Chapter 6 on page 45 a simulation model of the topology in PSCAD and a new switching pattern are explained.

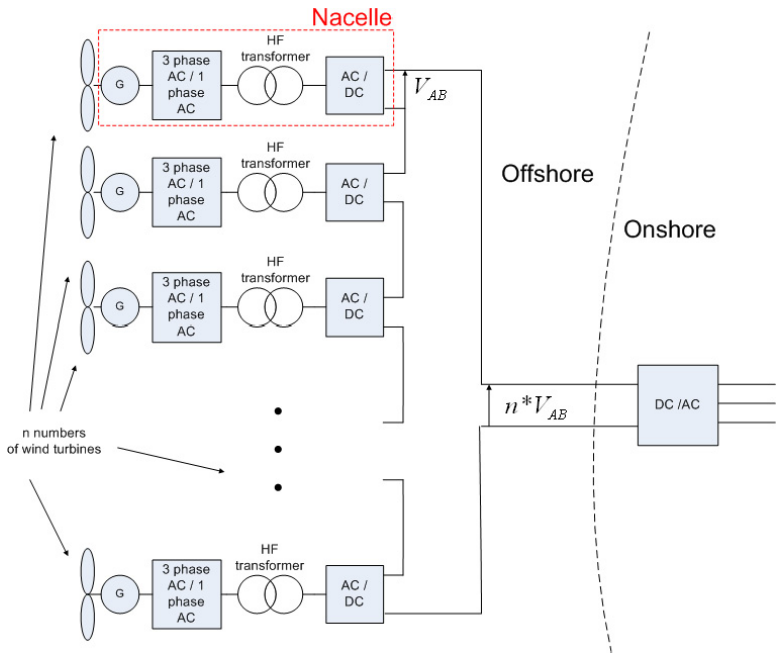

Figure 1.2: The proposed wind park layout

CHAPTER 2

INVESTIGATION OF WIND PARK TOPOLOGIES

2.1 Wind park layouts

Today there are many different topologies suggested for offshore wind parks. In [2] an overview of some topologies are given. The wind turbines can be connected in series, in parallel or in radial collection networks, see Figure 2.1. To the left in the figure the wind turbines are connected in radial. The end of the cable will either be connected to an offshore substation or to a collection point. For small parks with a short distances to shore, the radials with the wind turbines can be connected directly to shore. In a wind park there will be more cables with radially connected wind turbines. In Figure 2.2 on the following page an example of a radial connected wind park can be seen.

Figure 2.1: Different possibilities to connect wind turbines to the offshore collection network; radial (left), parallel (middle) and series (right)

In the middle of Figure 2.1 the wind turbines are connected in parallel. In this case all the wind turbines have their own cable which is connected to a substation. In Figure 2.3 on the following page a wind park with parallel connected wind turbines is shown. The turbines are connected in clusters to one of the two offshore substations (SS). Two substations might be needed to increase the voltage level to the required level for transmission. Only one substation is needed for the transformation if the output voltage from each turbine is high enough.

On the right side in Figure 2.1 the wind turbines are connected in series. In series connected networks both ends of the series connected turbines have to be connected to a substation or directly to shore. In the last case there should be DC transmission to reduce the number of transmission cables. That means that the collection network also has to be DC. If there is an offshore substation, the collection grid can be either DC or AC. The required voltage level will then be reached by having a transformer on the substation. An other option of series connected

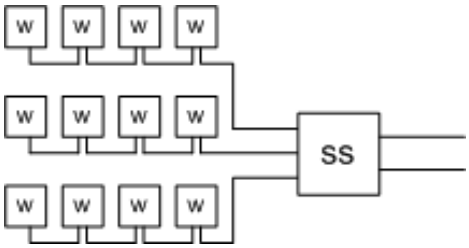

Figure 2.2: Radial connected wind turbines(W) with offshore substation(SS)

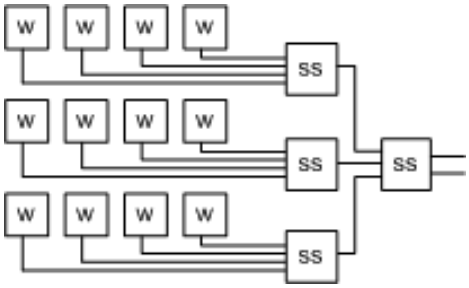

Figure 2.3: Parallel connected wind turbines(W) with two offshore substations(SS)

wind turbines, is to connect the turbines in series in clusters and then connect the clusters in parallel, Figure 2.5. The transmission voltage level can still be obtained when one cluster is disconnected.

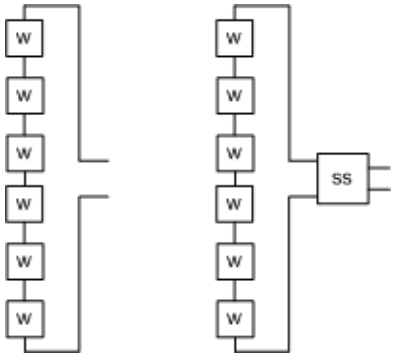

Figure 2.4: Series connected wind turbines(W) with and without offshore substation

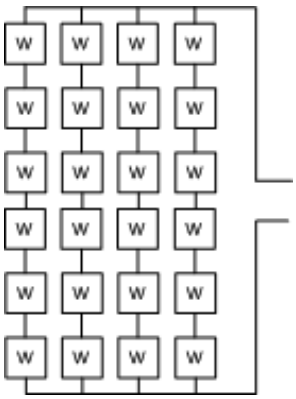

Figure 2.5: Parallel connected clusters with series connected wind turbines(W)

2.2 The conventional converter topology

One of the previously proposed DC based offshore wind park layouts is the parallel connected turbines, Figure 2.3 with one or more offshore substations. This layout must have offshore converter stations to raise the voltage before transmission to shore. It is assumed that only one transformer stage is needed if the output voltage of the wind turbine is 20-40 kV[2]. The wind turbines will then be connected in radials to the collecting point. With a lower output voltage of the wind turbine, about 5 kV, two transformer stages are needed. The wind turbines will then be divided into clusters and connected one by one to the first transformer stage. Then the clusters will be connected to the collecting point.

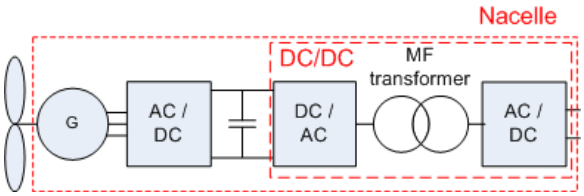

Figure 2.6: Conventional converter topology in the nacelle of the turbine as of [2]

For this type of wind park layout each wind turbine has an AC-DC converter, DC-DC converter and a capacitor between, as shown in Figure 2.6. DC-DC converters are also used for the two transformer stages in the layout. The AC-DC converter has either diode or IGBT switches depending on the type of machine used in the wind turbine, synchronous or induction machine. A DC-DC converter consists of one rectifier, one inverter and a medium frequency transformer. In [12] a loss and energy production cost study of different DC/DC converters for DC based offshore wind parks is carried out. Full-bridge converter, single active bridge converter and series parallel resonant converter are compared for the three different sites in the park, resulting in lowest losses for the resonant converter independent of the site. The single active bridge converter resulted in the highest losses, but the full-bridge converter gave slightly higher losses than the resonant converter. The resonant converter has a larger transformer and more IGBT modules than the full-bridge converter, which results in a higher energy production cost for some positions in the grid, even though the losses are lower. This topology also has a capacitor between the two converters to make sure the input to the DC-DC converter is smoothed properly.

2.3 The proposed converter topology

The proposed topology uses one cable with series connected turbines as the local grid, as can be seen in Figure 2.7 on the next page. Each wind energy conversion unit will consist of a generator, the turbine, a 3-phase AC to 1-phase AC converter, a high frequency (HF) transformer and a 1-phase AC-DC converter, see Figure 2.8 on the following page. All the components are located in the nacelle of the turbines. The turbines will be connected to an offshore DC network and the power will be transmitted directly to shore without any transformation stages. The DC side of the AC-DC converter of each turbine will be connected in series with the other wind turbines to obtain the required voltage level before transmission to shore. This is possible thanks to the transformer. It allows the current from the DC grid to flow through the secondary side of the transformer before entering the AC-DC converter again, but from the AC side. Then the current can continue further to the next wind turbine. This is possible since the turbines are connected in series and the voltage level required for transmission will be obtained by the series connection and/or the turn ratio of the HF transformer. By converting the AC voltage output from the generator to DC voltage directly in the nacelle of each turbine, a wind park layout without offshore substations is made possible. In [13] the similar conversion is proposed, but only the AC-AC converter is placed in the wind turbines. This leads to a square wave voltage

collection grid and an offshore substation for the AC-DC converter.

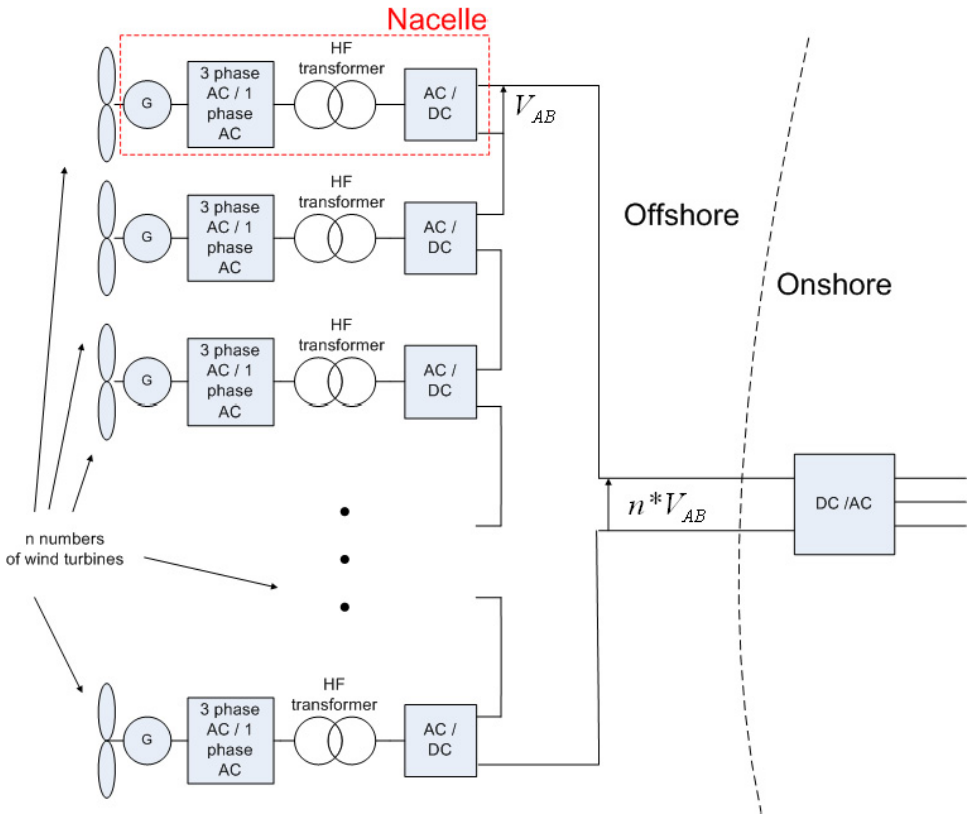

Figure 2.7: The proposed wind park layout

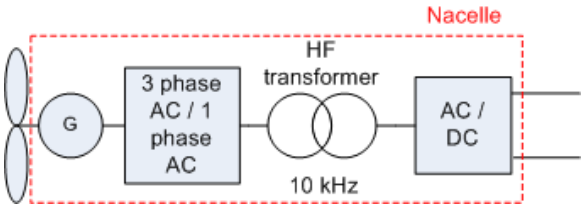

Figure 2.8: Converter topology in the nacelle of the turbine

The AC/DC converter in Fig. 2.8 is a full-bridge converter, also called an H-bridge, with switching modules consisting of IGBTs and diodes in anti parallel, Fig. 2.9 on the facing page. The converter has two legs, each with two switches (S1, S3) and (S2, S4), and is able to convert a DC voltage to a square wave voltage and vice versa. By connecting the converter to the DC bus and transformer, as shown in Fig. 2.9 on the next page, the required square wave form is obtained when starting the generator. To achieve square wave output when magnetizing the windings a PWM square wave switching scheme is used. The upper switch in one leg and the lower switch in the other are switched simultaneously, when not considering the blanking time. The two

switches form a switch pair, i.e. the converter has two switch pairs. The switch pairs are on for a half cycle of the output frequency (10 kHz), i.e. a duty ratio of 0.5.

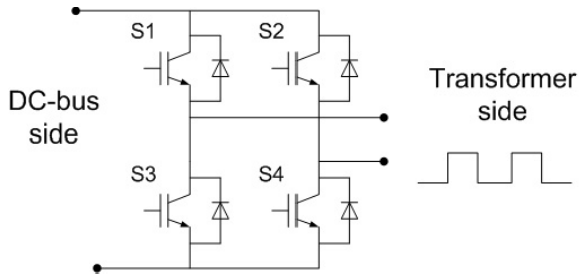

Figure 2.9: H-bridge with IGBTs and anti parallel diodes

The 3-phase AC to 1-phase AC converter in Figure 2.8 on the facing page consists of three legs each with two switches. The switches are made of two reverse-blocking IGBTs (RB-IGBT) in anti parallel and do not have any anti parallel diodes, see Figure 2.10. They therefore reduce the converter losses, due to fewer components for the current to pass through during on-state, see Chapter 3 on page 11. On the generator side of the converter there will always be an alternating voltage independent of the way the power flows. The switching technique used for the control of the switches in the converter results in a sinusoidal voltage wave when the generator is magnetized. When the generator produces power there will always be a square wave voltage entering the transformer from the AC-AC converter side. The switching pattern which is used to control the RB-IGBT is a new pattern which is based on the PWM technique but it inverts the reference signal for half of the switching period to reduce the switching actions. The pattern is thoroughly described in Section 6.2 on page 47.

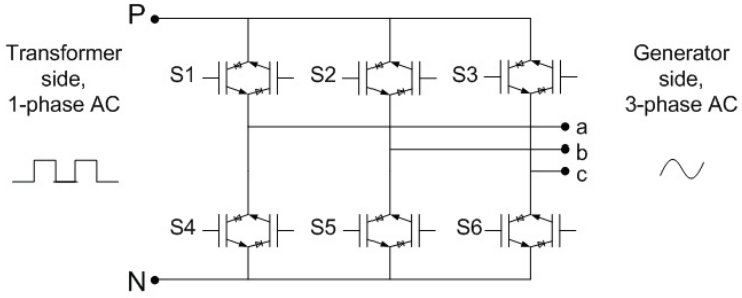

Figure 2.10: Bidirectional AC link with new reverse-blocking IGBTs

Another DC based layout option is to connect a few wind turbines in series to make clusters as in Figure 2.11 on the following page. These clusters will then be connected in parallel to the transmission line. By using this layout, the consequences during fault on cables might be less severe. Only the faulty cluster needs to be disconnected and the park can still produce power.

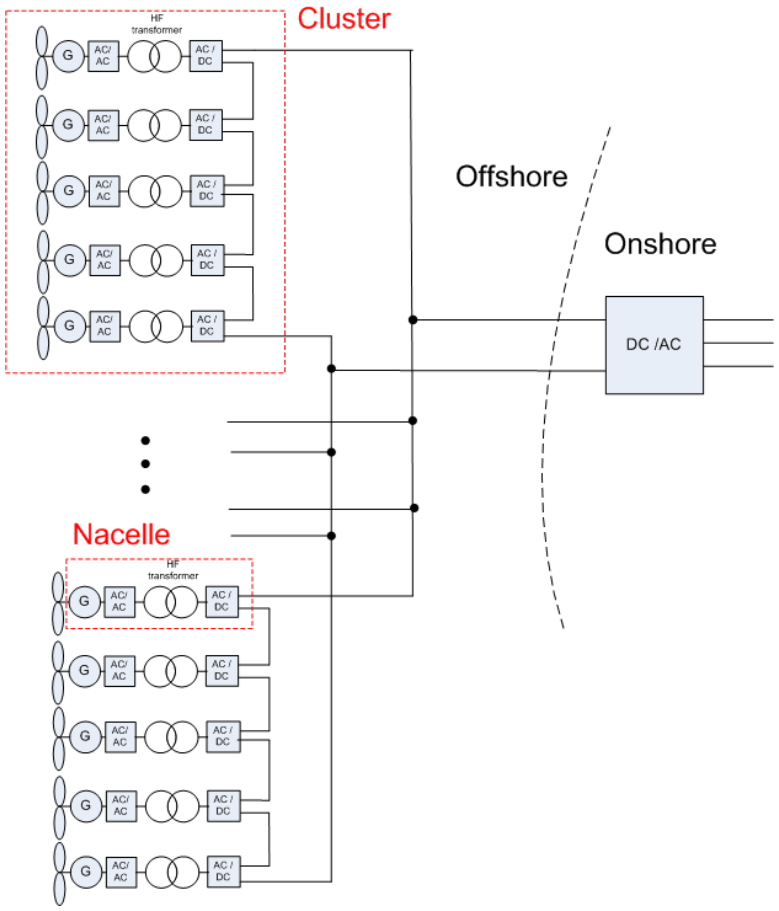

Figure 2.11: Series connected wind turbines in clusters

CHAPTER 3

REVERSE-BLOCKING IGBT

3.1 Insulated Gate Bipolar Transistor (IGBT)

The insulated gate bipolar transistor (IGBT) was invented when the BJT and the MOSFET were combined to improve the characteristics of the semiconductor devices. The BJT has low conduction losses, but switches slowly. The MOSFET switches fast but has high on-state conduction losses. Therefore they were combined to improve the characteristics of the device.

3.1.1 IGBT structure

The IGBT is formed from BJT and MOSFET and looks almost like a MOSFET with drain, source and gate connections. The names collector and emitter for drain and source can also be found in literature and will also be used in this thesis. The only difference from a MOSFET in the structure is one more layer to form the drain of the IGBT. The IGBT in Figure 3.1 on the next page is an n-channel IGBT and shows the structure of the device with the extra layer. This silicon layer is doped p^+, i.e. doped with an element with three valence electrons so that the atoms easily bond to the silicon and leaves free holes. The n-doped layers are doped with elements with extra valence electrons to create free electrons. The p^+ layer forms a junction with the n^+ layer which injects minority carriers, i.e. holes, into the drift region. The buffer layer in Figure 3.1 on the following page is not necessary for the main purpose and can be omitted. The type of IGBT without buffer layer is called non-punch-through IGBT (NPT-IGBT) and the one with buffer layer is called punch-through IGBT (PT-IGBT).

The IGBT has a parasitic thyristor due to the layer's structure n^+, p, n^- and n^+,Figure 3.1 on the next page. This thyristor should not be turned on during operation because it can not easily be turned off again. To turn off the IGBT after the thyristor is turned on forced commutation of the current has to be performed. To prevent this turn-on a source-body short is implemented in the IGBT. The source metallization is extended to include the body region as can be seen from Figure 3.1 on the following page.

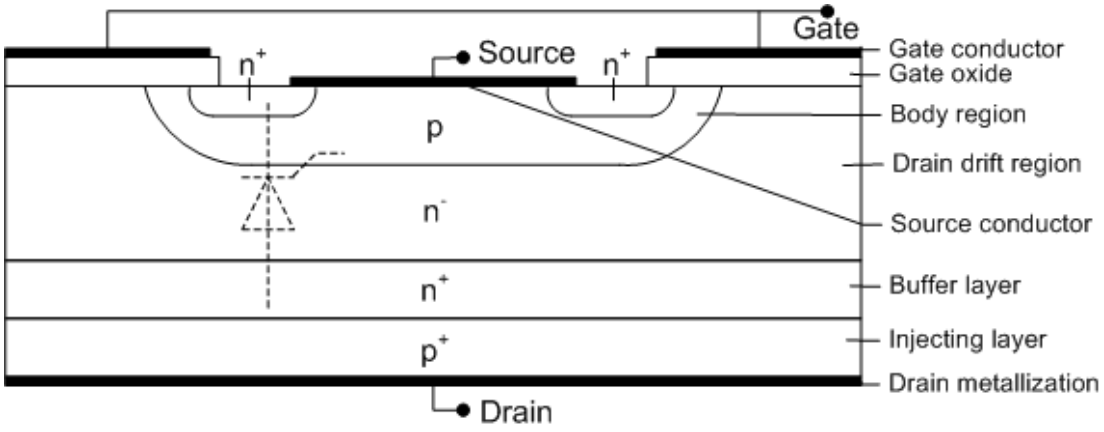

Figure 3.1: The architecture of an IGBT

3.1.2 Blocking capability

The body-drift region junction is the junction that blocks the forward voltage when the device is off and the junction between the p^+ injection layer and the n^- layer is the junction that blocks the reverse voltage. A punch-through IGBT is not capable of blocking any reverse voltage because of the high doping on both sides of the p^+-n^+ junction. The non-punch-through IGBT should theoretically be able to block a reverse voltage as high as the magnitude of the forward voltage. Due to roughness at the edges of the chip because of the cutting during the manufacturing this will not the reality. The roughnesses result in leakage currents on the edges causing breakdown of the blocking junction. In the NPT-IGBT the depletion region of the junction will extract into the n^- drift region because the body region has a higher doping than the drift region. The drift region is accommodated so that the depletion region never reaches the p^+ layer. This leads to a long drift region which leads to high conduction losses in on-state due to the resistance of the layer. To reduce these losses the drift region is made thinner. Then the depletion region of the body-drain drift junction might extend into the p^+ layer. Therefore the buffer layer is needed to prevent this extraction and a PT-IGBT i formed. By adding this buffer layer the revers blocking capability is almost absent.

3.1.3 Operation of the IGBT

To control the IGBT, a voltage V_{GS} is applied over gate and source. This voltage has to be higher than the threshold voltage $V_{GS(th)}$ to turn the IGBT on. If the V_{GS} is below the threshold voltage the IGBT will be in off-state. The voltage will then be blocked by the body-drift region junction. If the V_{GS} is higher than the threshold voltage the IGBT is in on-state and a inversion layer or channel will be build up beneath the gate. This layer shorts the n^- drift region to the n^+ source region. The electrons from the source will then flow into the drift region and attract holes from the p^+ drain layer. The holes will then move into the drift region and further into the body region.

When the holes are in the body region they attract electrons from the source and recombine. The holes from the p^+ layer will flow directly to the source metallization or to the inversion layer. This results in many holes flowing laterally through the body region. By doing that a resistance is created and this resistance causes a lateral voltage drop. This lateral voltage drop causes the n^+-p junction to be forward biased and the parasitic thyristor will be turned on. Therefore there are always given a maximum drain current and a maximum V_{GS} from the manufacturers to avoid this latchup. Latchup can also occur during turn-on and turn-off of the device.

Even though the IGBT is in conduction mode there will always be a voltage drop. The on-state drain-source voltage drop $V_{DS(on)}$ consists of the voltage drop over the p^+-n^+ junction, the voltage drop due to the resistance in the drift region and the voltage drop due to the resistance in the channel, Equation 3.1.

$$V_{DS(on)} = V_{junc} + V_{drift} + I_D R_{channel} \tag{3.1}$$

3.2 Bidirectional switches

Up to the last years bidirectional switches are made up of IGBTs and diodes in different constructions. Recently reverse-blocking IGBTs (RB-IGBTs) have been developed. They can be used for bidirectional switches and has advantages to the conventional switches. See Section 3.3 on page 15 for detailed information on RB-IGBT. Different configurations of bidirectional switches are described and studied for different converters in [14] and [15]. In Figure 3.2 on the next page four structures of switches are presented. The two bidirectional switches to the left in Figure 3.2 on the following page are made up of two IGBTs and two diodes in anti parallel. The switches are called common collector IGBT (CC-IGBT), seen in a), and common emitter IGBT (CE-IGBT), seen in b). The names are given because of the way the switch modules are series connected, collector to collector and emitter to emitter. These switches are easy to implement because conventional IGBT modules are used. The only changes that have to be made are the connections between the modules. The disadvantage of these switches is the high conduction losses. An advantage is that no snubber circuits are needed for the commutation[15].

Figure 3.2 on the next page also shows an IGBT embedded in a diode bridge. This type of bidirectional switch is convenient to control, but has high conduction losses. Another disadvantage is that snubber circuits are needed for the switching in some applications[15]. To the right in Figure 3.2 on the following page there are two reverse-blocking IGBTs (RB-IGBT) with intrinsic diodes. These reverse-blocking IGBTs can form a bidirectional switch without the use of diodes connected in anti parallel. In [14] the RB-IGBT is compared to a CE-IGBT module. The results of the experiments shows that the conduction losses of the RB-IGBT is halved compared to the CE-IGBT, but the switching losses is more than five times higher. The high switching losses is because of the high reverse recovery current in the intrinsic diode.

The new reverse-blocking IGBT leads to a reduction of the forward conduction state voltage drop of the switch[16]. This is due to less components in the switch and the architecture of

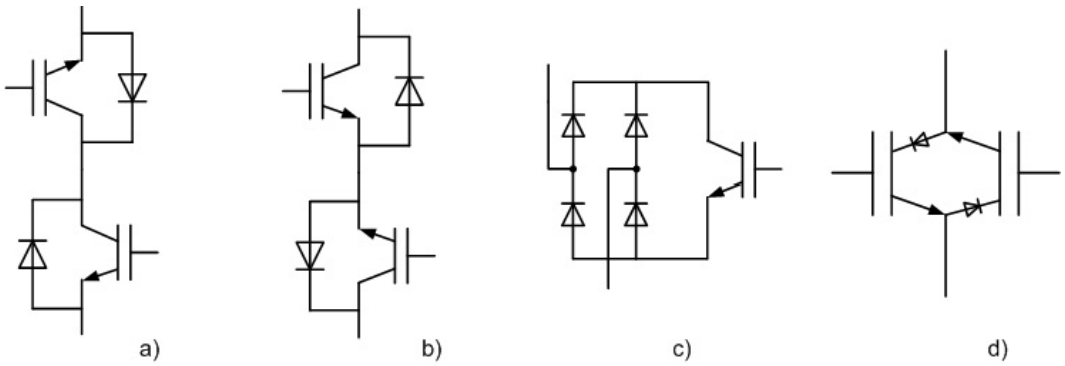

Figure 3.2: Bidirectional switches, a) common collector IGBT with diodes, b) common emitter IGBTs with diodes, c) diode embedded IGBT, d) reverse-blocking IGBT with intrinsic diodes

the RB-IGBT. This can be seen in Figure 3.2. The on-state conduction losses in a RB-IGBT is also reduced due to less components in the switch. In Figure 3.3 the conduction paths for the different bidirectional switches can be seen. For the CC-IGBT switch to the left and the CE-IGBT switch, the conduction path consists of two components in both directions, one IGBT and one diode. The diode embedded IGBT, Figure 3.3c), has three components for the current to pass through. All these configurations of bidirectional switches result in more on-state losses than the RB-IGBT on the right side in Figure 3.3. The RB-IGBT has just one component in both directions. The more components to pass through, the more on-state losses is generated.

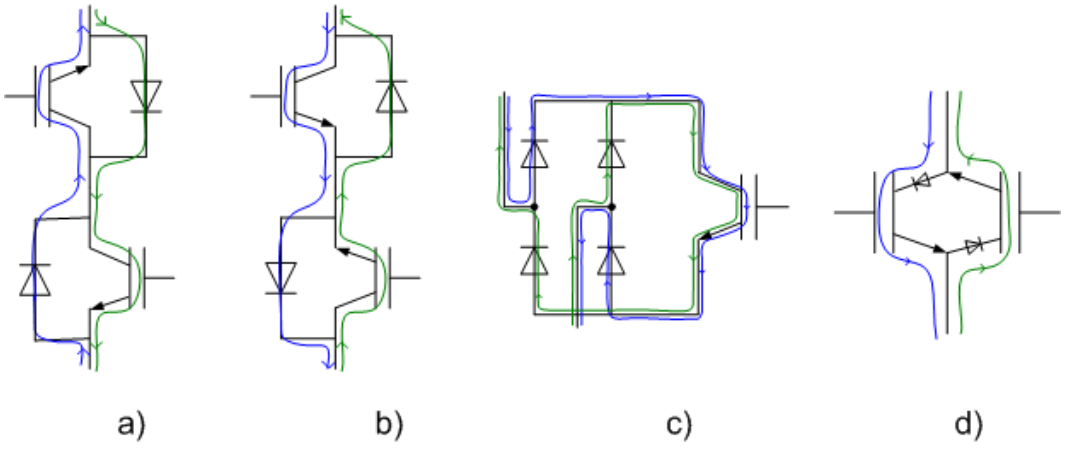

Figure 3.3: Current paths for the bidirectional switches, a) CC-IGBT, b) CE-IGBT, c) diode embedded IGBT, d) RB-IGBT with intrinsic diodes

3.3 Reverse-blocking IGBT(RB-IGBT)

Today there are five manufacturers of RB-IGBTs, IXYS, Fuji, SemiKron, Mitsubishi and Infineon, see Table 3.1 on page 17. They all have their own design, so the architecture of the RB-IGBT depends on the manufacturer. In [17] the architecture of a RB-IGBT from IXYS is described. They have modifying a non-punch-through IGBT (NPT-IGBT) by using the technique of isolation diffusion and folding up the lower p^+ layer at the chip edge. By doing that the p^+-n^- junction, which is the one who blocks the reverse voltage, prevents breakthrough at the chip edge. The p^+-n^- junction will continue to the isolation layer at the gate connection. These modifications make the IGBT capable of blocking negative collector-emitter voltages as a normal p-n diode and still have the operational behavior like a normal NPT-IGBT. The maximum reverse blocking voltage for this device is 1200 V.

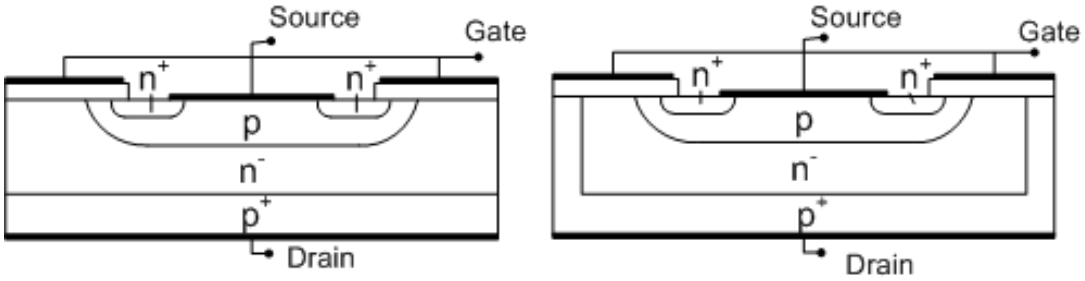

Figure 3.4: The architecture of a NPT-IGBT (left) and IXYS' RB-IGBT with an intrinsic diode (right)

In [18] different IGBT structures are tested by INFINEON. This includes a new type of reverse-blocking IGBT using a new concept of "dielectric charge traps". This technique obtains a "dynamical" buffering in both direction of the IGBT by trapping hole charges. There are specially formed dielectric structures which traps the holes and act as buffers for the electric field, see Figure 3.5. This might be possible by using technologies like Separation by implementation of oxygen (SIMOX) or wafer bonding. This type of RB-IGBT results in a switching loss reduction down to 50 % of the losses generated in series connected IGBTs, but is not commercial yet.

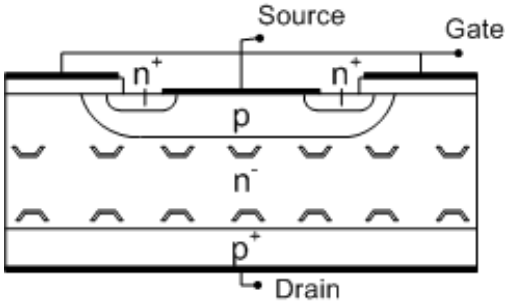

Figure 3.5: The architecture of a RB-IGBT with dynamical buffering from INFINEON

Fuji Electric has newly developed a RB-IGBT with a voltage rating of 1200 V. They have also managed to develop a device that can withstand 1600 V and 1800 V in the laboratory, but these devices are not yet commercially available[19]. In [20] a 600 V RB-IGBT from Fuji Electric is described. It is a NPT-IGBT which is etched to form a trench to electrically separate the side surface from the active region of the IGBT. The bottom of the etched trench reaches the substrate. By adding this trench there is no reverse leakage current from the side surface of the chip and the IGBT is able to block a reverse voltages. Experiments carried out in [20] shows that the RB-IGBT has a higher breakdown voltage than 600 V, but has both higher forward and reverse leakage current than a FZ-wafer NPT-IGBT (FZ-NPT-IGBT). Higher leakage currents are not good characteristics of an IGBT. Therefore Fuji improved the RB-IGBT by using helium irradiation to improve the carrier lifetime control at the collector side of the device. A high density of holes at the collector side results in a large value of the turn off losses E_{off}. The FZ-NPT-IGBT has a low-doped anode layer which will improve the FWD characteristics of the RB-IGBT. The only disadvantage is that for the FZ-NPT-IGBT the etched trench can not be made due to the thin collector layer. A technique used for the improvement of the FZ-NPT-IGBT is the junction separation technique, see Figure 3.6. For FUJIs 1200 V RB-IGBT the thin wafer technology and deep boron diffusion technique are used [21]. This leads to a total loss reduction of 20 % copared to the bidirectional switch with the IGBT and diode in anti parallel. The major loss reduction is in the on-state losses because of the lack of the ant parallel diode and since the RB-IGBT has the same on-state voltage drop as a normal IGBT. In [3] the new RB-IGBT is used in a AC-AC direct converter resulting in an efficiency increase of 1.9 point compared to a conventional device.

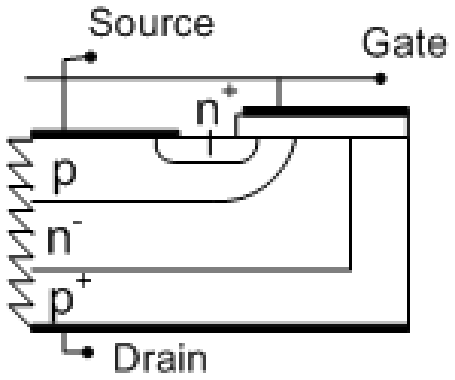

Figure 3.6: The architecture of the RB-IGBTs made by Fuji Electric with junction separation technique

In [22] the reverse recovery mode of an RB-IGBT is described. By having two RB-IGBT in the same switch and two switches in the leg of the converter, there will always be one switch which is outgoing and one switch which is incoming. The current has to commutate from the outgoing to the incoming device. When the voltage across the outgoing RB-IGBT is reversing polarity, the device will experience reverse recovery mode. With the normal bidirectional switch with IGBT and diode, the diode would not need to be turned on and off, so the IGBT will react

different than the RB-IGBT. In the commutation period the current in the outgoing RB-IGBT will start to decrease. But the voltage is still positive due to the excess carriers in the p^+-n^- junction, see Figure 3.7. The voltage will decrease a little due to the ohmic drop caused by the reverse current, but not much. When the current becomes negative the voltage will be reversed biased. The current will then decrease until a reverse recovery current I_{rr} is reached and increase back to almost zero. There will be a ”tail" in the current curve which will increase the reverse recovery loss. The voltage will get a peak before stabilizing in the reverse voltage. In [22] a control method to reduce the losses caused by the reverse recovery current is proposed.

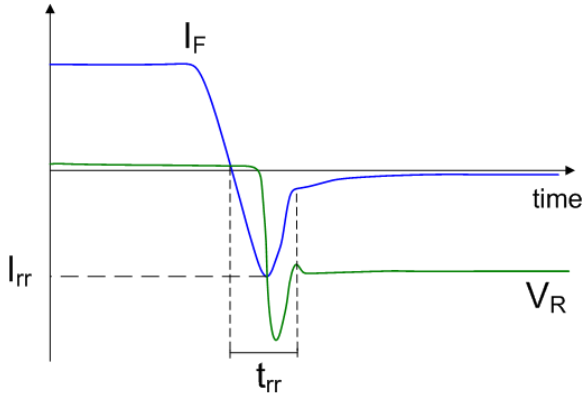

Figure 3.7: The current and voltage waveforms in reverse recovery

Manufacturer	IXYS	INFINEON	FUJI	SemiKron	Mitsubishi
Rating	1200 V / 40 A	-	1200 V / 35 A 600 V / 200 A	-	-

Table 3.1: Overview of the RB-IGBT manufacturers

3.4 IGBT vs. RB-IGBT

The main difference between the reverse-blocking IGBT and the normal IGBT is that the RB-IGBT is capable of withstanding reverse voltage, i.e. negative collector-emitter voltage. The architecture of the RB-IGBT is almost the same as the architecture of the normal IGBT, just with a few modifications. To make the IGBT withstand negative collector-emitter voltage, the chip edges need to be separated from the active region of the chip to prevent the leakage current from the side surface of the device.

The RB-IGBT can conduct in both directions, which the diode is not able to do. So by using two RB-IGBTs in anti parallel the power can flow in both directions. For the RB-IGBT the reverse conduction characteristics are the same as the forward conduction characteristics. The difference from the IGBT is the recovery mode. The conventional IGBT has no reverse recovery

mode but the RB-IGBT has and it is the same as for a diode. The forward voltage drop is about half compared to the normal IGBT and diode module[3].

The RB-IGBT has lower space requirement than the IGBT and diode modules due to less components. This is also the reason that lowers the costs.

CHAPTER 4

CONSIDERATION OF CONVERTER LOSSES

4.1 The AC-AC converter with the RB-IGBTs

The 3-phase AC to 1-phase AC converter consists of three legs each with two bidirectional switches, see Figure 4.1. The bidirectional switches are a new type of reverse-blocking IGBTs. They do not have any anti parallel diodes and they therefore reduce the converter losses. See Chapter 3 on page 11 for further explanation of the switch. The converter is connected to the generator on one side and the transformer on the other side. On the generator side of the converter there will always be an alternating voltage and on the transforme side a square wave voltage. The switching technique used for the control of the switches in the converter is a new switching pattern. The pattern is based on the PWM switching technique. A triangular carrier signal (10 kHz) is compared to a sinusoidal 50 Hz reference signal. The sinusoidal reference signal is inverted for half of the carrier signal period. There is one reference signal for each leg controlling the switching of the two switches in the leg. The switches in the same leg will never be on at the same time, but there will always be three switches on, one from each leg. For a thorough explanation of the switching technique, see Section 6.2 on page 47.

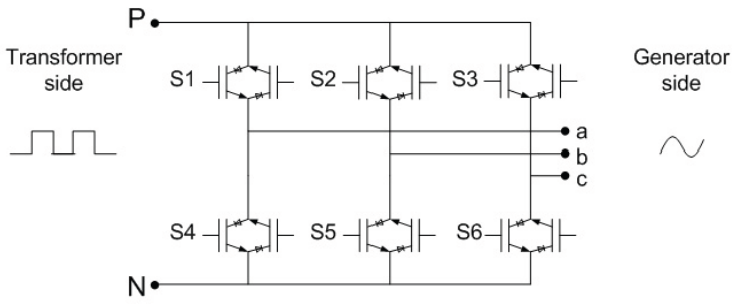

Figure 4.1: 3-phase AC to 1-phase AC converter with RB-IGBTs

4.2 Protection of the converter

To make a prototype of the converter protection is needed to prevent overcurrents and overvoltages which destroy the switches. To protect the RB-IGBTs from overvoltages a snubber circuit is added to each switch[23]. The snubber circuit consists of a diode and a zener diode from gate to collector, see Figure 4.2. If the voltage rating of the RB-IGBTs is 1200 V the device will be turned off if the voltage exceeds this limit. This type of snubber can only handle peaks with a small time range. If the peaks last for a long time, the diode will be warm and eventually be destroyed. It is therefore important to have a protection system to cope with these longer lasting peaks.

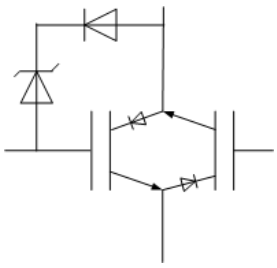

Figure 4.2: Snubber circuit for RB-IGBT switches

To protect the system from these longer lasting overvoltage periods, there should be current sensors on the DC grid side and on each phase on the generator side, red dots in Figure 4.3 on the next page[23]. These sensors give a signal to the control system if the current exceeds the maximum set value. The system will then be turned off. If this current is higher than the maximum set value it might be a short circuit in the converter close to the sensors. There should also be a voltage sensor close to the transformer. This sensor measures the voltage from the AC-DC converter before the transformer. If the voltage is over the set value, the system will be turned off to prevent damages on the system.

The protection circuit, red lines in Figure 4.3 on the facing page, should be added to the circuit to prevent peaks of the square wave voltage through the transformer [23]. The circuit consists of four diodes and a capacitor and resistance connected in parallel with one of the diodes. This circuit is to prevent the peaks in the voltage waveform which will destroy the switches in the converter. Since the switches can only withstand a maximum voltage of 1200 V, since that is the rating, the operational voltage should be a lot lower than the given withstand voltage of the device.

If the bidirectional switch was a normal IGBT with an anti parallel diode, there would be an RL snubber on the lower switch of the two switches in one leg. When the upper switch is conducting and should be turned off the lower diode would lead the current in a circuit through the RL snubber and the diode. Then the upper switch could be turned off without current flowing through it. This will be different for RB-IGBTs because they do not have any diodes. The upper left RB-IGBT S1 is conducting and should be turned off, Figure 4.4 on the next page. There are

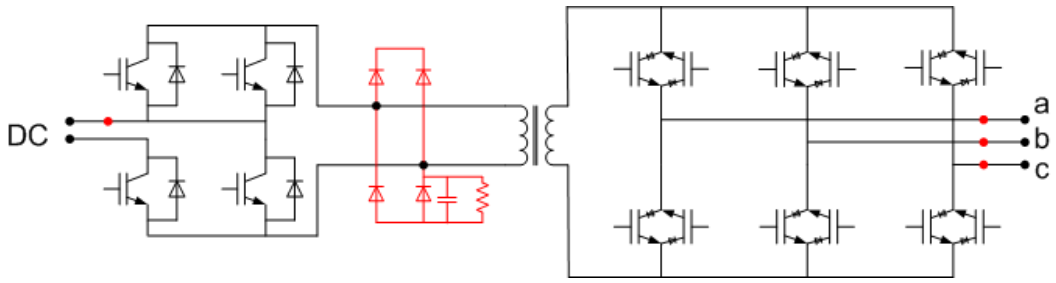

Figure 4.3: Protection circuit and sensors for the converter and the system

still an RL snubber connected over the lower switch, S3 and S4. Since there are no diodes, the lower right RB-IGBT S4 has to be turned on to make the current circling path. Then the upper switch S1 can be turned off.

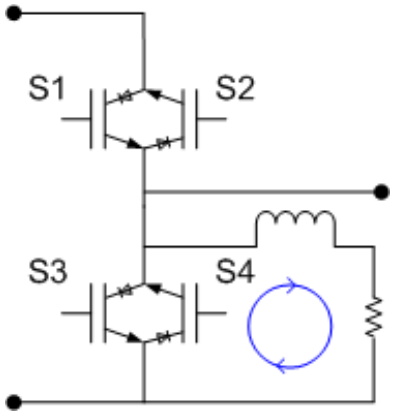

Figure 4.4: RL snubber for the switches

4.3 The converter losses

To calculate the losses in a converter the losses in every switch in the converter needs to be calculated. Which losses that will occur in the switches dependent on which type of semiconductor device that is used. For the controllable devices there are four different types of losses; conduction losses, turn-on losses, turn-off losses and reverse recovery losses. To calculate these losses the data sheet of the device is needed. In the AC-AC converter the switches consists of RB-IGBTs. The losses are calculated for one RB-IGBT and multiplied by the total number of devices in the converter. Each switch consists of two RB-IGBTs, so in this case the number is twelve. Figure 4.5 on the following page shows the principle of the time periods of the voltage and current waveforms when the turn on losses, conduction losses and turn off losses occur.

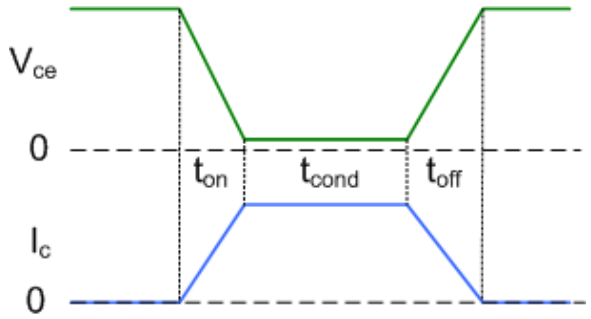

Figure 4.5: V_{CE} and I_C during turn on, conduction and turn off of an IGBT

4.3.1 Conduction losses

The conduction losses are the losses in the semiconductor device when the device is conducting, i.e. in on-state. There will always be some kind of voltage drop when conducting, see Equation 3.1 on page 13, and this voltage drop leads to losses. To calculate the conduction losses for the RB-IGBT the collector current I_C and the gate-emitter voltage V_{GE} has to be known. From the data sheet the curve Collector current vs. Collector-Emitter voltage for a given V_{GE} should give the on-state voltage V_{CE}. Using I_C and this curve the collector-emitter voltage can be found and multiplied with the current, Equation 4.1. Figure 4.6 shows the I_C-V_{CE} curve of a RB-IGBT to the left. The graphs are experimental results given in [3] so the real loss calculation should be carried out by using the real data sheet of the device. The figure also shows the I-V characteristics of an IGBT with an anti parallel diode FWD to the fight. The curves are for a given value of V_{GE}.

$$P_{cond} = V_{CE} I_C \tag{4.1}$$

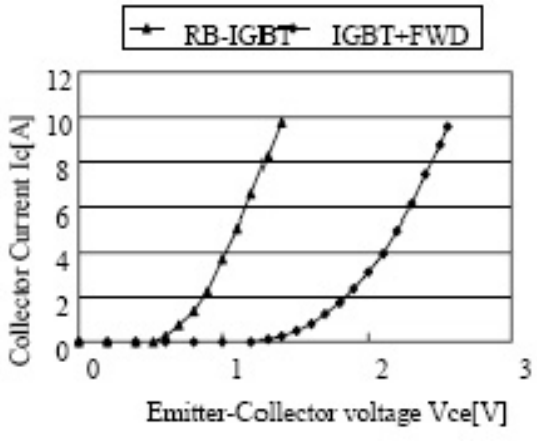

Figure 4.6: I_C-V_{CE} curve for the RB-IGBT [3]

4.3.2 Turn-on, turn-off and recovery losses

The turn-on and turn-off losses are the losses generated during turn-on and turn-off of the device. During turn-on it takes some time for the voltage to decrease and the current to increase to the on-state values. For the turn-off there will always be some time delay before the current is back to zero or a small leakage current value. The voltage will also need time to increase to the blocking voltage. These time delays will lead to the switching losses.

To find the switching losses of the RB-IGBT there will be a graph in the data sheet giving the different switching losses versus the collector current, see Figure 4.7, 4.8 on the next page and 4.9 on the following page for examples of graphs from [3]. The collector current I_C has to be known, so the energy losses for the turn-on, turn-off and recovery losses can easily be found. Since the losses are given in switching energy (J), they have to be converted to power losses (W). T in Equation 4.2 is the switching period for the device.

$$P_{loss} = \frac{E_{loss}}{T} \tag{4.2}$$

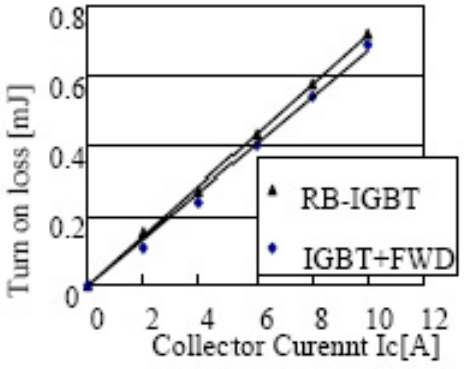

Figure 4.7: Turn-on losses vs. collector current curve for the RB-IGBT [3]

4.3.3 Total converter losses

The total losses per device will be the sum of all the four losses described above. Equation 4.3 shows the total losses of the switching period.

$$P_{tot} = P_{condRB-IGBT} + P_{on} + P_{off} + P_{rr} \tag{4.3}$$

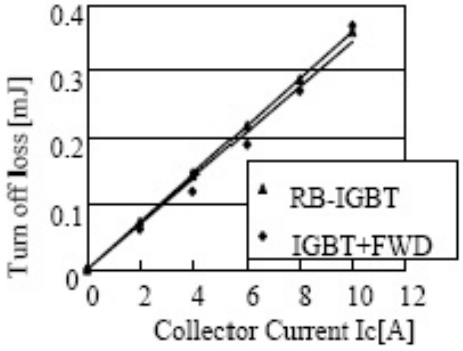

Figure 4.8: Turn-off losses vs. collector current curve for the RB-IGBT [3]

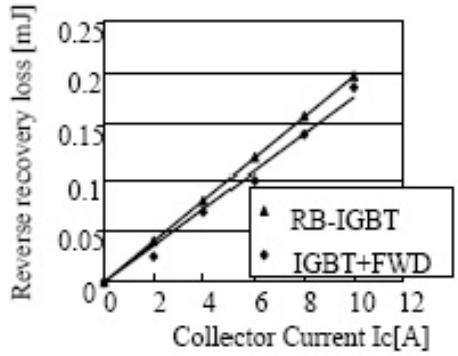

Figure 4.9: Reverse recovery losses vs. collector current curve for the RB-IGBT [3]

To find the average total losses for the frequency of the output f_{out}, Equation 4.4 can be used.

$$P_{totavr} = \int_0^t P_{tot} f_{out} \tag{4.4}$$

CHAPTER 5

HIGH FREQUENCY HIGH POWER TRANSFORMER DESIGN

Today transformers are indispensable electric components. They are found in many systems from large power transformers in the electric grid to small signal transformers in electronic circuits. The transformers used in power electronic converters are not mass-produced and have to be design individually [24]. To design a transformer there are many criteria to fulfill. Leakage inductance should not be too high, losses and weight should be minimized and cooling should be right dimensioned [25]. All these criteria must be considered during the design procedure.

5.1 Core materials

There are two different classes of materials used in cores when designing transformers. One is alloys especially iron alloys, often called electric steel, with large electric conductivity (compared to ferrite) and large values of saturation flux density, near 1.8 T. There are two types of losses found in iron alloys, hysteresis and eddy current losses. The cores must be laminated to reduce the eddy current losses. Because of these losses this material is mostly used in applications with low frequencies, 2 kHz or less. If the iron alloys are made of powder, they have greater resistivity and can be used for higher frequencies. Another type of alloys, amorphous alloys also called METGLAS, are also better suited for high frequencies. This is due to the small thickness because of the fabrication techniques and the larger resistivity due to no crystalline order in the structure. Amorphous alloys consist of iron, cobalt and nickel (70-80 atomic percent) in combination with boron, silicon and other glass-forming elements (approximately 20 atomic percent). One of the most suitable amorphous alloys for high frequencies includes cobalt.

The second class of materials are ferrite materials. Ferrite consists of oxide mixtures of iron and other magnetic elements. Due to the large electric resistivity the ferrite materials have only hysteresis losses. They have low saturation flux density compared to iron alloys, approximately 0.3 T. Because of the very low amount of eddy current losses, ferrite is the best choice for applications with frequencies of 10 kHz and above.

5.1.1 Hysteresis loss

There will always be hysteresis losses in magnetic materials and it will increase with increasing AC flux density,B_{ac} and with increasing operating or switching frequency, f. The loss per unit volume is often called specific loss $P_{m,sp}$ and the general form is

$$P_{m,sp} = kf^a(B_{ac})^d \tag{5.1}$$

with k, a and d as constants depending on the material. B_{ac} in 5.1 is the peak value of the ac flux density when the waveform has no time-average. If there exists a time-average, B_{avg}, the value used in Equation 5.1 should be $B_{ac} = \hat{B} - B_{avg}$. Usually the manufacturers give the specific loss of a material as a graph with $P_{m,sp}$ or P_v as a function of B_{ac} and with the frequency as a parameter[5], see Figure 5.1 and Figure 5.2. Equation 5.1 is not valid for ferrite materials at high frequencies due to reduction in the performance factor $PF = fB_{ac}$ of the material.

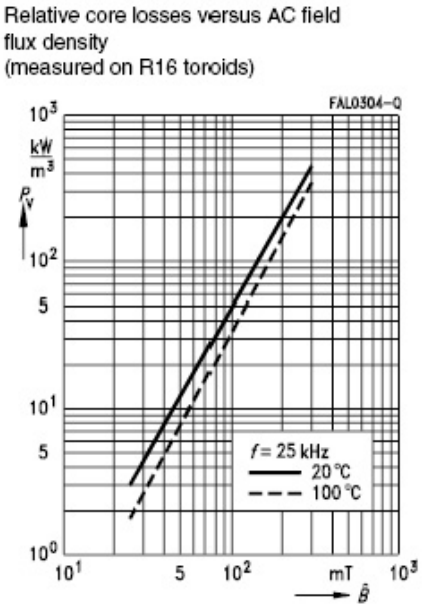

Figure 5.1: Relative core losses vs. AC field flux density for N27[4]

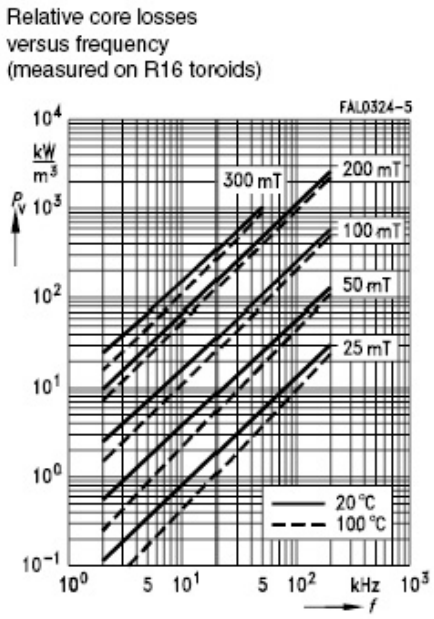

Figure 5.2: Relative core losses vs. frequency for N27[4]

5.1.2 Skin effect and eddy currents

Skin effect is circulating currents which arise in the magnetic materials used in cores due to the applied time varying magnetic field, see Figure 5.3 on the next page. These currents are called eddy currents and leads to core losses. The eddy currents produce magnetic fields which oppose

the applied magnetic field in the core. These magnetic field screens the interior of the core from the applied field and makes the total field decrease exponentially in the direction of the center of the core. The characteristic decay length of the magnetic field for materials is called skin depth δ. An example of a magnetic field distribution in a core with its skin depth can be seen in Figure 5.4. The skin depth is given by Equation 5.2 [5].

$$\delta = \sqrt{\frac{2}{\omega\mu\sigma}} \tag{5.2}$$

$\omega = 2\pi f$ where f is the frequency of the applied magnetic field, μ is the magnetic permeability and σ is the conductivity of the material. The length of the skin depth should be small compared to the cross-sectional dimension of the core to avoid ineffective use of the core. If the skin depth is small the interior of the core does not carry much of the applied magnetic flux which is the main purpose of the magnetic core.

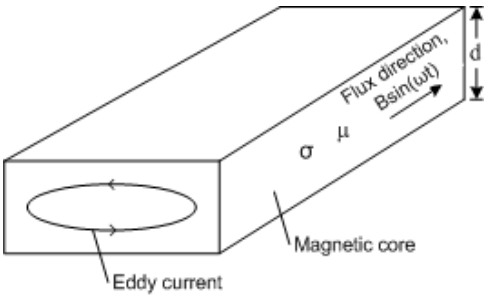

Figure 5.3: Part of transformer core with eddy current path

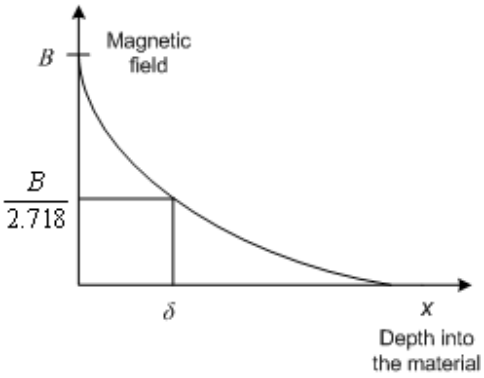

Figure 5.4: Exponential decrease of magnetic flux density in core material with skin depth δ

The losses produced by the eddy currents is due to power dissipation in the core. This power dissipation is called eddy current losses and lead to increasing core temperature. By applying a uniform time-varying magnetic field with flux density $B(t) = B\sin(\omega t)$ the specific eddy current loss $P_{ec,sp}$, i.e. loss per unit volume, can be derived. See [5]for a detailed derivation of Equation 5.3.

$$P_{ec,sp} = \frac{d^2\omega^2 B^2}{24\rho_{core}} \tag{5.3}$$

d in Equation 5.3 is the lamination thickness, $\omega = 2\pi f$ and $\rho = \frac{1}{\sigma}$ is the resistivity of the core material. To reduce the eddy current losses the cores can be made of many thin laminations separated by insulators. Another possibility is to add silicon to the material to increase the

resistivity. This will only be done in small percentage because by adding silicon the saturation flux is reduced more than the resistivity is increased. The ferrite materials have no eddy current losses due to their high resistivity.

5.2 Core geometry

There are many different shapes of cores available in the market RM (Rectangular Modular), PM (Pot core Module),P (Pot core) E, U, UI and toroid [4]. The RM and PM cores are normally used for telecommunication, broadband and other industrial applications. The pot cores have low magnetic leakage because the windings are completely enclosed by the core and are therefore mostly used for inductors and small signal transformers [4]. The E-core is shaped as the character E and has three legs as can be seen in Figure 5.5 at the bottom on the left side. This type of core is used in power applications and leads to power loss reduction. In the middle of Figure 5.5 is the U-core, formed as the character U, and is used for power and high-voltage transformers. The U-cores is often found in combination with the I-core, at the top of the U-core in Figure 5.5, or just two U-cores together. On the right side in Figure 5.5 a toroid shaped core can be seen. This type of core is mostly used in signal transformers but also in power applications. On the left side above the E-core, a horizontal cross-section of an E-core can be seen. The three legs have different shapes and this type of E-core is called ER-core, due to the shape of the legs. By having a circular shape of the center leg and curved legs on each side, the core is better suited for compact winding and reduces the leakage inductance. Therefore the ER cores are well suited for high power densities.

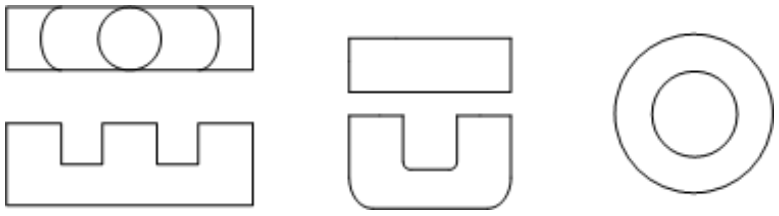

Figure 5.5: Core shapes: E-core (bottom left), ER-core (top left), U-core (bottom middle), I-core (top middle) and toroid core(right)

To make a transformer of the different core shapes two E-cores, two U-cores or U- and I-cores have to be used. The toroid core needs only one since both the primary and secondary windings are wound around the core as in Figure 5.6 on the facing page. In the figure only one winding is wound on the core to show the principle. The disadvantages of the toroid core are that they are difficult to wind and the cooling is also difficult. For the UU-core and the UI-core it is possible to separate the secondary and primary windings on the two legs. In Figure 5.6 on the next page the windings are shown for a UU-core transformer. For the ER-core and E-core type both of the windings have to be wound on the center leg of the core, Figure 5.6 on the facing page. This enables the possibility to use a bobbin. The windings can then be wound on the bobbin and then afterward the bobbin is placed in the core. A bobbin can also be used for the U-cores.

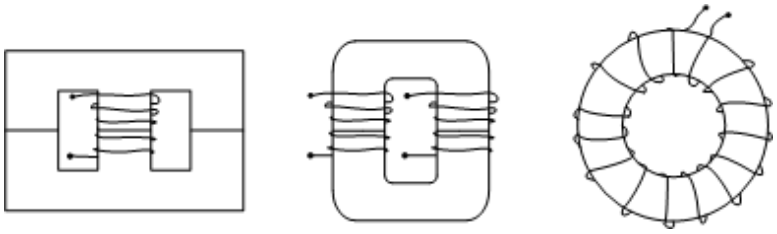

Figure 5.6: Transformer cores: double ER (left), UU (middle) and toroid (right)

5.3 Transformer windings

5.3.1 Winding material

For the material of the windings there are two possibilities which is used, copper and aluminium. Copper is mostly used due to the low conduction losses compared to aluminium. If aluminium is used it is either to reduce weight or to reduce costs. Copper is more expensive than aluminium (10 $ per kg for copper and 3 $ per kg for aluminium) [26]. The weight reduction is because the density of copper is 8.96 g/cm^3 and for aluminium it is 2.70 g/cm^3 (both in solid state at room temperature) [6]. Aluminium transformers can be found in airplanes for weight reduction and for other applications if the investment costs should be kept low, but it is very rare. If large amounts of current should be carried there will be more aluminium wires than copper wires needed to carry the current due to the electrical conductivity of the materials. Copper has an electrical conductivity of 59.6*10^6 S/m and aluminium has one of 37.8*10^6 S/m which shows that more aluminium wires are needed. The weight gain might therefore not be as big as first predicted.

5.3.2 Skin effect and eddy currents

There will also be skin effect and eddy currents in the windings, just like in the core. The conductor carries a time-varying current which generates a magnetic field. This magnetic field generates the eddy currents which flow in the opposite direction of the applied current. The current density will therefore be high at the surface and decrease exponentially into the center of the conductor. The skin depth describes also in this case the characteristic decay length of the conductor, Equation 5.2 on page 29. By using conductors with a radius equal to or less than the skin depth the skin effect can be neglected[5].

To reduce the skin effect and proximity effect at high frequencies Litz wires or foils are used for high frequencies. Litz wires consist of many small wires individually coated with an insulating film and twisted or woven together, as can bee seen in Figure 5.7 on the following page. It can also be used for lower frequencies, but as can be seen from the figure the available conducting area is smaller due to many small wires instead of one big one. There will be more unused space in the Litz wire compared to the wire with only one conductor. For high power transformer

one wire should be used because one wire can cope with higher currents than many individually isolated small ones. It is also more difficult to make thin windings of copper and the production process is more complicated which makes Litz wires more expensive [26].

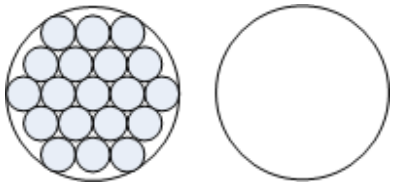

Figure 5.7: Conducting area of a Litz wire (left) and a one-conductor copper wire(right)

5.3.3 Winding losses

Every conductor has something called a DC resistance. This resistance leads to losses because of the current flowing in the conductor. The power dissipated in the windings due to this DC resistance is given by Equation 5.4. The current density $J_{rms} = \frac{I_{rms}}{A_{con}}$, where I_{rms} is the RMS value of the current flowing in the cable and A_{con} is the cross-sectional area of the conductor. Equation 5.4 shows the power dissipated per unit winding volume, which is the best way to express these losses. ρ_{con} is the resistivity of the material in the conductor and k_{con} is a constant called fill factor which will be explained in 5.3.4 on the next page.

$$P_{w,sp} = k_{con}\rho_{con}J_{rms}^2 \tag{5.4}$$

If a Litz wire or a foil is used the skin effect can be neglected and the only winding losses will be the losses caused by the DC resistance [5]. Normally a round or rectangular winding is used and they both have eddy currents. The skin effect caused by the eddy currents increases the resistance in the conductor because the current is flowing only close to the surface of the conductor. This leads to smaller cross-sectional area for the current to flow. In this case the losses will be higher than the DC resistance losses and Equation 5.4 is modified to Equation 5.5 to count for the eddy current losses. R_{dc} is the DC resistance and the R_{ac} is the effective resistance of the winding.

$$P_{w,sp} = k_{con}\rho_{con}\frac{R_{ac}}{R_{dc}}J_{rms}^2 \tag{5.5}$$

The total losses can also be written as in Equation 5.6. Here the losses due to the DC resistance and the eddy current losses are separated. The R_{ec} is the eddy current resistance.

$$P_w = P_{dc} + P_{ec} = R_{dc}I_{rms}^2 + R_{ec}I_{rms}^2 = R_{ac}I_{rms}^2 \tag{5.6}$$

5.3.4 Winding geometry

The winding area of a transformer is the area between the legs of the core which is suited for the windings. This space will never be totally filled with the windings because the windings normally have a shape which leaves some space between the wires and they are wound on a bobbin or an other coil former. Since the windings should be wound on the core the winding method also makes it impossible to fill the whole winding area. There will also be insulation between the windings which gives less conducting area. The constant describing the ratio of the area of conducting material, normally copper, to the winding area is called fill factor, k_{Cu} for copper. The fill factor can be calculated by using Equation 5.7 or by using the values of the different types of windings found in Table 5.1 [5]. N in Equation 5.7 is the number of turns, A_{Cu} is the copper area and A_w is the winding area.

$$k_{Cu} = \frac{NA_{Cu}}{A_w} \tag{5.7}$$

Type of winding	**Fill factor**
`Litz wire`	0.3
`Round wire`	0.55
`Foil/rectangular wire`	0.6

Table 5.1: Fill factor for different types of windings

There are two ways to wind the windings in a transformer. The first one is as shown on the left side in Figure 5.8 on the following page. In the figure a part of the core can be seen in the middle and the windings are wound around the core every second primary and every second secondary. This way of winding the windings is very complicated [26]. The second option is to have the secondary and primary windings separated in layers as shown in the middle in Figure 5.8 on the next page. This technique is easier, but results in high eddy current losses when many layers are wound in one section. Each layer will generate eddy currents in the other layers which leads to more losses. This effect is called proximity effect since it is caused by the conductors in the proximity of a conductor. The windings wound in layers can also be split to reduce the eddy current losses. An example of splitting primary windings is shown on the right side in Figure 5.8 on the following page. Nearest the core a section of primary windings is wound. Outside the primary layers secondary layers are wound. Then outside this secondary layers the other section of primary windings is placed. The primary and secondary windings can be split in many sections but the more sections the more insulation is needed. Since the insulation area is increased the fill factor will decrease which means the conducting area is decreased. The inter-winding capacitance is also increased when the number of sections is increased. The more sections the more complicated is the winding of the windings.

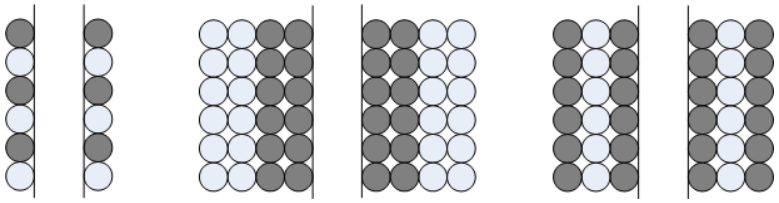

Figure 5.8: Winding techniques: every second primary and every second secondary (left), layers (middle) and split windings (right)

5.4 Temperature considerations and cooling

The temperature of the transformer will increase above normal room temperature due to the power dissipation in the core and windings. This heat has to be transfered away from the transformer to prevent damage of the component. The heat will transfer to the surrounding air and the other components in the system. At the end the whole system will have the same temperature. The maximum allowable temperature has to be decided by the component with the lowest maximum temperature. This temperature is normally around 100 °C according to [5]. The ampient temperature is normally about 25-40 °C.

For transformers with power ratings above 100 kW the best cooling alternative will be water cooling [26]. The water pipes are wound around the windings and a pump is needed to make the water circulating. Thus technique requires a lot of space. The core will then have to be bigger in size to also fit the water pipes. This and the pipes will give an increase in both weight and size.

The other option is air cooling. Then the transformer will be naturally cooled and the core has to be big enough to let the air through. It is also possible to use a fan to increase the effect of the air cooling.

5.5 Losses and weight

For this transformer the losses and the weight is important to reduce. The losses in a transformer consist of the core losses and the winding losses. These losses can be found by using Equation 5.8 and Equation 5.9. V_w and V_{core} are the volumes of the windings and the core and $P_{w,sp}$ and $P_{sp,core}$ are the specific losses.

$$P_w = P_{w,sp} V_w \tag{5.8}$$

$$P_{core} = P_{sp,core} V \tag{5.9}$$

The weight of the transformer can be calculated by using Equation 5.10 on the next page where ρ_{Cu} and ρ_{core} are the density of the copper windings and the core material.

$$M_{transformer} = V_w \rho_{Cu} + V_{core} \rho_{core} \tag{5.10}$$

5.6 Proposed transformer design

The transformer which should be designed for the prototype of the converter topology will have a rated power of 50 kVA and a frequency of 10 kHz. Such a transformer is not as often made as the normal power transformers because of the high frequency combined with high power. As core material ferrite will be used because it has no eddy current losses. Ferrite materials are also suited for high frequencies, but the maximum flux densities is about 0.5 T [27]. The N27 manufactured by EPCOS is preferred due to the sizes available. This material has a flux density of about 0.41 T.

For the windings copper foil is chosen. Copper has lower conduction losses than aluminium which means higher electrical conductivity. The shape of the windings will be foil to reduce the eddy current losses. Aluminium is easier to flatten than copper, but because of the low conductivity of aluminium more foils are needed to carry the same amount of current. Foil windings has a high fill factor because each foil covers the whole hight of the bobbin, 0.6. The thickness should be equal or less than the skin depth. Litz wires could also have been chosen to reduce the eddy current losses but it is expensive and has a fill factor of 0.3.

In [5] a transformer design method is described. To follow this method, the data sheets of the core materials are needed. An Excel program with these data sheets included can be found on the CD following the book. This program is made to ease the transformer design process and can be found in Appendix A on page 65. By inserting the input into the program it seems like there are some upper voltage limits of 1000 V which leads to a maximum V-A rating of 21 199 W using the N27 material. The current is in this case increased to give the highest possible VA- rating. This V-A rating is not high enough to be able to use for the transformer. The other materials in the database are also tested together with the input parameters but no one gives a high enough V-A rating, see Appendix A on page 65.

Since there are no satisfying output of the above mentioned design program, the method is then manually carried out using Excel, see Appendix A on page 65. This is to see if it is possible to find the size of the transformer by putting together more standard cores. The preferred shape of the core is a double E-core. It is easy to wind because of the bobbin which can be placed on the core after the windings are wound on it. Both the primary and secondary windings can be wound on the center leg to minimize the leakage inductance. According to [5] the optimal dimensions of a double E-core can be given by a relative parameter a, Table 5.2 on page 37, Figure 5.9 on the following page and Figure 5.10 on the next page.

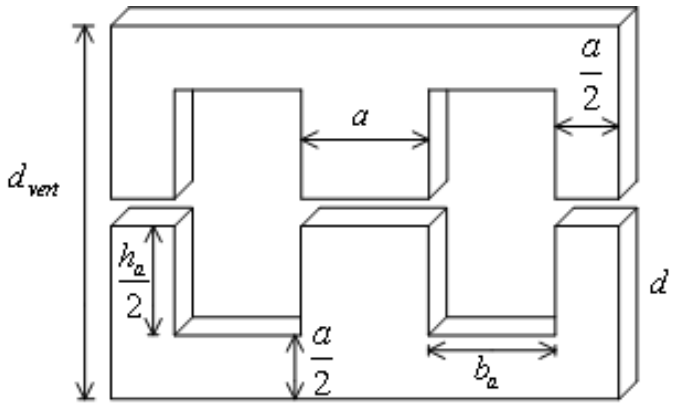

Figure 5.9: Optimal relative dimensions for an E-core

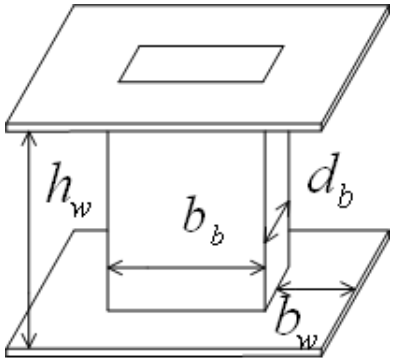

Figure 5.10: Optimal relative dimensions of a bobbin for a E-core transformer

Physical parameter	Relative value
Width of center leg, a	a
Width of winding window, b_a	a
Thickness of the core, d	$1.5a$
Hight of the winding window, h_a	$2.5a$
Width of winding area of bobbin, b_w	$0.7a$
Hight of winding area of bobbin, h_w	$2a$
Width of leg of bobbin, b_b	$1.4a$
Thickness of leg of bobbin, d_b	$1.9a$
Core area, A_{core}	$1.5a^2$
Core volume, V_{core}	$13.5a^3$
Winding area, A_w	$1.4a^2$
Winding volume, V_w	$12.3a^3$
Area product $AP = A_w A_{core}$	$2.1a^4$
Total surface area of core, A	$59.6a^2$
Vertical hight if the body, d_{vert}	$3.5a$
Mean turn length of windings, l_w	$9a$

Table 5.2: Optimal dimensions of an E-core and bobbin

5.6.1 Design method

The design method is split into eight steps. An Excel sheet is made to ease the calculations and to make adjustments easier, see Appendix A on page 65.

Step 1: Input

The input should be determined and an assumption about the wave form is made. The method is meant for sinusoidal waves, not a square wave, so the wave is assumed to be sinusoudal.

Input parameter	Value
Primary rms current I_{pri}	$38.46A$
Primary rms voltage V_{pri}	$1300V$
Frequency f	$10000Hz$
Turns ratio $N_{pri}/N_{sec} = n$	1
Surface temperature T_s	$100°C$
Ambient temperature T_a	$40°C$

Table 5.3: Transformer design input

Step 2: Volt-ampere rating

The volt-ampere rating needs to be calculated to be able to compare it to the apparent power of the proposed design, Equation 5.11.

$$S = V_{pri} I_{pri} = 38.46 * 1300 = \underline{50kVA} \tag{5.11}$$

Step 3: Core material, shape and size

The third step is to decide the core material, the core shape and the size of the core. Considering the options given in Section 5.1 on page 27 it seems like ferrite materials or amorphous alloys are the best alternatives for this frequency and power rating. According to Figure 5.11 there are no ferrite materials that are preferred for the required frequency of 10 kHz. In the figure the material with the highest power factor (PF) for a given frequency is the one which should be chosen. According to [28] N27 is still an option. Since the ferrite materials might not be the best option, amorphous alloys will also have to be considered.

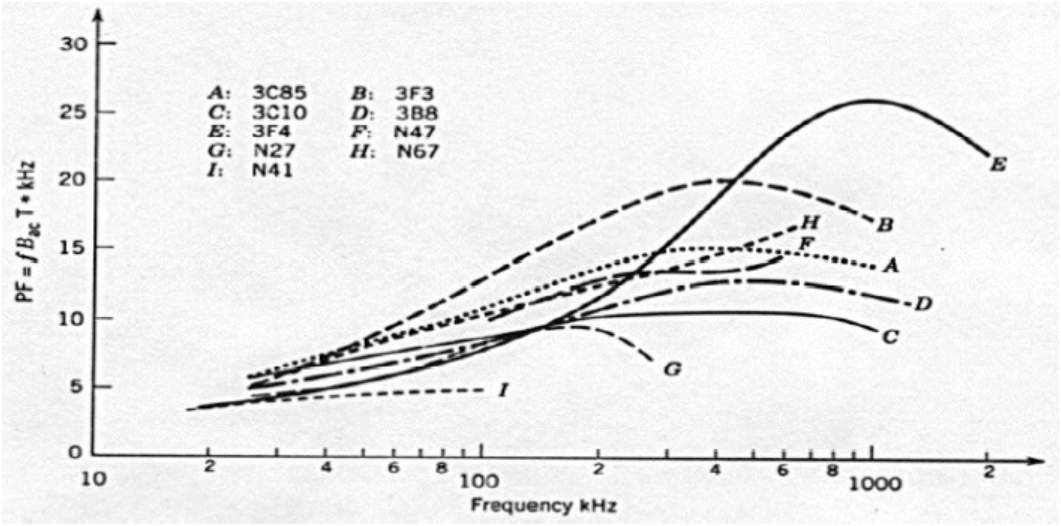

Figure 5.11: Power factor of ferrite cores vs. frequency [5]

Regarding the shape of the core different shapes are discussed in Section 5.2 on page 30. The double E-core is the easiest and cheapest one. The size of the double E-core should be decided using Equation 5.12 on the next page and comparing it to the V-A rating. The V-A rating of the transformer should be bellow the apparent power of the core. If it is higher, a bigger core needs to be chosen. The equation or value of the apparent power S can be given in the data sheet of the cores. I not S is given the type of winding, i.e. the fill factor, has to be chosen, see Table 5.1 on page 33 to be able to compare these values.

$$S = 2.22 k_{Cu} f J_{rms} \widehat{B} A_{core} A_w \tag{5.12}$$

As mentioned above, foil windings will be used and the fill factor will then be 0.6. To decide the size of the E-core different values of a, the centre leg of the transformer, are tested in the Excel sheet found in Appendix A on page 65. Since the Excel sheet with the transformer design method has all the steps included, the right size can be found easier and $\widehat{B}$ which should be found in step 5 can be used. The optimum value of a is somewhere between 4 and 4.5 cm. Since there are some inaccurate numbers given from graphs and assumptions made, the further calculations will be carried out with a = 4.5 cm to be more sure to have a core which can cope with the power flow. The dimension of the core can be found in Table 5.4.

Physical parameter	**Value**
Width of center leg, a	4.5
Width of winding window, b_a	4.5
Thickness of the core, d	6.75
Hight of the winding window, h_a	11.25
Width of winding area of bobbin, b_w	3.15
Hight of winding area of bobbin, h_w	9
Width of leg of bobbin, b_b	6.3
Thickness of leg of bobbin, d_b	8.55
Core area, A_{core}	30.375
Core volume, V_{core}	1230.18
Winding area, A_w	28.35
Winding volume, V_w	1120.8375
Area product $AP = A_w A_{core}$	861.13
Total surface area of core, A	1206.9
Vertical hight if the body, d_{vert}	15.75
Mean turn length of windings, l_w	40.5

Table 5.4: Optimal dimensions of an E-core and bobbin with $a = 4.5cm$

Step 4: $R_{\theta sa}$ and P_{sp}

In this step the $R_{\theta sa}$ and P_{sp} should be found. They can both be found in the data sheet of the material or be calculated using Equation 5.13, 5.14 on the following page, 5.15 on the next page and 5.16 on the following page. The values of the T_s and T_a is given as input parameters and d_{vert}, A, V_{core} and V_w can be found in Table 5.4.

$$R_{\theta,sa} = \frac{R_{\theta,rad} R_{\theta,conv}}{R_{\theta,rad} + R_{\theta,conv}} = \underline{0.5829 °C/W} \tag{5.13}$$

$$R_{\theta,rad} = \frac{\Delta T}{5.1A((\frac{T_s}{100})^4 - (\frac{T_a}{100})^4)} = \underline{0.9989^\circ C/W} \tag{5.14}$$

$$R_{\theta,conv} = \frac{1}{1.34A}(\frac{d_{vert}}{\Delta T})^{\frac{1}{4}} = \underline{1.3996^\circ C/W} \tag{5.15}$$

$$P_{sp} = P_{w,sp} = P_{core,sp} = \frac{T_s - T_a}{R_{\theta,sa}(V_{core} + V_w)} = 22k_{Cu}J_{rms}^2 = \underline{43.7840mW/cm^3} \tag{5.16}$$

Step 5: Core flux density and number of turns

The core flux density $\widehat{B}$ and the number of turns of the primary and the secondary windings should be found in this step. $\widehat{B}$ can either be found in the data sheet or by using the value of P_{sp} found in step 4 combined with the graph of the core losses in the data sheet of the material or the equation describing the core losses of the material. The P_{sp} and the frequency is used in the equation and to read the flux density of the graph. The general loss equation is given in 5.1 on page 28 and graphs of the losses for the ferrite material N27 is given in Figure 5.1 on page 28 and Figure 5.1 on page 28. The value of $\widehat{B}$ for the material N27 is given in the data sheet to be approximately 200mT for a P_{sp} of 44 kW/m^3. By using this figures found in the data sheet, it is assumed that there are no significant difference in the P_{sp} for 25 kHz compared to 10 kHz.

To calculate the primary windings Equation 5.17 is used. $\omega = 2\pi f$ and the frequency is given as input parameter. The peak primary voltage $\widehat{V}$ can be calculated using Equation 5.18 and A_{core} can be found in Table 5.4 on the previous page.

$$\widehat{V}_{pri} = N_{pri}A_{core}\omega\widehat{B}_{core} \Rightarrow N_{pri} = \frac{\widehat{V}_{pri}}{\widehat{B}_{core}A_{core}\omega} = \underline{48} \tag{5.17}$$

$$\widehat{V}_{pri} = \sqrt{2}V_{pri} = \underline{1838,48V} \tag{5.18}$$

After founding the numbers of primary turns the number of secondary turns can easily be calculated using Equation 5.19.

$$N_{sec} = \frac{N_{pri}}{n} = \underline{48} \tag{5.19}$$

Step 6: Conductor size

In step 6 the conductor sizes should be calculated. If Litz wires are used, the eddy current losses can be neglected and the copper area of the primary windings $A_{Cu,pri}$ and of the secondary windings $A_{Cu,sec}$ can be found using Equation 5.20 and 5.21.

$$A_{Cu,pri} = \frac{k_{Cu}A_w}{2N_{pri}} = \underline{12,82mm^2} \tag{5.20}$$

$$A_{Cu,sec} = \frac{k_{Cu}A_w}{2N_{sec}} = \underline{12,82mm^2} \tag{5.21}$$

If round wires or foils are used, the copper areas should be calculated but the dimension of the conductors should also be found. Figure 5.12 on the next page can be used to decide how many layers of windings there should be per section of windings. Φ in the figure can be calculated using Equation 5.22 where δ is the skin depth, h is the effective hight of the conductor and F_l is the copper layer factor which indicates the ratio between the copper and the insulation in the wires. For foils or rectangular wires the effective hight is the real hight, but for round wires the effective hight $h = \sqrt{\frac{\pi}{4}}d$ where d is the conductor diameter. F_l is normally assumed to be 0.9 for foils. Using Equation 5.2 on page 29 and the values in Table 5.5 to calculate the skin depth for a frequency of 10 kHz gives δ = 0.66 mm.

Property	**Value**
`Magnetic permeability of copper` μ_r $[kgm/(s^2A^2)]$`:`	1
`Conductivity of copper` σ $[S/m]$`:`	$5,84 * 10^7$
`Density of copper` ρ $[g/cm^3]$`:`	8,96

Table 5.5: Copper properties[6]

$$\Phi = \frac{\sqrt{F_l}h}{\delta} \tag{5.22}$$

$$h = \frac{A_{Cu,pri}}{F_l H_w} \tag{5.23}$$

To decide the number of layers and number of sections, an iterative procedure has to be used [5]. First it is assumed that there are one section of primary and one section of secondary windings and that every layer consists of only one single turn. The procedure has to be carried out for both of the windings. The layer thickness of the primary windings h is 0.1582 mm calculated by using Equation 5.23 and normalized primary conductor thickness Φ is 0.2279 given by Equation 5.22. By using the value of Φ to get the number of layers from Figure 5.12 on the next page it seems like the calculated Φ is higher than the optimal Φ for 48 layers from the figure. This means that

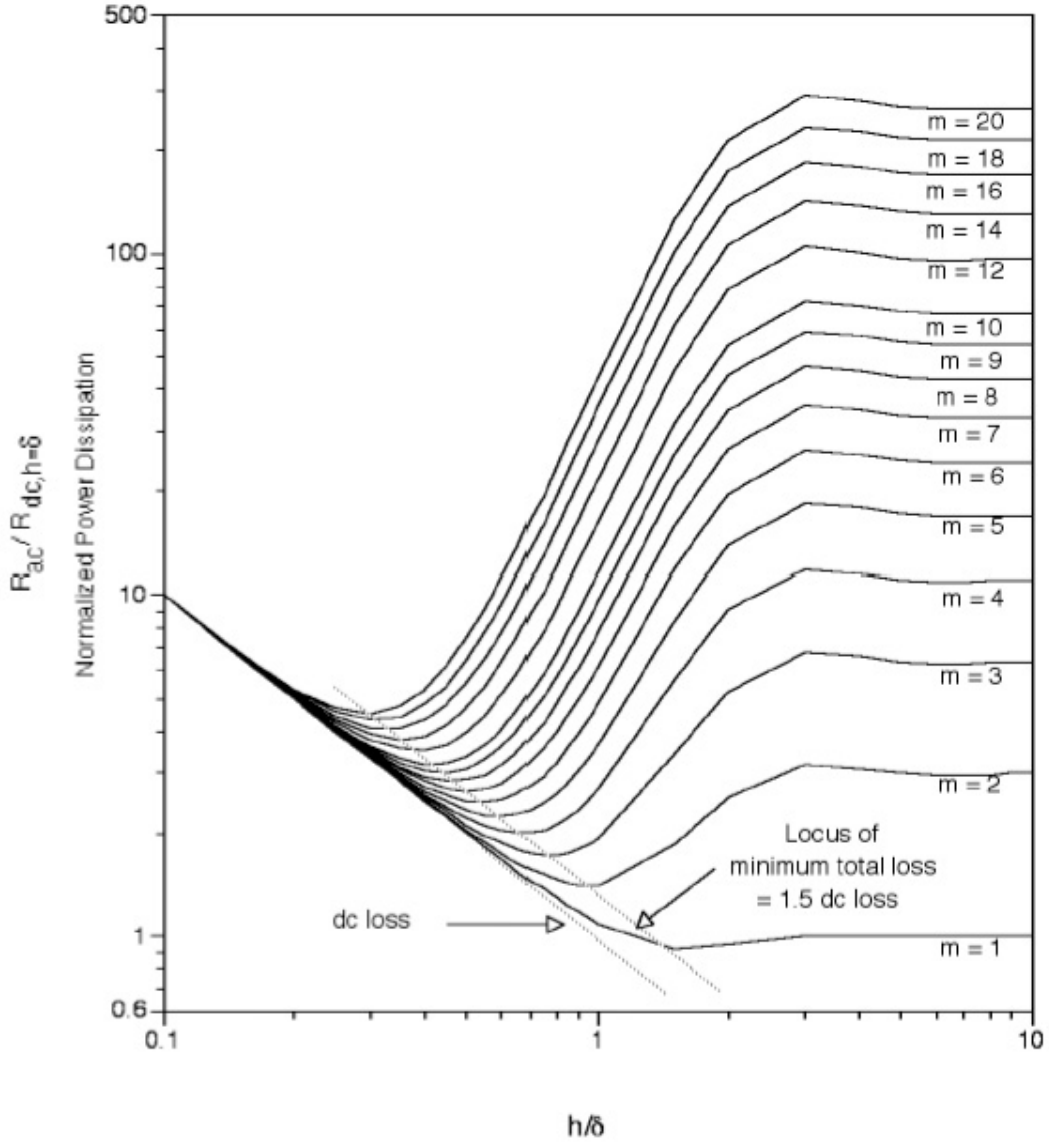

Figure 5.12: Power dissipation in a winding section vs. Φ for different numbers of layers m [5]

the primary windings should be split. The same value of h and Φ are also valid for the secondary windings.

Since the primary windings need to be split, the primary windings are split in two sections and the secondary is sandwiched between, see Figure 5.13. The secondary winding section has to be considered as two sections. The number of layers of the primary sections is then 24 layers with one turn and the secondary is 2 times 24 layers with one turn each. From the figure it can be seen that the optimal Φ for 24 layers is approximately 0.3. This is over 20% higher than the calculated value of Φ of 0.22.

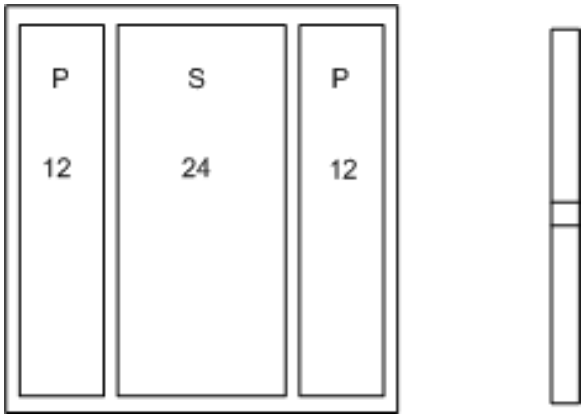

Figure 5.13: The split transformer windings (left) and the layer with two conductors (right)

Since the value of the optimal Φ is higher than the calculated one, it might be better to increase the number of turns per layer, Figure 5.13. By increasing the number of turns per layer to two for the primary winding, h is 0.3165 mm and Φ is 0.4557. Comparing the calculated value of Φ to the optimal one for 12 layers, Φ is 0.4, shows that the calculated one is less than 20% higher than the optimal one. This means that the hight of the conductor foils are 4.5 cm and the thickness is 0.3165 mm and it will be the same when it comes to the secondary windings.

Step 7: Leakage inductance

The leakage inductance should be calculated using Equation 5.24 to see if it is below the maximum allowable value. By splitting the windings the leakage inductance is reduced. By using the Excel sheet for the calculation of the steps, the leakage inductance and the windings can be calculated at the same time. Since the transformer should be near converters, the leakage inductance should be made small. The value of leakage inductance L_{leak} will be 34.18 μH.

$$L_{leak} = \frac{\mu_0 (N_{pri})^2 l_w b_w}{3 h_w} = \mu_0 (N_{pri})^2 1.05a = \underline{34.18\mu H} \tag{5.24}$$

To further decrease the leakage inductance the winding sections can be split into more sections

in combination with more turns per layer. By doing this it will be more difficult to wind the windings on the bobbin and there will be a trade-off between these to criteria.

Step 8: Maximum V-A rating

The apparent power rating of the transformer should be calculated using Equation 5.12 on page 39. The value should be compared to the V-A rating of the transformer. This is done by using the Excel sheet in step 3 to decide the right dimensions of the core.

The losses for the proposed design are calculated as explained in Section 5.5 on page 34. The winding losses are 49 W and the core losses are 54 W. The total losses will then be 103 W. The weight of the transformer using the permeability of the N27 material, 4800 kg/m^3, as given in the data sheet, is 15.9 kg.

CHAPTER 6

SIMULATION MODEL AND SWITCHING PATTERN

6.1 PSCAD simulation model

To be able to test the proposed converter topology a model has to be built. A model of the wind turbine is made in PSCAD to simulate the losses in the converters. The model consists of the components from the generator connected to the rotor of the wind turbine to the converter connected to the DC collection grid in the offshore wind park. The DC collection grid is modelled as a DC voltage source with a resistance and a large capacitor in parallel. The voltage source and the resistance are implemented as a Single Phase Voltage Source Model 2 from the Master Library in PSCAD. The values used in the model are found in Appendix B on page 69. The lowest possible DC voltage at the DC bus needed to get the desired square wave voltage output of the H-bridge is calculated in Appendix B on page 69. By assuming the transformer to be ideal with turn ratio 1:1, the DC value of the DC grid is found to be 1.02 kV. When this is implemented in the model the output voltage of the H-bridge will not be 1.3 kV. This might be due to the blanking time implemented in the switching of the H-bridge, because when a blanking time is used a voltage drop will occur [5].

As can be seen from Figure 6.1 on the next page the system also consists of a wind generator, bidirectional converter, high frequency transformer and a DC/AC converter (H-bridge). The wind generator in the model is a squirrel cage induction machine with an Explicit Interface. The machine parameters are from Vestas 750 kVA (660 kW) wind generator given in Appendix B on page 69 [29]. The mutual saturation and the leakage saturation are not allowed for, i.e. are set to disable in the model. The two-state switch named Spd_Trq in Figure 6.1 on the next page is the starter for the wind turbine. In on-position, corresponding to 1, the generator gets power to magnetize the windings. In off-position, corresponding to 0, the generator delivers power to the grid. When the switch is pointing toward Spd in the control panel the switch is in on-position. The machine will then rotate with the speed given as input parameter W. The switch must be switched manually over to torque (off) position by clicking on the switch in the control panel after the initial transients of the generator reaches steady-state. In torque position the machine will rotate at a speed calculated based on the machine inertia, damping, the input torque T, given as an input parameter, and the output torque.

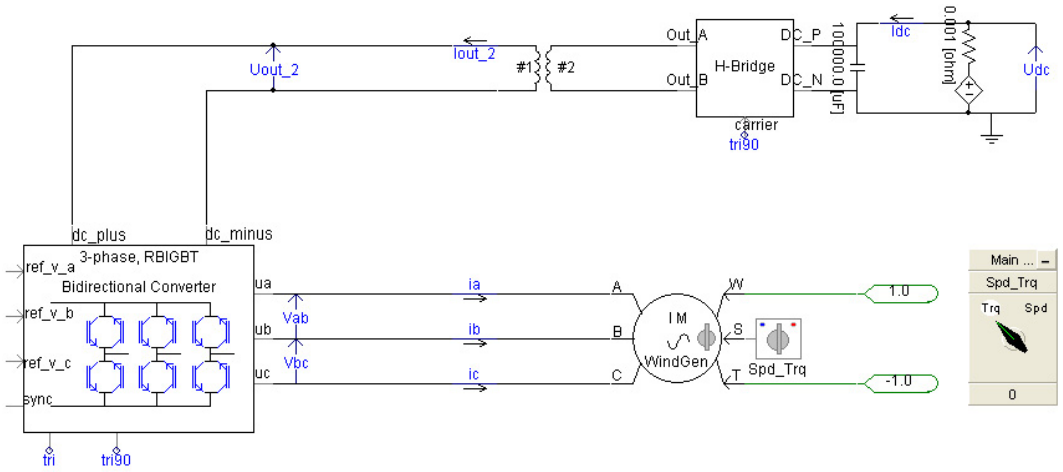

Figure 6.1: The PSCAD model of the system

The transformer in the model is a single phase two winding transformer with a rated power of 0.75 MVA. The frequency is 10 kHz because that is the switching frequency of the converters which leads to the frequency of the square wave voltage in the transformer. The rated voltage is 1.3 kV for both windings which is the calculated output of the bidirectional converter. As mentioned in Chapter 5 on page 27 every high frequency high power transformer is designed for a specific system. Therefore it is not easy to find parameters to use for the simulation model. PSCAD suggests some parameters which are used in the model for the rest of the parameters needed to do the simulation. See Appendix B on page 69 for a list of the used parameters.

The bidirectional converter has three legs each with two switches. The switches consists of two RB-IGBTs in anti parallel. The values for the switches are the standard values in PSCAD given in Table B.2 on page 70 in Appendix B on page 69. The switches are controlled by using the switching pattern described in Section 6.2 on the facing page.

The full-bridge converter, also called H-bridge, has two legs with two switches. The switches consist of one IGBT and one diode in anti parallel. The parameters used for the diodes and the IGBTs in the converter are the standard one suggested by PSCAD, Appendix B on page 69. Each switch gets a control signal from the control system, 1 for ON and 0 for OFF. They are controlled by using a PWM square wave switching scheme.

To simulate the losses in the converter a simulation file programmed in C is implemented in the model. This file uses the equations from Section 4.3 on page 21 to calculate the losses for the switch. As can be seen in Figure 6.2 on the next page there are two ampere meters, Iup and Idn, to measure the current flowing in and out of one switch and a volt meter, Ea, to measure the voltage over the switch. The voltage and current is measured every time step and is used for the calculation performed by the C-program.

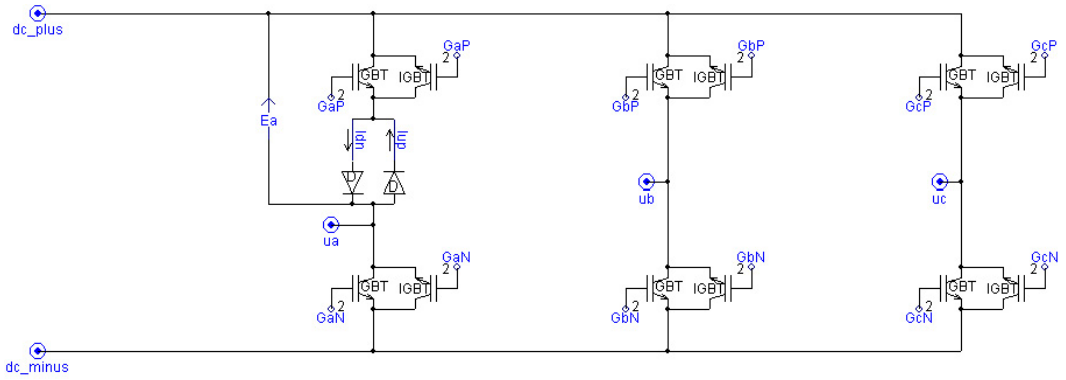

Figure 6.2: The PSCAD model of the one-phase AC-three-phase AC converter with loss measurements

6.2 Switching pattern

The bidirectional converter uses a new switching pattern for the switching of the RB-IGBT switches. Considering the switching of the two switches in one leg, the upper and the lower switch will never be on at the same time. When the upper one is on, i.e. the control signal to the switch is 1, the lower one will be off, control signal 0, and vice versa. The violet curve, number three from the top in Figure 6.4 on page 49, shows when the upper switch is on and off with a DC input into the converter. This switching control can be obtained by using a switching technique called Pulse Width Modulation (PWM). This technique can be explained by looking at the second graph from the top in Figure 6.4 on page 49 and only considering the upper one of the two blue lines (made up of dark and light blue pieces). This blue line is actually a sinusoidal reference signal for one leg or phase (50 Hz) and will decide the frequency of the output. The green triangular signal is called a carrier and it decides the frequency with which the switches are switched. Since this carrier has a frequency of 10 kHz, the sinusoidal reference signal can be considered as a straight line for small time intervals as in Figure 6.4 on page 49. When the sinusoidal reference signal is higher than the carrier signal the upper switch of the phase leg will be turned on and the lower switch will be turned off. They will remain on and off until the reference signal is lower than the carrier signal. At that moment the upper switch turns off and the lower one turns on, until the reference signal again is higher than the carrier signal. This leads to a positive output of the leg when the upper one is on and a negative output when the lower one is on, as the yellow curve, fourth one from the top, in Figure 6.4 on page 49.

The orange curve at the top of Figure 6.4 on page 49 shows the square wave voltage input to the converter from the transformer. To obtain the sinusoidal output as required for the converter the switches need to be switch oppositely for the negative period of the square wave input as for the positive period. Considering the upper switch S1 in the a-phase leg the red curve, second one from the bottom in Figure 6.4 on page 49 shows how the switch is switched. In the beginning the upper connection point P in Figure 6.3 on the next page is positive and the lower connection point N is negative. S1 is ON connecting the a-phase to the positive P-pole. Then after a while

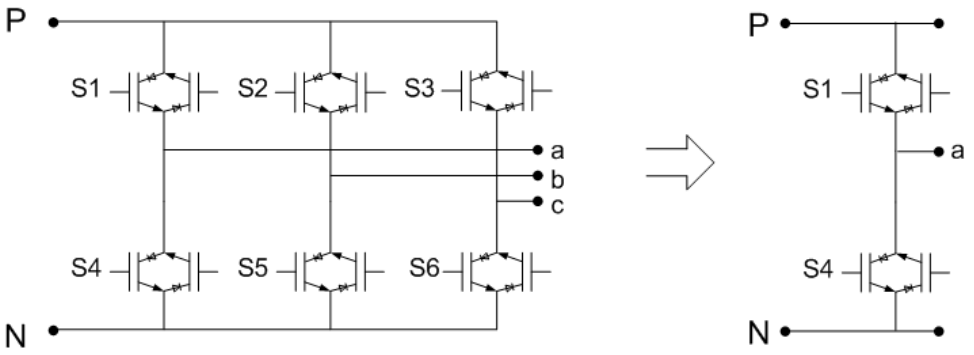

Figure 6.3: AC-AC converter leg analysed in Figure 6.4 on the facing page

S1 is turned OFF and the lower one S4 is turned ON.

The lower switch then connects the a-phase to the negative N-pole. Since the voltage between P and N is a square wave the polarity of P becomes negative after a while, and the polarity of N becomes positive. Phase a still has to be negative so S1 is turned ON and S4 OFF since P now is negative and N is positive. To get a positive output on phase a in this period, the lower switch S4 will have to be turned ON and the upper switch OFF. The square wave will then enter a period where P again becomes positive and N negative. This switching pattern is the pattern that would have given the desired output.

With the dedicated switching pattern, a sinusoidal output can be achieved with less number of switching sequences. The sinusoidal reference signal is inverted for half of the carrier period, the dark blue curve, second from the top in Figure 6.4 on the facing page. Using this blue reference signal and the green carrier for the PWM switching technique, the upper switch will be ON and OFF as shown in the brown curve at the bottom in Figure 6.4 on the next page. In the beginning the switch is ON because the blue reference signal is above the green carrier signal. Almost at the end of the first half period, the positive one of the input, the switch is turned OFF due to higher carrier than reference signal. For the negative half of the input period, the reference is inverted and remains below the carrier for a longer time than if it where not inverted. The switch will be turned ON before the second positive half period of the input begins. The reference signal in this positive half period is not inverted and the switch will remain ON until the reference signal again is below the carrier signal and so forth.

6.3 Simulation results

With the dedicated switching pattern the number of times switched each period is reduced. The red and brown patterns, the second one and the one at the bottom in Figure 6.4 on the facing page, gives the switching sequence of one switch with the virtual pattern and the dedicated pattern. Considering these patterns, the brown one shows that the number of times switched per switch is halved, from four times to two. This is important at high voltage levels because of slower

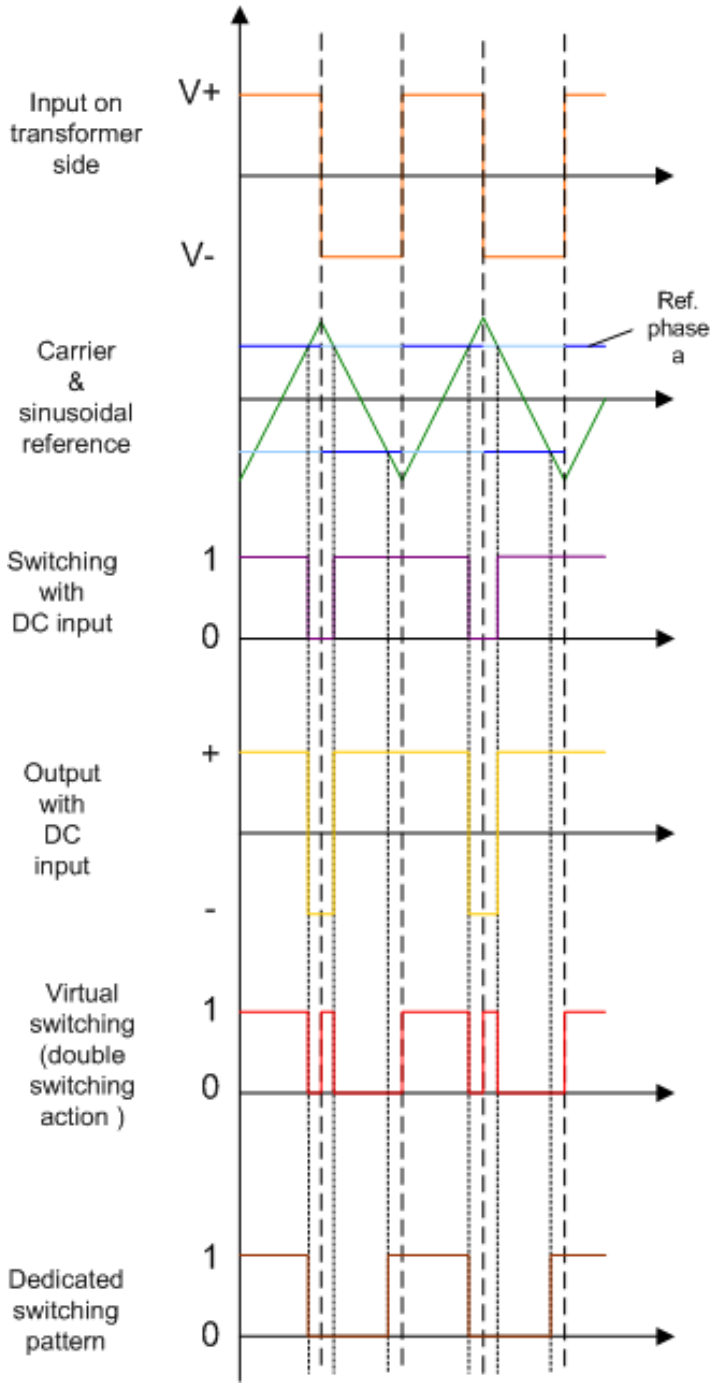

Figure 6.4: Switching technique

devices, due to longer delay time. By reducing the number of times switched, the switching losses are reduced and this results in less converter losses.

In the simulation model the dedicated switching pattern is used for the bidirectional converter. The triangular carrier signal (10 kHz) and a sinusoidal reference signal for one phase (50 Hz) is shown in the top of Figure 6.5. As can be seen from the figure, the sinusoidal reference signal is inverted for half of the carrier signal period which is 100 μs. There is one sinusoidal reference signal for each phase just delayed with 120° and 240°. By using this technique there will always be three switches on at any instant of time. The square wave voltage, U_{out} in Figure 6.5, is the input to the converter on the transformer side. Figure 6.6 on the next page shows the output phase-to-phase voltage V_{ab} from the converter. This voltage is the voltage between the a-phase leg and the b-phase leg in the converter in Figure 6.6 on the facing page. By using filters this will result in a sinusoidal output voltage.

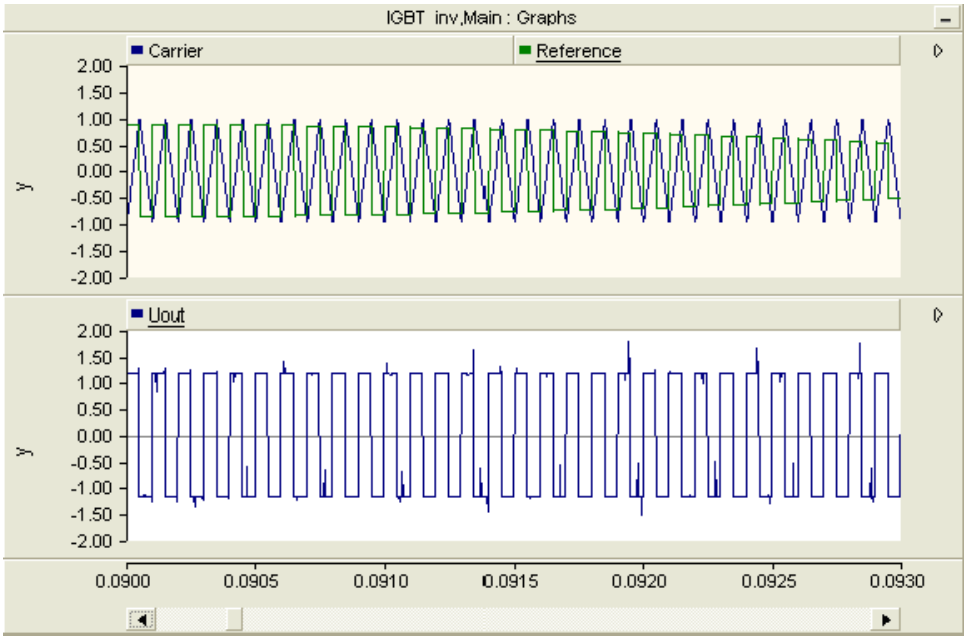

Figure 6.5: Switching pattern, top: sinusoudal reference for one phase, bottom: output voltage on transformer side

By assuming that the RB-IGBT has the same forward V-I characteristics and the same switching loss curves as a normal IGBT, the loss curves can be seen in Figure 6.7 on the next page and Figure 6.8 on page 52. The numbers implemented in the model is taken from the data sheet of SEMIKRON's SEMITRANS 4. The blue curves in Figure 6.8 on page 52 are the conduction losses and the green peaks are the switching losses. The green peak on the left side of the conduction losses is the turn-on losses and the green one on the right side is the turn-off losses. The maximum value of the conduction losses 0.01 W is too small to be seen in Figure 6.7 on the facing page.

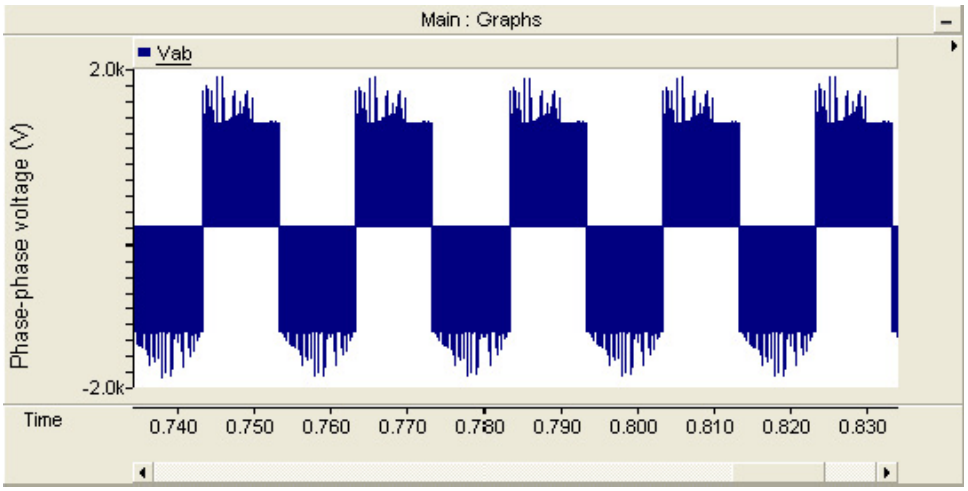

Figure 6.6: Phase-to-phase voltage output on generator side

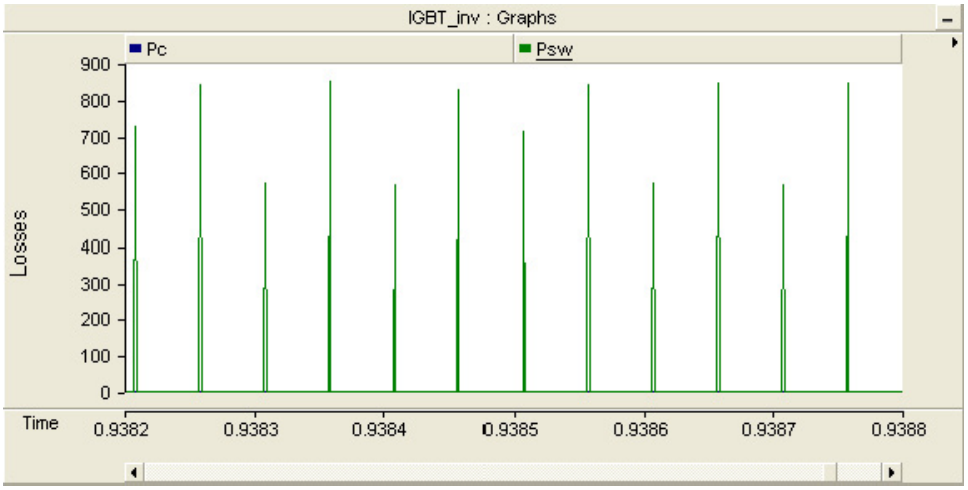

Figure 6.7: Switching losses for one switch in the converter

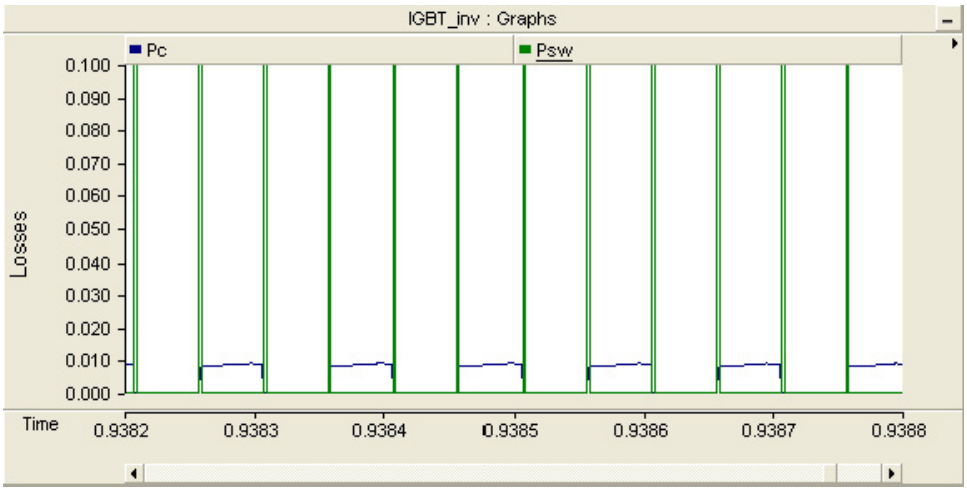

Figure 6.8: Conduction and switching losses for one switch in the converter

CHAPTER 7

DISCUSSION

7.1 Wind parks

The different types of collection networks for wind parks have both advantages and disadvantages. A series connected wind farm is to prefer due to no transformer substation, but the economical risk at faults in the cables or turbines will be higher than with parallel or radial connected turbines[30]. When the turbines are connected in series the economical consequences of a cable fault is much larger than if they were connected in parallel. In parallel, only the single turbine which is connected to the cable with a fault needs to be disconnected. If the fault is on the cable from the cluster to the connecting point, only this cluster needs to be disconnected. Therefore there will always be some wind turbines producing, even though there are faulty cables in the park.

For the series connected wind turbines in Figure 2.4 on page 6, there need to be some extra cables connecting different parts of the park together to prevent the whole park from being disconnected during cable faults. If a fault arises, the current will need another path to flow, so extra cable connections have to be connected to keep the park running. Where and how many of these extra cables to install in the offshore collection grid, will be a trade off between installation cost of the cables and the lost revenue due to lost turbine production during fault and post-fault period. If series connected wind turbines are connected in clusters, the risk will be decreased. Since the clusters will be connected in parallel, the cluster with the faulty cable can be disconnected and the rest of the park can still be running.

With a radial network the loss of production due to cable faults depend on where the fault on the cable is located. If it is located near the substation, all the turbines connected to the faulty cable will be disconnected. If it is located between some of the turbines, the turbines between the substation and the fault will still be able to continue production.

If a turbine fault arises in a series connected wind park, i.e. a turbine must be disconnected, there should be switchgears disconnecting the turbine, but allowing the rest of the turbines to produce power. To obtain the same voltage across the turbines, the remaining turbines have to increase their production accordingly by the transformer turns ratio or the transmission voltage will decrease. This voltage increase in the turbines can be avoided if the turbines are connected in clusters. Then the cluster with the faulty turbine can be disconnected and the rest of the

clusters can still be in operation.

There should also be switchgears for turbine disconnection in a radial park allowing the rest of the turbines in the radial to continue production. For the parallel connected turbines, there is only one turbine connected to one cable, so the other turbines are not affected of the faulty one.

If there is a fault in the main transmission cables to shore, the whole park will be shut down independent of the layout. The only possibility to still deliver power to shore during such faults is to install extra cables. Independent of the layout, a cable fault always leads to a decrease in revenue due to lower production.

7.2 Converter topologies

Considering the converter topologies, i.e. the conventional one and the proposed one, some important differences are worth noticing. In the proposed one on the top in Figure 7.1 there will be three steps of conversion, 3-phase AC-1-phase AC, transformer (AC-AC) and AC-DC. As seen from the bottom in Figure 7.1, there will be four steps in the conventional converter topology, AC-DC, DC-AC, transformer (AC-AC) and AC-DC. One converter less in the proposed topology leads to fewer switches. Fewer switches give less switching losses. This is a great advantage since the converter losses contribute a lot to the total losses. The conventional topology also has a capacitor to smoothen the DC output of the rectifier before it enters the DC-DC converter. A capacitor is normally a heavy component, which is a disadvantage for a wind turbine. For wind turbines, especially floating ones, the weight of the components should be minimized to minimize the counterbalance of the foundation. For the same reason, the new topology has a high frequency (HF) transformer in stead of a medium frequency transformer. Transformers' size and weight is reduced with increasing frequency. Both the reduction in weight and the reduction in switching and ON-state losses are great advantage of the proposed topology.

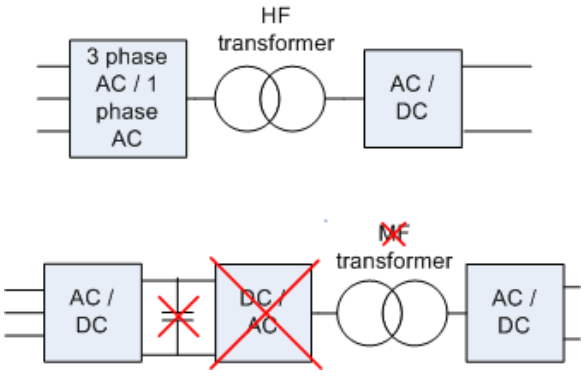

Figure 7.1: Top: proposed converter topology, bottom: conventional converter topology

Frequency	Winding loss [W]	Core loss [W]	Total loss [W]	Weight [kg]
10 kHz	49,07	53,86	102,94	15,9
2 kHz	92,95	102,02	194,98	43,8

Table 7.1: Losses and weight at different frequencies

7.3 Transformer design

A transformer with the dimensions calculated in Chapter 5 on page 27 can not be found as a standard component. If the transformer with these dimensions and the ferrite material N27 should be built, it has to be made of more components put together. By putting together four U-cores the right size may be able to realize. According to [31] there will then be some problems with heat accumulation and the manufacturing process.

By decreasing the frequency to 2 kHz the losses will increase and the weight will be more than double. The flux density is assumed to be the same for the to frequencies, but the size has been increased as can be seen in Table 7.1. For a frequency of 2 kHz amorphous alloys might be better suited as core material. As mentioned previous alloys give eddy current losses, but the amorphous alloys are made for higher frequencies than the normal alloys. The amorphous alloys also have higher flux density which makes the size smaller, according to Equation 5.11 on page 38. The density of an amorphous alloys has to be found in the data sheet because it consists of many different elements. Since iron is on of the main component it can be assumed to have a density about 7-8 g/cm^3. Comparing this to the ferrite material N27 which has a density of 4800 kg/m^3, the decrease in size might not give a significant weight reduction after all. Design using amorphous alloys should be carried out to be able to compare the weight and losses.

CHAPTER 8

CONCLUSION AND FURTHER WORK

8.1 Conclusion

In this thesis a new converter topology for large offshore wind parks have been explained and compared with a conventional one. A thorough investigation of a high frequency high power transformer, a RB-IGBT switch and the losses in a one-phase AC to three-phase AC converter is carried out. These components are important parts of the proposed converter topology for offshore wind park.

The wind turbines are connected in series and directly connected to shore without any transformer stages. Since the voltage across the series connected wind turbines are high enough to be transmitted directly, offshore transformer substations are unnecessary. The risk of such a series connected park has to be considered and a trade off between extra cable installations and lost revenue at cable faults is unavoidable. The new converter topology consists of fewer converter stages than the conventional topology. With one converter less the converter system has fewer switches and less switching losses come in to being. This is important because the converter losses are a great contributor to the total losses in the entire wind park. The proposed converter topology does not include a heavy capacitor and the transformer is smaller due to higher frequency. This is a weight reduction which is important to achieve for floating wind turbines.

The RB-IGBT is compared to other bidirectional switches made of IGBTs and diodes in anti parallel. Compared to the normal IGBT/diode module the on-state voltage drop is halved. The on-state losses is also reduced due to the lack of the diode and since a RB-IGBT has the same on-state voltage drop as a normal IGBT. The architecture of the RB-IGBT is almost the same as the IGBT. The only difference is that the chip edges need to be separated from the active region of the chip to prevent the leakage current from the side surface of the device. This can be done by different techniques but the most common one is to extend the extra p^+ layer on the edges to reach all the way up to the gate isolation.

The losses in the one-phase AC to three-phase AC converter is calculated based on the behavior of the RB-IGBT found in the data sheet of the switch. The conduction losses, reverse recovery losses, turn-on and turn-off losses for one switch is calculated and multiplied with the number of switches in the converter. An equation of the total losses is given and there are performed loss simulations for the converter in PSCAD with good results.

By introducing a new switching pattern the switching frequency is halved. The sinusoidal reference signal for the PWM switching is inverted for half of the carrier period. With a square wave input to the converter, a visual switching pattern is obtained by inverting the switching sequences for half of the carrier period. With the new pattern number of times switched is halved compared to the visual switching.

A design of a high power high frequency transformer is proposed. The core of the transformer is made of the ferrite material N27 and the windings are made of copper foil. A model is made in Excel to calculate the needed values for the design procedure. The shape of the core is a double E-core with a centre leg of 4.5 cm. The primary windings will be separated in two sections each section having 12 layers with two turns per layer. The secondary windings will be sandwiched between the primary sections and will consist of 24 layers with two turns per layers. Each conductor will have a hight of 4.5 cm and a thickness of 0.3165 mm. By decreasing the frequency the weight will increase.

The wind farm topology which is newly proposed is based on series connection of turbines connected to shore with DC cables. The topology is without offshore substation which makes it better suited for offshore parks. The reliability of the park during faults is a concern which has to be further investigated.

On the basis of the mentioned weight reduction and the layout without offshore substation, the proposed topology might be better suited for the large offshore wind parks. The reduction of switches, reduction of times switched with the new pattern and the new RB-IGBT reduce the converter losses which is the great contributor to the total losses in the electrical system.

8.2 Further work

This thesis is just the beginning of an extensive study of offshore wind parks at the Norwegian University of Science and Technology. There are a lot of interesting topics for further investigation. Both the converter topology and the whole park need to be investigated. Here are some suggestions for the further studies:

- Simulations in PSCAD of a model with a generator with the characteristics of a real wind turbine
- Further investigation and development of a prototype of the high frequency transformer
- Development of prototype, implementation of switching pattern and loss measurements
- Simulations of the whole wind park and its connection to the onshore grid during operation and faults, especially when one turbine is disconnected.

Bibliography

[1] P. Bresesti, W. L. Kling, R. L. Hendriks, and R. Vailati. HVDC connection of Offshore Wind Farms to the Transmission System. *IEEE Transactions of Energy Conversion*, 22(1):37–43, 2007.

[2] S. Lundberg. Evaluation of wind farm layouts. *NORPIE*, 2004.

[3] Jun ichi Itoh, T. Iida, and A. Odaka. Realization of High Efficiency AC link Converter System based on AC/AC Direct Concersion Techniques with RB-IGBT. *IEEE*, pages 1703–1708, 2006.

[4] EPCOS. *Data book Ferrites and Accessories*. Epcos AG, 2007.

[5] Ned Mohan, Tore M. Undeland, and William P. Robbins. *Power Electronics – Converters, Application and Design*. John Wiley & Sons, INC. 3rd ed., 2003.

[6] Gordon Aylward and Tristan Findlay. *SI Chemical Data*. John Wiley & Sons Australia, Ltd. 5rd ed., 2002.

[7] A. R. Henderson, C. Morgan, B. Smith, H. Sørensen, R. J. Barthelmie, and B. Boesmans. Offshore Wind Energy in Europe - A Review of the State-of-the-Art. *ELSEVIER, Science Direct*, 2003.

[8] V. G. Agelidis and C. Mademlis. Technology of Offshore Wind Turbines and Farms and Novel Multilevel Converter-based HVDC Systems for Their Grid Connections. *Wind Energy*, 26(6):383–395, 2002.

[9] N. Barberis Negra, J. Todorovic, and T. Ackermann. Loss evaluation of HVAC and HVDC transmission solutions for large offshore wind farms. *ELSEVIER Electric Power System Research, Science Direct*, (76):916–927, 2005.

[10] OffshoreCenterDanmark. Offshore wind farms. Online. Available: http://www.offshorecenter.dk/OffshoreWindFarms/.

[11] T. Ackermann. Transmission Systems for offshore Wind Farms. *IEEE Power Engineering Review*, pages 23–27, 2002.

[12] Lena Max. *Energy Evaluation for DC/DC Converters in DC based Wind Farms*. PhD thesis, Chalmers University of Technology, Sweden, 2007.

[13] S. Meier and P.C. Kjær. Benchmark of Annual Energy Production for Different Wind Farm Topologies. *IEEE 0-7803-9033-4*, pages 2073 – 2080, 2005.

[14] M. J. Bland, P. W. Wheeler, J. C. Clare, and L. Empringham. Comparison of Bi–directional Switch Components for Direct AC–AC Converters. *35th Annual IEEE Power Electronics Specialists Conference*, pages 2905–2909, 2004.

[15] Christian Klumpner and Frede Blaabjerg. Using Reverse–Blocking IGBTs in Power Converters for Adjustable–Speed Drives. *IEEE Transactions on Industry Applications*, 42(3):807–816, 2006.

[16] M. Takei, T. Naito, and K. Ueno. The Reverse Blocking IGBT for Matrix Converter With Ultra-Thin Wafer Technology. *IEEE 15th International Symposium on Power Semiconductor Devices and ICs*, pages 156 – 159, 2003.

[17] A. Lindemann. A New IGBT with Reverse Blocking Capability. *EPE 2001, Graz*, 2001.

[18] H. Kapels and D. Drücke. Optimized device concepts for reverse blocking IGBTs. *ISPSD*, pages 148–151, 2003.

[19] Jun ichi Itoh, April 2008. Conversation at Nagaoka University of Technology, Japan.

[20] M. Takei, Y. Harada, and K. Ueno. 600V–IGBT with Reverse Blocking Capability. *International Symposium on Power Semiconductor Devices and ICs*, pages 413–416, 2001.

[21] T. Naito, M. Takei, M. Nemoto, T. Hayashi, and K. Ueno. 1200V Reverse Blocking IGBT with low losses for Matrix Converter. *International Symposium on Power Semiconductor Devices and ICs*, pages 125–128, 2004.

[22] Shuyun Jia, K. J. Tseng, and Xiao Wang. Study on Reverse Recovery Characteristics of Reverse-Blocking IGBT Applied in Matrix Converter. *IEEE*, pages 1917–1921, 2005.

[23] Fumihiro Hayashi, April 2008. Conversation at Nagaoka University of Technology, Japan.

[24] Neeltran. High frequency transformer. Online. Available: http://www.neeltran.com/hf_trns.htm.

[25] M.H. Kheraluwala, D.W. Novotny, and D.M. Divan. Coaxially Wound Transformers for High-Power High-Frequency Applications. *IEEE Transactions on Power Electronics*, 7(1):54–62, 1992.

[26] Nagai Shin ichiro from Pony Electric, April 2008. Conversation at Nagaoka University of Technology, Japan.

[27] Colonel Wm. T. McLyman. *Transformer and inductor design handbook*. Marcel Dekker INC, 1978.

[28] Arne Nysveen, May 2008. Conversation at NTNU.

[29] J. A. Suul. Use of standard frequency converters in power plants and Wind power and preproject to master thesis: Pumped-storage power plant with variable rotational speed(in

norwegian). Technical report, Norwegian University of Science and Technology (NTNU), 2004.

[30] J. Pechey, P. Taylor, R. Dixon, M. Lawson, and A. Dinning. The Role of Medium Voltage Electrical System Design in Risk Management for Offshore Wind farms. *Wind Engineering*, 28(5):489–502, 2004.

[31] Andre Büttner, June 2008. Conversation at NORPIE 2008.

Appendices

APPENDIX A

TRANSFORMER DESIGN

A.1 Design program on CD

In Figure A.1 the main file of the transformer design program is shown. The design input of the transformer is inserted and the output is shown. The upper limit of the primary and secondary voltage of 1000 V is reached and the current is adjusted to see if the required power of 50 kVA is reached. As can be seen in the figure, the power is not reached. This is the device with the highest power rating available using N27 material. The other lines in the design output in the figure show that there are no design using this shape which suite the specified input parameters.

Design Inputs

kcu	Ta (°C)	Ts (°C)	Freq. [kHz]	Material	Vpri,rms	Ipri,rms	Vsec,rms	Isec,rms	Throughput Power	δ [cm]
0,67	40	100	10	N27	1000	10,5	1000	10,50	21000	0,07462875

Design Outputs

Core Type	Core #	V-A Rating [watts]	Jrms [A/mm²]	Bac [mT]	Npri [#]	Nsec [#]	Acu,pri [mm²]	Acu,sec [mm²]	Skin, Prox. Effects?	Vc+Vw [cm³]	[nH] Lleakage	Efficiency [%]
E-core	#N/A	0	#N/A	#N/A	#N/A	#N/A	#N/A	#N/A	#N/A	#N/A	#N/A	#N/A
EC-core	#N/A	0	#N/A	#N/A	#N/A	#N/A	#N/A	#N/A	#N/A	#N/A	#N/A	#N/A
EFD-core	#N/A	0	#N/A	#N/A	#N/A	#N/A	#N/A	#N/A	#N/A	#N/A	#N/A	#N/A
EP-core	#N/A	0	#N/A	#N/A	#N/A	#N/A	#N/A	#N/A	#N/A	#N/A	#N/A	#N/A
ER-core	#N/A	0	#N/A	#N/A	#N/A	#N/A	#N/A	#N/A	#N/A	#N/A	#N/A	#N/A
ETD-core	#N/A	0	#N/A	#N/A	#N/A	#N/A	#N/A	#N/A	#N/A	#N/A	#N/A	#N/A
PM-core	PM 114/93	21199	1,6	200	65	65	6,70	6,70	YES	899	26613	99,69 %
Potcore	#N/A	0	#N/A	#N/A	#N/A	#N/A	#N/A	#N/A	#N/A	#N/A	#N/A	#N/A
PQ-core	#N/A	0	#N/A	#N/A	#N/A	#N/A	#N/A	#N/A	#N/A	#N/A	#N/A	#N/A
RM-I core	#N/A	0	#N/A	#N/A	#N/A	#N/A	#N/A	#N/A	#N/A	#N/A	#N/A	#N/A
U-core	#N/A	0	#N/A	#N/A	#N/A	#N/A	#N/A	#N/A	#N/A	#N/A	#N/A	#N/A

Notes

Any row having a cell entry of #N/A indicates that the core in that row cannot meet the input specifications.

Figure A.1: Excel program for transformer design with the highest possible design using N27

The input parameters are kept the same and different materials a chosen to see if anyone is better than the N27. There are no materials that give a high enough V-A rating. The highest one is U-cores with the material 3C94. The rating is then 34 413 VA, as can be seen in Figure A.2.

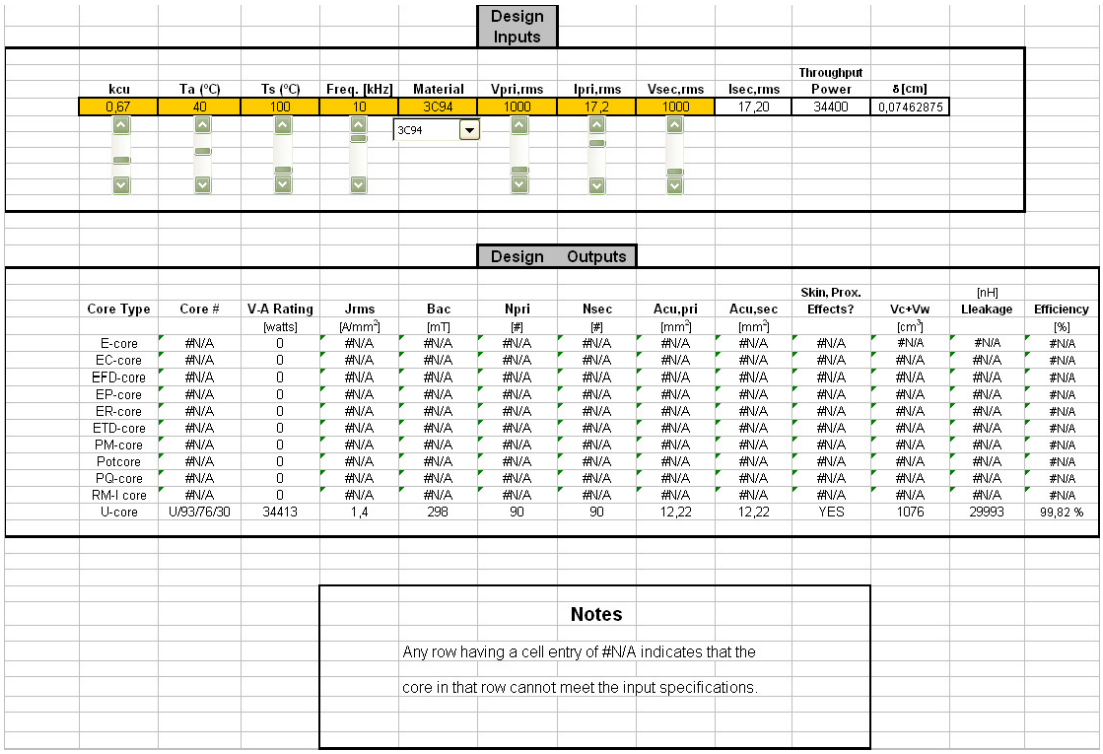

Design Inputs

kcu	Ta (°C)	Ts (°C)	Freq. [kHz]	Material	Vpri,rms	Ipri,rms	Vsec,rms	Isec,rms	Throughput Power	δ [cm]
0,67	40	100	10	3C94	1000	17,2	1000	17,20	34400	0,07462875

Design Outputs

Core Type	Core #	V-A Rating	Jrms	Bac	Npri	Nsec	Acu,pri	Acu,sec	Skin, Prox. Effects?	Vc+Vw	[nH] Lleakage	Efficiency
		[watts]	[A/mm²]	[mT]	[#]	[#]	[mm²]	[mm²]		[cm³]		[%]
E-core	#N/A	0	#N/A	#N/A	#N/A	#N/A	#N/A	#N/A	#N/A	#N/A	#N/A	#N/A
EC-core	#N/A	0	#N/A	#N/A	#N/A	#N/A	#N/A	#N/A	#N/A	#N/A	#N/A	#N/A
EFD-core	#N/A	0	#N/A	#N/A	#N/A	#N/A	#N/A	#N/A	#N/A	#N/A	#N/A	#N/A
EP-core	#N/A	0	#N/A	#N/A	#N/A	#N/A	#N/A	#N/A	#N/A	#N/A	#N/A	#N/A
ER-core	#N/A	0	#N/A	#N/A	#N/A	#N/A	#N/A	#N/A	#N/A	#N/A	#N/A	#N/A
ETD-core	#N/A	0	#N/A	#N/A	#N/A	#N/A	#N/A	#N/A	#N/A	#N/A	#N/A	#N/A
PM-core	#N/A	0	#N/A	#N/A	#N/A	#N/A	#N/A	#N/A	#N/A	#N/A	#N/A	#N/A
Potcore	#N/A	0	#N/A	#N/A	#N/A	#N/A	#N/A	#N/A	#N/A	#N/A	#N/A	#N/A
PQ-core	#N/A	0	#N/A	#N/A	#N/A	#N/A	#N/A	#N/A	#N/A	#N/A	#N/A	#N/A
RM-I core	#N/A	0	#N/A	#N/A	#N/A	#N/A	#N/A	#N/A	#N/A	#N/A	#N/A	#N/A
U-core	U/93/76/30	34413	1,4	298	90	90	12,22	12,22	YES	1076	29993	99,82 %

Notes

Any row having a cell entry of #N/A indicates that the core in that row cannot meet the input specifications.

Figure A.2: Transformer design output with 3C94 material

A.2 Excel sheet for transformer design

Figure A.3 on the next page shows the part where the input and the constants are given in the Excel sheet for the transformer design. The input column is where the electrical characteristics from the converter circuit are given. The constant column is constants and material properties. The decision column is parameters needed to do the calculations and are either constants found in books or read from graphs. Figure A.4 on page 68 shows the steps used in the method to design the transformer.

Transformer design

Step 1: INPUT				**Constants:**	
Primary current, Ipri [A]:	38,462			μ0 [H/m]	1,26E-06
Primary voltage, Vpri [V]:	1300			π	3,14
Frequency, f [Hz]:	10000			Magnetic permeability of copper [kg*m/(s^2*A^2)]:	1
Transformer turns ratio, n:	1			Conductivity of copper σ [S/m]:	5,84E+07
Maximum body temperature, Ts [°C | K]:	100	373		Density of copper [g/cm^3]:	8,96
Ambient temperature, Ta [°C | K]:	40	313			
Decisions:					
Core size, a [cm]:	4,5				
Fill factor, kCu [Litz=0.3, round=0.5, foil=0.6]:	0,6				
Bpeak from data sheet [T]:	0,200				
Number of interfaces between windings sections:	2				
Current density [A/mm^2]:	3				

Figure A.3: Input part of the Excel sheet made for transformer design

Step 2: Volt-Ampere rating				
Volt-ampere rating, S [VA]:	50000,6			
Step 3: Core material, shape and size				
Core dimensions:	cm	m		
ba [cm | m]:	4,50	0,0450		
d [cm | m]:	6,75	0,0675		
ha [cm | m]:	11,25	0,1125		
bw [cm | m]:	3,15	0,0315		
hw [cm | m]:	9,00	0,0900		
Acore [cm^2 | m^2]:	30,38	0,0030		
Vcore [cm^3 | m^3]:	1230,19	0,0012		
Aw [cm^2 | m^2]:	28,35	0,0028		
Vw [cm^3 | m^3]:	1120,84	0,0011		
AP [cm^4]:	861,13			
A [cm^2 | m^2]:	1206,90	0,1207		
dvert [cm | m]:	15,75	0,1575		
lw [cm | m]:	40,50	0,4050		
Step 4: Rθsa and Psp				
Radiative heat transfer resistance, Rrad [°C/W]:	0,9989			
Convective heat transfer resistance, Rcon [°C/W]:	1,3996			
Rθsa [°C/W]:	0,5829			
Psp [mW/cm^3]:	43,7840			
Step 5: Core flux density and number of turns				
Flux density peak, Bpeak [T]:	0,200			
Primary voltage peak, Vpeak [V]:	1838,48			
Number of primary windings, Npri [-]:	48,19	48		
Number of secondary windings, Nsec [-]:	48,19	48		
Step 6: Copper area of foils				
Copper area of primary windings, Acu,pri [mm^2 | m^2]:	12,82	1,28E-05		
Copper area of secondary windings, Acu,sec [mm^2 | m^2]:	12,82	1,28E-05		
Figure 30-19:				
Skin depth δ [m | mm]:	0,000659	0,66		
Layer thickness primary windings, hp [mm]:	0,15828			
Normalized primary conductor thickness Φ:	0,227884			
Layer thickness secondary windings, hs [mm]:	0,15828			
Normalized secondary conductor thickness Φ:	0,227884			
Hw	4,5			
h	0,31656			
Φ	0,455767			
Step 7: Leakage inductance				
Leakage inductance, Lleak [H | µH]:	3,42E-05	34,18		
Step 8: Smax vs. S				
Current density, Jrms [A/mm^2 | A/m^2]:	3,00	3000000,00		Smax should be
Smax:	68821,61			higher than S
S:	50000,60			which leads to a
Difference:	18821,01			positive difference.

Figure A.4: Calculation step part of the transformer design

APPENDIX B

SIMULATION PARAMETERS

To calculate the lowest possible DC voltage at the DC bus needed to get the desired square wave voltage output of the H-bridge Equation B.1 is used [5].

$$\widehat{V_{square}} = \frac{4}{\pi} V_d = 1.273 V_d \tag{B.1}$$

The desired square wave voltage is found by using Equations B.2, B.3, B.4, and B.5. Equation B.2 calculates the amplitude modulation ratio for the bidirectional converter by dividing the amplitude of the sinusoidal reference signal by the amplitude of the carrier signal. The values are found from the graph in the PSCAD model.

$$m_a = \frac{\widehat{V_{ref}}}{\widehat{V_{car}}} = \frac{0.867}{0.960} = 0.903 \tag{B.2}$$

The peak value of the fundamental-frequency component in one of the converter legs is given by B.3 where V_d is the amplitude of the square wave output. The line to line voltage $V_L L$ on the generator side of the converter is given by B.4.

$$\widehat{V_{AN}} = m_a \frac{V_d}{2} \tag{B.3}$$

$$V_{LL} = \frac{\sqrt{3}}{\sqrt{2}} \widehat{V_{AN}} = 0.612 m_a V_d \tag{B.4}$$

By reversal of Equation B.4 the amplitude of the square wave output is given by Equation B.5 and calculated to be about 1.3 kV. The line-to-line voltage of the generator is given by B.6 and the phase voltage is found in Table B.3 on page 71 in Appendix B.

$$V_d = \frac{V_{LL}}{0.612 m_a} = \frac{690}{0.612 * 0.903} = 1249V \approx 1.3kV \tag{B.5}$$

$$V_{LL,rms} = \sqrt{3} V_{ph,rms} = \sqrt{3} * 398 = 690V \tag{B.6}$$

DC link parameter	**Value**
Capacitor	$100mF$
Single phase voltage source	
Source impedance	Resistive
Grounded	No
Resistance	0.001Ω
Voltage	$1.3kV$
Ramp up time	$0.01sec$

Table B.1: DC link data

Power Electronic Switch	**Value**
Thyristor On Resistance	0.001Ω
Thyristor Off Resistance	$1.0E6\Omega$
Forward Voltage Drop	0
Forward Breakover Voltage	$1.0E5kV$
Reverse Withstand Voltage	$1.0E5kV$
Minimum Extinction Time	0

Table B.2: Semiconductor device data

$$\frac{V_1}{N_1} = \frac{V_2}{N_2} \tag{B.7}$$

The transformer is assumed to be ideal with turn ratio 1:1. Then Equation B.7 gives $V1 = V2$ and the amplitude of the square wave voltage output of the H-bridge will also be 1.3 kV. Using this value in B.1 on the previous page the DC value of the DC grid is found to be 1.02 kV.

In Table B.1 the parameters used in the DC link in the simulation model can be found. As generator a squirrel cage induction motor is used. In the induction motor an Explicit Interface with machine parameters from Vestas 750 kVA (660 kW) wind generator are used. These parameters are listed in Table B.3 on the next page. The mutual saturation and the leakage saturation are not allowed for, i.e. are set to disable in the model. For the transformer the parameters in the model are found in Table B.4 on the facing page. The frequency of 10 kHz is decided by the switching frequency of the converters. The winding voltages are calculated and the power rating is given by the generator. For the switches in the converters in the model, each IGBT and diode has the parameters as listed in Table B.2. These values are suggested by PSCAD.

Input parameter	**Value**
W	1
T	-1
S (from switch Spd_Trq)	1/0
Machine parameter	
Rated RMS Phase Voltage	0.398 kV
Rated RMS Phase Current	0.628 kA
Base Angular Frequency	314,149 p.u.
Stator Resistance	0.0092 p.u.
First Cage Resistance	0.0076 p.u.
Second Cage Resistance	10 p.u.
Stator Unsaturated Leakage Current	0.1580 p.u.
Unsaturated Magnetizing Reactance	3.8693 p.u.
Rotor Unsaturated Mutual Reactance	0.0651 p.u.
Second cage Unsaturated	10 p.u.
Polar Moment of Inertia (J=2H)	2.0 MW/MVA
Mechanical Damping	0.008 p.u.

Table B.3: Induction machine parameters

Transformer parameter	**Value**
Transformer MVA	$0.75MVA$
Base Operation Frequency	$10kHz$
Leakage Reactance	$0.01p.u.$
No Load Losses	$0p.u.$
Copper Losses	$0p.u.$
Winding 1 Voltage RMS	$1.3kV$
Winding 2 Voltage RMS	$1.3kV$
Saturation	No
Air Core Reactance	$0.2p.u.$
Inrush Decay Time Current	$1.0sec$
Knee Voltage	$1.25p.u.$
Time to Release Flux Clipping	$0.1sec$
Magnetizing Current	1%

Table B.4: Transformer data

APPENDIX C

CONFERENCE PAPERS

During the work with this master thesis an article with the title ”Power Collection and Integration on the Electric Grid from Offshore Wind Parks" has been written for the Nordic Workshop on Power and Industrial Electronics 2008 (NORPIE 2008). The conference is held in Helsinki, Finland in June 2008. There is also written an abstract for the IEEE Industrial Electronics Society’s conference IECON 2008 in Orlando, Florida, USA in November 2008. The title of the article is ”A power conversion system for offshore wind parks". Both of the articles can be found below.

Power Collection and Integration on the Electric Grid from Offshore Wind Parks

Anne Berit Mogstad, Marta Molinas
Norwegian University of Science and Technology
Department of Electric Power Engineering, Trondheim, Norway

Corresponding author: Anne Berit Mogstad
O.S. Bragstad plass 2E, 7491 Trondheim, Norway
Tel.: +47 7359 3796
Fax: +47 7359 4279
mogstad@stud.ntnu.no

***Abstract*—There is a lot of potential in offshore wind parks due to the amount of available area. The parks get bigger in size and will continue to grow in the future. In this article a new converter topology for offshore wind parks is proposed. This topology is meant to be for large offshore wind parks sited far from shore and it is based on DC collection and transmission. All the converters are located in the nacelle of the wind turbines and the turbines are connected in series directly connected to shore without any transformation stages. The electrical system, from the generator to the grid connection of the turbine, is modeled in PSCAD. The model consists of an induction machine, a 3-phase AC to 1-phase AC converter, a high frequency high power transformer and a full-bridge converter. The AC-AC converter has a new type of reverse-blocking IGBTs and the switches are controlled with a dedicated switching pattern. The simulations show that the switching pattern gives the expected square wave voltage from the AC-AC converter. The new converter topology reduces the converter losses due to fewer converter stages, the architecture of the reverse-blocking IGBT and the new switching pattern.**

***Index Terms*—Bidirectional/AC-AC converter, reverse-blocking IGBT, offshore wind parks, HVDC, switching pattern AC-AC converter, high frequency transformer**

I. Introduction

The existing offshore wind parks are connected to the onshore grid with high voltage AC (HVAC) cables. They are not located far from shore, and the maximum size in operation is 166 MW [1]. In future, the size of offshore wind parks will increase and the distance to shore will be longer. In HVAC cables there will be generated reactive current due to high capacitance which reduces the active current-carrying capacity. This leads to limitations of the length of the cable without compensation devices [2]. According to [3] HVAC systems lead to the lowest transmission losses for distances up to 55-70 km depending on the size of the wind parks. For longer distances high voltage DC (HVDC) transmission has the lowest losses, as shown in Fig.1. The figure is based on an average wind speed of 9 m/s. In the figure the blue line indicates the border between AC and line commutated converter (LCC) HVDC transmission. The dashed red lines show the percentage loss variation.

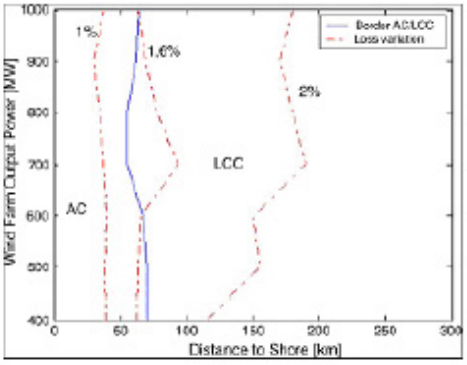

Fig. 1. Comparison of LCC HVDC and HVAC transmission for different wind park sizes and distances to shore for an average wind speed of 9 m/s [3]

Today there are two different HVDC link types, line commutated converter (LCC) HVDC and voltage source converter (VSC) HVDC. The LCC is cheaper than the VSC solution [2] but has a large offshore substation required for the converters and the auxiliary equipment. Because of the PWM technique used in VSC, this technology requires fewer auxiliary filters than the LCC technology. There is no need for switchable AC harmonic filters for reactive power control in VSC technology, because the converters are able to control reactive power in both ends of the cable. VSC converter stations take only half of the area of an LCC transmission station [4] but the price for the total VSC HVDC offshore substations can be about 10 times higher than an AC substation [5]. One disadvantage with the VSC is the high switching losses which leads to higher power losses (3.5 % at full load) than LCC (1.5 %) [4]. The need for large offshore substations and auxiliary equipment makes LCC not so well suited for large scale offshore wind parks.

Despite of heavy transformers at line frequency, heavy capacitors and converter losses VSC is a promising technology.

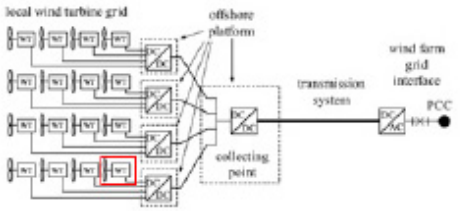

Fig. 2. Parallel connected wind turbines with offshore substations as presented in [7]

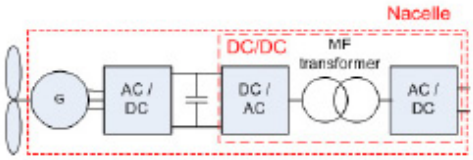

Fig. 3. Conventional converter topology in the nacelle of the turbine as of [7]

The purpose of this article is to illustrate a possible offshore wind park topology made by using the reverse-blocking IGBT type of semiconductor device with a dedicated switching pattern to reduce the converter losses [6].

II. New topology for DC based offshore wind parks

A. The conventional converter topology

One of the previously proposed DC based offshore wind park layouts is the parallel connected turbines with one or more offshore substations, Fig. 2. This layout must have offshore converter stations to raise the voltage before transmission to shore. It is assumed that only one transformer stage is needed if the output voltage of the wind turbine is 20-40 kV[7]. Then the wind turbines will be connected in radials to the collecting point in Fig. 2. With a lower output voltage of the wind turbine, about 5 kV, two transformer stages are needed. The wind turbines will then be divided into clusters and connected one by one to the first transformer stage. Then the clusters will be connected to the collecting point as shown in Fig. 2.

For this type of wind park layout each wind turbine (WT), marked with a red rectangle in Fig. 2, has an AC-DC converter, DC-DC converter and a capacitor between, as shown in Fig. 3. DC-DC converters are also used for the two transformer stages in the layout. The AC-DC converter has either diode or IGBT switches depending on the type of machine used in the wind turbine, synchronous or induction machine. A DC-DC converter consists of one rectifier, one inverter and a medium frequency transformer. In [8] a loss and energy production cost study of different DC/DC converters for DC based offshore wind parks is carried out. Full-bridge converter, single active bridge converter and series parallel resonant converter are compared for the three different sites in the park, resulting in lowest losses for the resonant converter independent of the site. The single active bridge converter resulted in the highest losses, but the full-bridge converter gave slightly higher losses than the resonant converter. The resonant converter has a larger transformer and more IGBT modules than the full-bridge converter, which results in a higher energy production cost for some positions in the grid, even though the losses are lower. This topology also has a capacitor between the two converters to make sure the input to the DC-DC converter is smoothed properly.

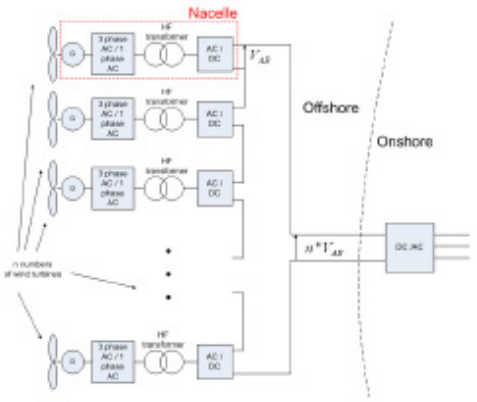

Fig. 4. DC based wind park with proposed converter topology

B. The proposed converter topology

The proposed topology uses only one cable with series connected turbines as the local grid, as can be seen in Fig. 4. Each wind energy conversion unit will consist of a generator, the turbine, a 3-phase AC to 1-phase AC converter, a high frequency (HF) transformer and a 1-phase AC-DC converter. The turbines will be connected to an offshore DC network and the power will be transmitted directly to shore without any transformation stages. This is possible since the turbines are connected in series and the voltage level required for transmission will be obtained by the series connection and/or the turn ratio of the HF transformer. By converting the AC voltage output from the generator to DC voltage directly in the nacelle of each turbine, a wind park layout without offshore substations is made possible [9]. In [10] the similar conversion is proposed, but only the AC-AC converter is placed in the wind turbines. This leads to a square wave voltage collection grid and an offshore substation for the AC-DC converter.

In the proposed topology the DC side of the AC-DC converter of each turbine will be connected in series with the other wind turbines to obtain the required voltage level before the transmission to shore. This is possible through the high frequency transformer. It allows the current from the DC grid to flow through the secondary side of the transformer before entering the AC-DC converter again, but from the AC side. Then the current can continue further to the next wind turbine.

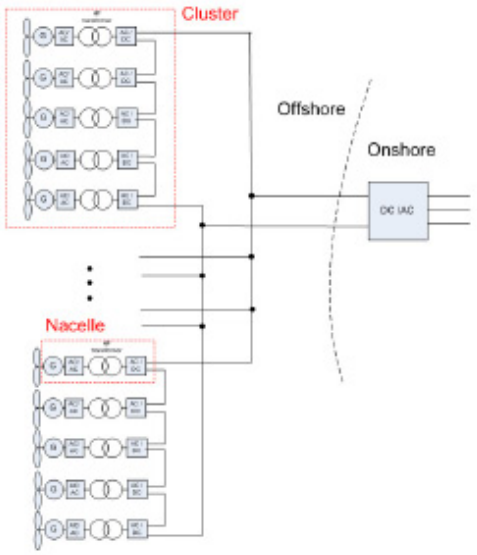

Fig. 5. Series connected wind turbines in clusters

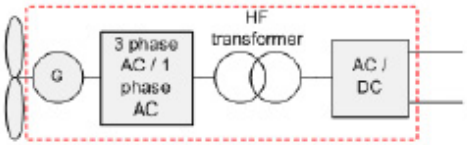

Fig. 6. Wind turbine with proposed topology

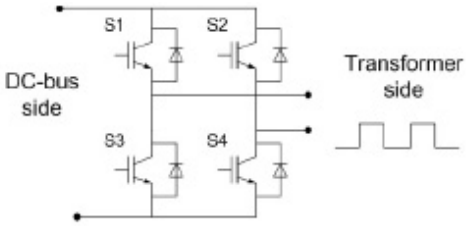

Fig. 7. H-bridge with IGBTs and anti parallel diodes

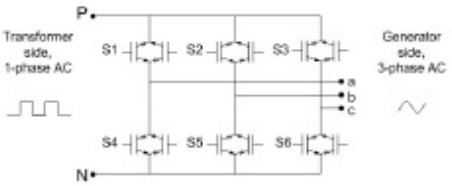

Fig. 8. Bidirectional AC link with new reverse-blocking IGBTs

Another DC based layout option is to connect a few wind turbines in series to make clusters. These clusters will then be connected in parallel to the transmission line, see Fig. 5. By using this layout, the consequences during fault on cables might be less severe. Only the faulty cluster needs to be disconnected and the park can still produce power.

The generator in Fig. 6 is a squirrel cage induction machine with a rated line-to-line voltage of 690 V and a rated power of 750 kVA (660 kW). The future generators will be able to generate more than today, so an output higher than 1000 V and a power rating of up to 10 MW can be assumed as realistic for use in these wind turbines. This leads to fewer turbines needed in series to obtain the required voltage level for transmission and perhaps lower ratio of the transformers.

The AC/DC converter in Fig. 6 is a full-bridge converter, also called an H-bridge, with switching modules consisting of IGBTs and diodes in anti parallel, Fig. 7. The converter has two legs, each with two switches (S1, S3) and (S2, S4), and is able to convert a DC voltage to a square wave voltage and vice versa. By connecting the converter to the DC bus and transformer, as shown in Fig. 7, the required square wave form is obtained when starting the generator. To achieve square wave output when magnetizing the windings a PWM square wave switching scheme is used. The upper switch in one leg and the lower switch in the other are switched simultaneously, when not considering the blanking time. The two switches form a switch pair, i.e. the converter has two switch pairs. The switch pairs are on for a half cycle of the output frequency (10 kHz), i.e. a duty ratio of 0.5.

The 3-phase AC to 1-phase AC converter consists of three legs each with two switches. The switches are a new type of reverse-blocking IGBTs, as can be seen in Fig. 8. They do not have any anti parallel diodes and therefore reduce the converter losses. On the generator side of the converter there will always be an alternating voltage independent of the way the power flows.

1) Proposed high frequency high power transformer: A 1.3 kV and 750 kW transformer is not often made. For a frequency of 10 kHz transformers with power ratings of 100 kW would not be a problem, but with higher power ratings the frequency is normally about 1-2 kHz. The weight will decrease with increasing frequency, but smaller size makes the cooling difficult and that will increase the losses. For the prototype of this system a 50 kW transformer with 10 kHz will be designed.

As material for the cores there are two options, amorphous alloys or ferrite materials. The amorphous alloys have higher saturation flux density than the ferrite materials, which is good for high currents, but the ferrite material has no eddy current losses. The shape of the core could be E, U or toroid. The disadvantages with the toroid cores are that they are difficult to wind and the cooling is also difficult. For the U-core it is possible to separate the secondary and primary windings on to legs, but this will lead to more leakage inductance. It is also possible to wind both windings on one leg. The E-core is easy to use and has low leakage inductance since both of the windings are wound on the center leg. The windings can be wound on a bobbin and then afterward the bobbin is placed

on the core.

For the material of the windings there are two possibilities, copper and aluminium. Copper is the most used one because of the low conduction losses compared to aluminium. Copper is more expensive than aluminium (10 $ to 3 $ per kg) so if aluminium is used it is to reduce the cost. The density of copper is 8.96 g/cm3 and 2.70 g/cm3 for aluminium (both in solid state at room temperature), so aluminium can also be used to reduce the weight of the transformer. Aluminium transformers can be found in airplanes for weight reduction and for other applications if the investment costs should be kept low, but it is very rare. For this application losses are important and should be reduced. Therefore copper windings should be chosen. The shape of the windings can be wire or foil. Foils reduces the skin and proximity effect of the winding. If aluminium where chosen, it would not be a problem to make foils. Since copper is the preferred material due to lower conduction losses, it is more difficult to make foil windings. Copper is not as easy flattened as aluminium.

To reduce the skin effect and proximity effect at high frequencies litz wires are used for frequencies above 100 kHz. Litz wire consists of many small wires individually coated with an insulating film and twisted or woven together. It can also be used for lower frequencies, but the available conducting area is smaller due to many small wires instead of one big one. There will be more unused space in the litz wire compared to the wire with only one copper wire. For high power transformer one copper wire should be used because one wire can cope with higher currents than many individually isolated small ones. It is also more difficult to make thin windings of copper.

For the cooling of transformers with a power rating above 100 kW the best one will be water cooling. The water pipes will take a lot of space when they are wound around the windings and a pump and pipes from the ground are needed. This will give a weight increase and might not be the best alternative for wind turbines. The other option for cooling of transformers is air cooling. To make air cooling possible the core has to be bigger to let the air through.

For the design of the prototype transformer leakage inductances, flux densities and the size of the core and windings should be calculated. Ferrite material should be used for the core and as mentioned the windings should be of copper not aluminium. Even though weight reduction is important for offshore wind turbines, the weight gain will not be so remarkable since more aluminium wires are required to carry the same current as the copper wires.

2) New reverse-blocking IGBT: The reverse-blocking IGBT can form a bidirectional switch without the use of diodes. This leads to a voltage drop reduction of the switch [6]. The same functionality of reverse-blocking IGBTs (RB-IGBTs) can be obtained by two IGBTs with anti parallel diodes in series, left side in Fig. 9. The new reverse-blocking IGBTs do not have the anti parallel diodes as shown in Fig. 9 on the right side. In [11] the new RB-IGBT is used in a AC-AC direct converter resulting in an efficiency increase of 1.9 point compared to a conventional device. As can be seen from Fig. 9, for the switch

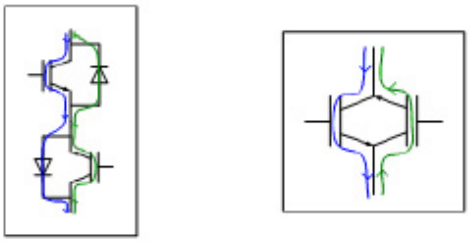

Fig. 9. Bidirectional switches with IGBTs, left: two IGBTs with anti parallel diodes in series, right: new reverse-blocking IGBT

consisting of two IGBT modules in series, the current has to pass through two components independent of the direction of the current flow. Both the current flowing from the top to the bottom of Fig. 9, the blue line, and the current flowing from the bottom to the top, the green line, have to pass through one IGBT and one diode. This would result in more on-state losses than the new RB-IGBT, which has just one component to pass through in both directions. The more components to pass through, the more on-state losses is generated.

C. Converter losses

To calculate the losses in a converter the losses in every switch in the converter need to be calculated. Which losses that will occur in the switches is dependent on which type of semiconductor device that is used. For the controllable devices there are four different types of losses; conduction losses, turn on losses, turn off losses and recovery losses. To calculate these losses the data sheet of the device has to be used. In the AC-AC converter the switches consists of RB-IGBTs. The losses are calculated for one RB-IGBT and multiplied by the total number of devices in the converter. Each switch consists of two RB-IGBTs, so in this case the number is twelve.

The conduction losses are the losses in the semiconductor device when the device is conducting, i.e. in on-state. There will always be some kind of voltage drop in on-state and this voltage drop leads to losses. To calculate the conduction losses for the RB-IGBT the collector current I_C and the gate-emitter voltage V_{GE} has to be known. From the data sheet the curve Collector current vs. Collector-Emitter voltage should give the on-state voltage V_{CE}. By knowing the I_C and V_{GE} the collector-emitter voltage can be found and multiplied with the current 1.

$$P_{cond} = V_{CE} I_C \tag{1}$$

The turn on and turn off losses are the losses connected/involved to the on and off switching of the device. The current and voltage need some time to go back to zero or to increase to max during to turn on and off of the device. These delays will lead to switching losses. To find the switching losses of the RB-IGBT there will be a graph in the data sheet giving the different switching losses, Switching losses vs. Collector current. The collector current I_C has to be known, so

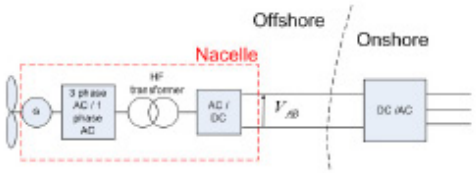

Fig. 10. Model implemented in PSCAD for simulation

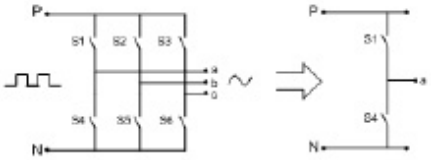

Fig. 11. AC-AC converter leg analysed in Fig.12.

the energy losses for the turn-on, turn-off and recovery losses can easily be found. Since the losses are given in switching energy(J), they have to be converted into power losses(W) with T in 2 as the switching period for the device:

$$P_{loss} = \frac{E_{loss}}{T} \quad (2)$$

The total losses per device will be the sum of all the four losses described above:(total loss of switching frequency period)

$$P_{tot} = P_{condIGBT} + P_{condDiode} + P_{on} + P_{off} + P_{rr} \quad (3)$$

Averaging total losses:

$$P_{totavr} = \int_0^t P_{tot} f_{out} \quad (4)$$

f_{out} is the frequency of the output, not the switching frequency.

III. Simulation system

A. Simulation model

To be able to test the proposed converter topology a model was built. A model of the wind turbine is made in PSCAD to simulate the losses in the converters [9]. The model consists of the components from the generator connected to the rotor of the wind turbine to the converter connected to the DC collection grid in the offshore wind park. The DC collection grid is modelled as a DC voltage source with a resistance and a large capacitor in parallel. As can be seen from Fig. 10 the system also consists of a wind generator, bidirectional converter, high frequency transformer and a DC/AC converter (H-bridge).

The wind generator in the model is a squirrel cage induction machine. The machine parameters are from Vestas 750 kVA (660 kW) wind generator found in [12]. The transformer in the model is a single phase two winding transformer with a rated power of 0.75 MVA. The frequency is 10 kHz because that is the switching frequency of the converters which leads to the frequency of the square wave voltage in the transformer. The rated voltage is 1.3 kV for both windings which is the calculated output of the bidirectional converter. Every high frequency high power transformer is designed for a specific system. Therefore it is not easy to find parameters to use for the simulation model. PSCAD suggests some parameters which are used in the model for the rest of the parameters needed to do the simulation.

The 3-phase AC-1-phase AC converter in Fig. 10 is a bidirectional converter consisting of three legs with two switches, Fig. 8. The switching frequency is 10 kHz and the bidirectional switches are made of two IGBTs of the new type described in II.B.1). The parameters for the IGBTs are the standard PSCAD values for semiconductor devices. The P and N connection points in Fig. 8 are connected to the transformer side and there is always a square wave voltage input from the transformer. Each leg in the converter is connected to one phase on the generator side. The switches are controlled by using a dedicated switching pattern. A triangular carrier signal (10 kHz) is compared to the 3-phase sinusoidal 50 Hz reference signal. The sinusoidal reference signal is inverted for half of the carrier signal period. There is one reference signal for each leg controlling the switching of the two switches in the leg. The reference signals are generated by a control box. The switches in the same leg will never be ON at the same time, but there will always be three switches ON, one from each leg.

The full-bridge converter, also called H-bridge, has two legs with two switches, Fig. 7. The switches consist of one IGBT and one diode in anti parallel. The parameters used for the diodes and the IGBTs in the converter are the standard one suggested by PSCAD. Each switch gets a control signal from the control system, 1 for ON and 0 for OFF.

B. New switching pattern

The bidirectional converter uses a dedicated switching pattern for the switching of the RB-IGBT switches. Considering the switching of the two switches in one leg, see Fig.11, the upper and the lower switch will never be ON at the same time. When the upper one is ON, i.e. the control signal to the switch is 1, the lower one will be OFF, control signal 0, and vice versa. The violet curve, number three from the top in Fig. 12, shows when the upper switch is ON and OFF with a DC input into the converter. This switching control can be obtained by using a switching technique called Pulse Width Modulation (PWM) [13]. This technique can be explained by looking at the second graph from the top in Fig. 12 and only considering the upper one of the two blue lines (made up of dark and light blue pieces). This blue line is actually a sinusoidal reference signal for one leg or phase (50 Hz) and will decide the frequency of the output. The green triangular signal is called a carrier and it decides the frequency with

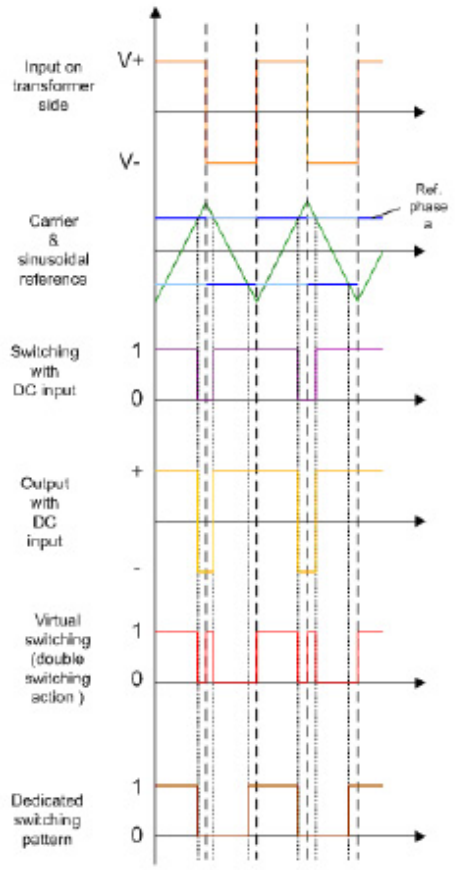

Fig. 12. Dedicated switching pattern for the RB-IGBTs [9]

which the switches are switched. Since this carrier has a frequency of 10 kHz, the sinusoidal reference signal can be considered as a straight line for the small time intervals as in Fig. 12. When the sinusoidal reference signal is higher than the carrier signal the upper switch of the phase leg will be turned ON and the lower switch will be turned OFF. They will remain ON and OFF until the reference signal is lower than the carrier signal. At that moment the upper switch turns OFF and the lower one turns ON, until the reference signal again is higher than the carrier signal. This leads to a positive output of the leg when the upper one is ON and a negative output when the lower one is ON, as the yellow curve, fourth one from the top, in Fig. 12 shows.

The orange curve at the top of Fig. 12 shows the square wave voltage input to the converter from the transformer. To obtain the sinusoidal output as required for the converter the switches need to be switch oppositely for the negative period of the square wave input as for the positive period. Considering the upper switch S1 in the a-phase leg in Fig. 11 the red curve, second one from the bottom in Fig. 12 shows how the switch is switched. In the beginning the P-pole is positive and the N-pole is negative. S1 is ON connecting the a-phase to the positive P-pole. Then after a while S1 is turned OFF and the lower one S4 is turned ON.

The lower switch then connects the a-phase to the negative N-pole. Since the voltage between P and N is a square wave the polarity of P becomes negative after a while, and the polarity of N becomes positive. Phase a still has to be negative so S1 is turned ON and S4 OFF since P now is negative and N is positive. To get a positive output on phase a in this period, the lower switch S4 will have to be turned ON and the upper switch OFF. The square wave will then enter a period where P again becomes positive and N negative. This switching pattern is the pattern that would have given the desired output.

With the dedicated switching pattern, a sinusoidal output can be achieved with less number of switching sequences. The sinusoidal reference signal is inverted for half of the carrier period, the dark blue curve, second from the top in Fig. 12. Using this blue reference signal and the green carrier for the PWM switching technique, the upper switch will be ON and OFF as shown in the brown curve at the bottom in Fig. 12. In the beginning the switch is ON because the blue reference signal is above the green carrier signal. Almost at the end of the first half period, the positive one of the input, the switch is turned OFF due to higher carrier than reference signal. For the negative half of the input period, the reference is inverted and remains below the carrier for a longer time than if it where not inverted. The switch will be turned ON before the second positive half period of the input begins. The reference signal in this positive half period is not inverted and the switch will remain ON until the reference signal again is below the carrier signal and so forth.

C. Simulation results

With the dedicated switching pattern the number of times switched each period is reduced. The red and brown patterns, the second one and the one at the bottom in Fig. 12, gives the switching sequence of one switch with the virtual pattern and the dedicated pattern. Considering these patterns, the brown one shows that the number of times switched per switch is halved, from four times to two. This is important at high voltage levels because of slower devices, due to longer delay time. By reducing the number of times switched, the switching losses are reduced and this results in less converter losses.

In the simulation model the dedicated switching pattern is used for the bidirectional converter. The triangular carrier signal (10 kHz) and a sinusoidal reference signal for one phase (50 Hz) is shown in the top of Fig. 13. As can be seen from the figure, the sinusoidal reference signal is inverted for half of the carrier signal period which is 100 s. There is one sinusoidal reference signal for each phase just delayed with 120° and 240°. By using this technique there will always be three switches on at any instant of time. The square wave voltage, U_{out} in Fig. 13, is the input to the converter on

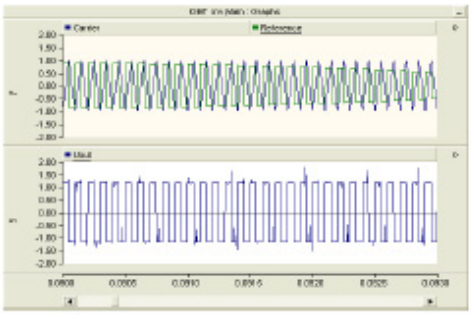

Fig. 13. Switching pattern, top: sinusoidal reference for one phase, bottom: output voltage on transformer side

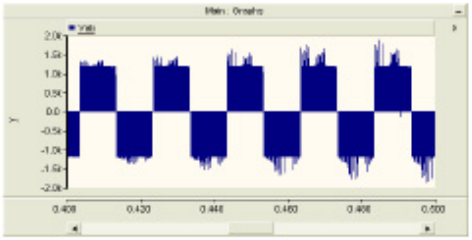

Fig. 14. Phase-to-phase voltage output on generator side

the transformer side. Fig. 14 shows the output phase-to-phase voltage V_{ab} from the converter. This voltage is the voltage between the a-phase leg and the b-phase leg in the converter in Fig. 12. By using filters this will result in a sinusoidal output voltage.

IV. Discussion

A series connected wind farm is to prefer due to no transformer substation, but the reliability at faults in the cables or turbines can be lower than with parallel or radial connected turbines [14]. When the turbines are connected in series the economical consequences of a cable fault is much larger than if they were connected in parallel. In parallel, Fig. 2, only the single turbine which is connected to the cable with a fault needs to be disconnected. If the fault is on the cable from the cluster to the connecting point, only this cluster needs to be disconnected. Therefore there will always be some wind turbines producing, even though there are faulty cables in the park. For the series connected wind turbines in Fig. 4, there need to be some extra cables connecting different parts of the series connected turbines together to prevent the whole park from being disconnected during cable faults. If a fault arises, the current will need another path to flow, so the extra cable connections have to be connected to keep the park running. Where and how many of these extra cables to install in the offshore grid, will be a trade off between installation costs of the cables and the lost revenue due to lost production during fault and post-fault period [14]. This will also be a subject for

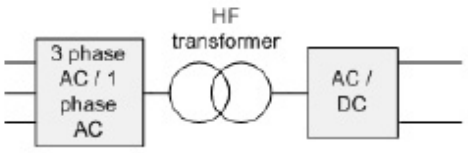

Fig. 15. Proposed converter topology

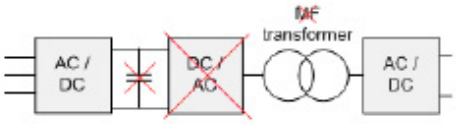

Fig. 16. Conventional converter topology

further investigation.

By connecting a few wind turbines in series in clusters and the clusters in parallel the reliability increases. Now only the faulty cluster needs to be disconnected and the park can still produce some power. With a radial network the loss of production due to turbine disconnection depends on where the fault on the cable is located. If it is located near the connection to the substation, all of the turbines connected to the cable will be disconnected. If it is located between some of the turbines, the turbines between the substation and the fault will still be able to continue production.

If a turbine fault arises in a series connected wind park, i.e. a turbine must be disconnected, there should be switchgears disconnecting the turbine, but allowing the rest of the turbines to produce power. To obtain the same voltage across the turbines, the remaining turbines have to increase their production accordingly. There should also be switchgears allowing turbine disconnection in a radial park so the rest of the turbines in the radial can continue production. For the parallel connected turbines, there is only one turbine connected to one cable, so the other turbines are not affected by the faulty line. If there is a fault in the main transmission cables to shore, the whole park will be shut down independent of the layout. The only possibility to still deliver power to shore during such faults is to install extra cables to shore. Independent of the layout, a cable fault always leads to a decrease in revenue due to lower production.

Considering the converter topologies, i.e. the conventional one and the proposed one, some important differences are worth noticing. In the proposed one in Fig. 15 there will be three steps of conversion, 3-phase AC-1-phase AC, transformer (AC-AC) and AC-DC. As seen from Fig. 16, there will be four steps in the conventional converter topology, AC-DC, DC-AC, transformer (AC-AC) and AC-DC. One converter less in the proposed topology leads to fewer switches. Fewer switches give less switching losses. This is a great advantage since the converter losses contribute a lot to the total losses.

The conventional topology also has a capacitor to smoothen the DC output of the rectifier before it enters the DC-DC converter. A capacitor is normally a heavy component, which is a disadvantage for a wind turbine. For wind turbines, especially floating ones, the weight of the components should be minimized to minimize the counterbalance of the foundation. For the same reason, the new topology has a high frequency (HF) transformer in stead of a medium frequency transformer. Transformers' size and weight is reduced with increasing frequency. Both the reduction in weight and the reduction in switching and ON-state losses are great advantage of the proposed topology.

V. Conclusion/Further work

In this paper a new converter topology for large offshore wind parks has been presented, explained and compared with a conventional one. A PSCAD model of the converter topology is explained and results described. The turbines are connected in series and directly connected to shore without any transformer stages. Since the voltage across the series connected wind turbines are high enough to be transmitted directly, offshore transformer substations are unnecessary. The risk of such a series connected park has to be considered and a trade off between extra cable installations and lost revenue at cable faults is unavoidable. The new topology with a 3-phase AC to 1-phase AC converter, a HF transformer and a full-bridge converter, consists of fewer converter stages than the conventional topology. With one converter less the converter system has fewer switches and less switching and ON-state losses come in to being. This is important because the converter losses are a great contributor to the total losses in the entire wind park. The proposed converter topology does not include a heavy capacitor and the transformer is smaller due to higher frequency. This is a weight reduction which is important to achieve for floating wind turbines.

The switches used for the AC-AC converter are a new type of reverse-blocking IGBT. This switch replaces the series connected IGBTs with anti parallel diodes. By using this new reverse-blocking IGBT without the anti parallel diode, the on-state losses are reduced due to fewer devices for the current to pass through. By introducing the dedicated switching pattern the number of switching actions is reduced. Compared to the virtual pattern the number of times is halved.

On the basis of the mentioned weight reduction and the no offshore substation, the proposed topology might be better suited for the large offshore wind parks. The reduction of switches, reduction of times switched with the new pattern and the new RB-IGBT reduce the converter losses which is the great contributor to the total losses in the electrical system.

The study of this offshore wind park topology has just started. The converter topology and its work in the whole system need to be further investigated. The switching pattern and the switch need to be tested and simulated to document good results. Some further tasks to prove the results of this report:

- Simulations in PSCAD of a model with a generator with the characteristics of a real wind turbine
- Design of the high frequency transformer
- Loss calculations and simulations in PSCAD for the switches and the total converter system
- Development of prototype, implementation of switching pattern and loss measurements
- Simulations of the whole wind park and its connection to the onshore grid during operation and faults, especially when one turbine is disconnected.

References

[1] OffshoreCenterDanmark, "Offshore wind farms," Online, available: http://www.offshorecenter.dk/OffshoreWindFarms/.

[2] P. Bresesti, W. L. Kling, R. L. Hendriks, and R. Vailati, "HVDC connection of Offshore Wind Farms to the Transmission System," *IEEE Transactions of Energy Conversion*, vol. 22, no. 1, pp. 37–43, 2007.

[3] N. B. Negra, J. Todorovic, and T. Ackermann, "Loss evaluation of HVAC and HVDC transmission solutions for large offshore wind farms," *ELSEVIER Electric Power System Research, Science Direct*, no. 76, pp. 916–927, 2005.

[4] L. Xu and B. Andersen, "Grid Connection of Large Offshore Wind Farms Using HVDC," *Wind Energy*, no. 9, pp. 371–383, 2006.

[5] T. Ackermann, "Transmission Systems for offshore Wind Farms," *IEEE Power Engineering Review*, pp. 23–27, 2002.

[6] M. Takei, T. Naito, and K. Ueno, "The Reverse Blocking IGBT for Matrix Converter With Ultra-Thin Wafer Technology," *IEEE 15th International Symposium on Power Semiconductor Devices and ICs*, pp. 156 – 159, 2003.

[7] S. Lundberg, "Evaluation of wind farm layouts," *NORPIE*, 2004.

[8] L. Max, "Energy Evaluation for DC/DC Converters in DC based Wind Farms," Chalmers University of Technology, Sweden, Licentiate dissertation, 2007.

[9] A. B. Mogstad, "New switching pattern for AC/AC converters with RB-IGBTs for offshore wind parks," Norwegian University of Science and Technology (NTNU), Tech. Rep., 2007.

[10] S. Meier and P. Kjr, "Benchmark of Annual Energy Production for Different Wind Farm Topologies," *IEEE 0-7803-9033-4*, pp. 2073–2080, 2005.

[11] J. ichi Itoh, T. Iida, and A. Odaka, "Realization of High Efficiency AC link Converter System based on AC/AC Direct Conversion Techniques with RB-IGBT," *IEEE*, pp. 1703–1708, 2006.

[12] J. A. Suul, "Use of standard frequency converters in power plants and Wind power and preproject to master thesis: Pumped-storage power plant with variable rotational speed(in norwegian)." Norwegian University of Science and Technology (NTNU), Tech. Rep., 2004.

[13] N. Mohan, T. M. Undeland, and W. P. Robbins, *Power Electronics – Converters, Application and Design*. John Wiley & Sons, INC. 3rd ed., 2003.

[14] J. Pechey, P. Taylor, R. Dixon, M. Lawson, and A. Dinning, "The Role of Medium Voltage Electrical System Design in Risk Management for Offshore Wind farms," *Wind Engineering*, vol. 28, no. 5, pp. 489–502, 2004.

A power conversion system for offshore wind parks

Anne Berit Mogstad, Marta Molinas, Paal Keim Olsen, Robert Nilssen
Norwegian University of Science and Technology
Department of Electric Power Engineering, Trondheim, Norway

Corresponding author: Anne Berit Mogstad
O.S. Bragstad plass 2E, 7491 Trondheim, Norway
Tel.: +47 7359 3796
Fax: +47 7359 4279
mogstad@stud.ntnu.no

Abstract—**This article presents a power conversion system for offshore wind parks based on a high voltage generation, high frequency AC link with bidirectional switches and DC power collection and transmission to shore. All the converters are located in the nacelle of the wind turbines and the turbines are connected in series on the output side of the AC/DC converter and connected to shore without any further transformation stages. The electrical system, from the generator to the grid connection of the turbine, is modeled in PSCAD. The model consists of an induction machine, a 3-phase AC to 1-phase AC converter, a high frequency high power transformer and a full-bridge converter. The AC-AC converter is based on bidirectional switches with reverse-blocking IGBTs and the switches are controlled with a dedicated switching pattern. The simulations show that the switching pattern gives the expected square wave voltage from the AC-AC converter. The new converter topology reduces the converter losses due to fewer converter stages, the architecture of the reverse-blocking IGBT and the new switching pattern.**

Index Terms—**Bidirectional/AC-AC converter, reverse-blocking IGBT, offshore wind parks, HVDC, switching pattern AC-AC converter, high frequency transformer**

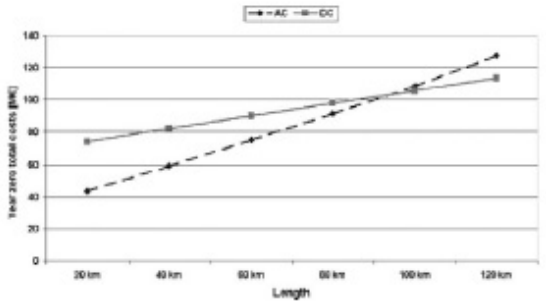

Fig. 1. Economic results of sensitivity analysis for different transmission lengths of AC and DC transmission [2]

I. Introduction

The existing offshore wind parks are connected to the onshore grid with high voltage AC (HVAC) cables. They are not located far from shore, and the maximum size in operation is 166 MW [1]. In future, the size of offshore wind parks will increase and the distance to shore will be longer. In HVAC cables there will be generated reactive current due to high capacitance which reduces the active current-carrying capacity. This leads to limitations of the length of the cable without compensation devices [2]. According to [3] HVAC systems lead to the lowest transmission losses for distances up to 55-70 km depending on the size of the wind parks. For longer distances high voltage DC (HVDC) transmission has the lowest losses. HVDC also gives the lowest year zero total costs for distances above 90 km, as can be seen in Fig. 1 [2]. Fig. 1 shows the year zero total cost of AC and DC transmission for different transmission lengths. The costs considered in [2] are the cost of cable installation and protection, the cost of converter stations and the losses in the converter stations.

Today there are two different HVDC link types, line commutated converter (LCC) HVDC and voltage source converter (VSC) HVDC. The LCC is cheaper than the VSC solution [2] but has a large offshore substation required for the converters and the auxiliary equipment. Because of the PWM technique used in VSC, this technology requires fewer auxiliary filters than the LCC technology. There is no need for switchable AC harmonic filters for reactive power control in VSC technology, because the converters are able to control reactive power in both ends of the cable. VSC converter stations take only half of the area of an LCC transmission station [4] but the price for the total VSC HVDC offshore substations can be about 10 times higher than an AC substation [5]. One disadvantage with the VSC is the high switching losses which leads to higher power losses (3.5 % at full load) than LCC (1.5 %) [4]. The need for large offshore substations and auxiliary equipment makes LCC not so well suited for large scale offshore wind parks. Despite of heavy transformers at line frequency, heavy capacitors and converter losses VSC is a promising technology.

The purpose of this article is to illustrate a possible offshore wind park topology made by using the reverse-blocking IGBT type of semiconductor device with a dedicated switching pattern to reduce the converter losses [6].

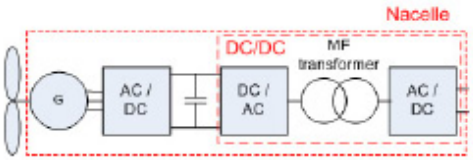

Fig. 2. Conventional converter topology in the nacelle of the turbine as of [7]

II. New topology for DC based offshore wind parks

A. The conventional converter topology

One of the previously proposed DC based offshore wind park layouts is the parallel connected turbines with one or more offshore substations. This layout must have offshore converter stations to raise the voltage before transmission to shore. It is assumed that only one transformer stage is needed if the output voltage of the wind turbine is 20-40 kV [7]. The wind turbines will then be connected in radials to the collecting point. With a lower output voltage of the wind turbine, about 5 kV, two transformer stages are needed. The wind turbines will then be divided into clusters and connected one by one to the first transformer stage. Then the clusters will be connected to the collecting point.

For this type of wind park layout each wind turbine has an AC-DC converter, DC-DC converter and a capacitor between, as shown in Fig. 2. DC-DC converters are also used for the two transformer stages in the layout. The AC-DC converter has either diode or IGBT switches depending on the type of machine used in the wind turbine, synchronous or induction machine. A DC-DC converter consists of one rectifier, one inverter and a medium frequency transformer. In [8] a loss and energy production cost study of different DC/DC converters for DC based offshore wind parks is carried out. Full-bridge converter, single active bridge converter and series parallel resonant converter are compared for the three different sites in the park, resulting in lowest losses for the resonant converter independent of the site. The single active bridge converter resulted in the highest losses, but the full-bridge converter gave slightly higher losses than the resonant converter. The resonant converter has a larger transformer and more IGBT modules than the full-bridge converter, which results in a higher energy production cost for some positions in the grid, even though the losses are lower. This topology also has a capacitor between the two converters to make sure the input to the DC-DC converter is smoothed properly.

B. The proposed converter topology

The proposed topology uses only one cable with series connected turbines as the local grid, as can be seen in Figure 3. Each wind energy conversion unit will consist of a generator, the turbine, a 3-phase AC to 1-phase AC converter, a high frequency (HF) transformer and a 1-phase AC-DC converter. The turbines will be connected to an offshore DC network

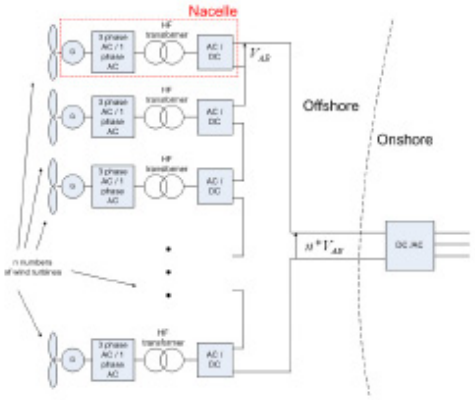

Fig. 3. DC based wind park with proposed converter topology

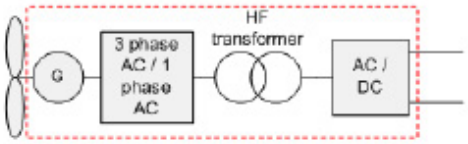

Fig. 4. Wind turbine with proposed topology

and the power will be transmitted directly to shore without any transformation stages. This is possible since the turbines are connected in series and the voltage level required for transmission will be obtained by the series connection and/or the turn ratio of the HF transformer. By converting the AC voltage output from the generator to DC voltage directly in the nacelle of each turbine, a wind park layout without offshore substations is made possible [9]. In [10] the similar conversion is proposed, but only the AC-AC converter is placed in the wind turbines. This leads to a square wave voltage collection grid and an offshore substation for the AC-DC converter.

In the proposed topology the DC side of the AC-DC converter of each turbine will be connected in series with the other wind turbines to obtain the required voltage level before the transmission to shore. This is possible through the high frequency transformer. It allows the current from the DC grid to flow through the secondary side of the transformer before entering the AC-DC converter again, but from the AC side. Then the current can continue further to the next wind turbine.

Another DC based layout option is to connect a few wind turbines in series to make clusters. These clusters will then be connected in parallel to the transmission line. By using this layout, the consequences during fault on cables might be less severe. Only the faulty cluster needs to be disconnected and the park can still produce power.

The AC/DC converter in Fig. 4 is a full-bridge converter, also called an H-bridge, with switching modules consisting of IGBTs and diodes in anti parallel, Fig. 5 on the next page. The converter has two legs, each with two switches (S1, S3)

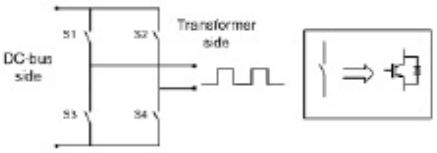

Fig. 5. H-bridge with IGBTs and anti parallel diodes

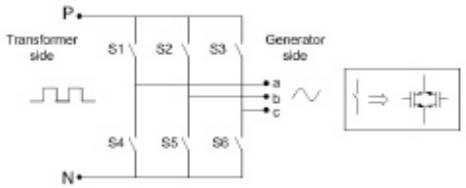

Fig. 6. Bidirectional AC link with new reverse-blocking IGBTs

and (S2, S4), and is able to convert a DC voltage to a square wave voltage and vice versa. By connecting the converter to the DC bus and transformer, as shown in Fig. 5, the required square wave form is obtained when starting the generator. To achieve square wave output when magnetizing the windings a PWM square wave switching scheme is used. The upper switch in one leg and the lower switch in the other are switched simultaneously, when not considering the blanking time. The two switches form a switch pair, i.e. the converter has two switch pairs. The switch pairs are on for a half cycle of the output frequency (10 kHz), i.e. a duty ratio of 0.5.

The 3-phase AC to 1-phase AC converter consists of three legs each with two switches. The switches are a new type of reverse-blocking IGBTs, as can be seen in Fig. 6. They do not have any anti parallel diodes and therefore reduce the converter losses. On the generator side of the converter there will always be an alternating voltage independent of the way the power flows.

1) New reverse-blocking IGBT: There are many ways to make a bidirectional switch. In [11] and [12] different configurations of bidirectional switches are described and analysed for different converters. In Fig. 7 four configurations of switches are presented. The two bidirectional switches to the left in Fig. 7 are made of two IGBTs and two diodes in antiparallel. The switches are called common collector IGBT (CC-IGBT), seen in a), and common emitter IGBT (CE-IGBT), seen in b), depending on how the switch modules are series connected. Fig. 7c) shows an IGBT embedded in a diode bridge. To the right in Fig. 7 there are two reverse-blocking IGBTs (RB-IGBT) with intrinsic diodes connected in antiparallel. These reverse-blocking IGBTs can form a bidirectional switch without the use of diodes. In [13] the new RB-IGBT is used in a AC-AC direct converter resulting in an efficiency increase of 1.9 point compared to a conventional device.

The new reverse-blocking IGBT leads to a reduction of the forward conduction state voltage drop of the switch [6]. It can

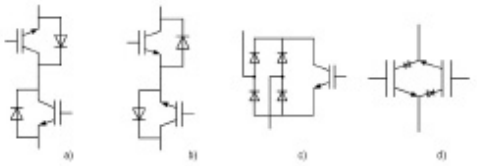

Fig. 7. Bidirectional switches, a) common collector IGBT with diodes, b) common emitter IGBTs with diodes, c) diode embedded IGBT, d) reverse-blocking IGBT with intrinsic diodes

also be seen from Fig. 7, that for the CC-IGBT switch and the CE-IGBT switch the conducting path has two components in both directions, one IGBT and one diode. For the diode embedded IGBT the number of components to pass through is three. All these configurations of bidirectional switches results in more on-state losses than the new RB-IGBT, which has just one component in both directions of the conduction path. The more components to pass through, the more on-state losses is generated. A thorough consideration about losses will be presented in the final paper.

The architecture of the RB-IGBT depends on the manufacturer. In [14] the architecture of a non-punch-through IGBT (NPT-IGBT) is modified by using the technique of isolation diffusion and folding up the lower p^+ layer at the chip edge. By doing these modifications the IGBT can block reverse voltages and still have the operational behaviour like a normal NPT-IGBT. In [15] a new concept of "dielectric charge traps" to obtain a "dynamical" buffering in both direction of the IGBT by trapped hole charges is suggested. This might be possible by using technologies like SIMOX or wafer bonding. In [16] a NPT-IGBT is etched to form a trench to electrically separate the side surface from the active region of the IGBT. This leads to no reverse leakage current from the side surface and the IGBT is able to block a reverse voltages of 600 V. A 1200 V RB-IGBT is also made by using deep boron diffusion technique and thin wafer technology [17].

C. Preliminery investigation of a medium voltage generator

The power output of todays wind turbines have exceeded 3 MW, companies like Repower and Enercon have developed WTs with power rating in the range of 5-7 MW. The interest in using offshore wind potential could push the power ratings above 10 MW. Although power rating has increased rapidly the last decade, the voltage rating of the generators have stayed below 690 V, some companies, like Harakosan [18] and Multibrid [19], have developed WTs with rated voltage above 3 kV. If the trend of increasing the power rating continues the voltage rating will increase to deal with high current losses. Initially it can be assumed that the generator will have an output higher than 3 kV and a power rating higher than 5 MW. This leads to fewer turbines needed in series to obtain required voltage level for transmission and perhaps lower ratio of the transformers.

Modern, land based wind turbines often use geared doubly fed inductions generators, but these generators need extensive

maintenance on slip rings, brushes and gear. It is especially important to avoid the gear, some offshore wind farms have already experienced severe problems with the gear system [20]. Permanent magnet synchronous generator technology makes it possible to design gearless drive trains with very high total efficiency and power to weight ratio [21]. Low speed, gearless drives must utilize a high pole count in the generator to increase electric frequency and induced voltage. Induction generators for gearless application are not in use because the high pole number would demand a very big magnetizing current. For low speed application, characteristic for large wind turbines, synchronous generators with high pole number are superior. Since the field ampereturns increase with pole count permanent magnets should be used in the rotor [22], this will lower the field circuit losses as well.

D. Design considerations of high frequency high power transformer

Between the two converters there is a high frequency high power transformer to electrically isolate the generator from the grid. The transformer also raises the voltage to a higher level which is better suited for transmission to shore. By having a transformer, the series connection of the DC output of each turbine is made possible. The transformer has to be able to cope with 10 kHz and 0.75 MVA. According to [23] that should not be a problem, but there are no reported works in that up to the power level this project is investigating. To design such a high frequency high power transformer many criteria must be fulfilled. The transformer must be specially designed and matched for each case [24]. The main issues to consider according to [25] are the losses, weight and leakage inductance.

The losses consist mainly of core and copper losses. The copper losses are dependent on the leakage flux distribution in the window region. The window region is formed by the core and winding geometry of the transformer. The copper losses are mainly due to eddy current effect in the conductors, i.e. skin and proximity effects. Skin effect is an increase in the resistance in a cable due to alternating current moving towards the surface because of the magnetic field made up of the current itself. The proximity effect is circulating currents in the cable arisen due to time-varying magnetic field from nearby current carrying conductors. Both of these effects are frequency and field dependent. According to [26] the eddy current and hysteresis losses will increase in non-sinusoidal ecited transformers with high frequencies. The core losses change from material to material for a given frequency and flux density. In [25] different core materials are tested and a material with high permeability gives the lowest core losses. Therefore, and due to the geometry of the transformer's core, the proposed design will be made of SIFERRIT N27 [27]. The core losses can be found in data sheets for the different materials.

The weight of the transformer is decreased with increasing frequency. This is of course an advantage when it comes to offshore installations, but a small size makes the cooling of the electrical parts difficult. At this moment the proposed design has a geometry as in Fig. 8 consisting of two U-cores and two I-cores made of SIFERRIT N27 [27]. The optimal shape of the core for high power transformers is orbital according to [28]. The windings are made of aluminum foil.

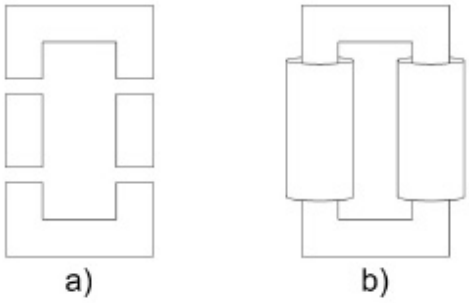

Fig. 8. Geometry of high frequency high power transformer

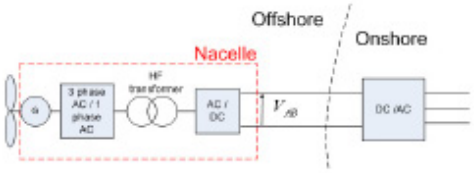

Fig. 9. Model implemented in PSCAD for simulation

III. Simulation System

A. Simulation model

To be able to test the proposed converter topology a model was built. A model of the wind turbine is made in PSCAD to simulate the losses in the converters [9]. The model consists of the components from the generator connected to the rotor of the wind turbine to the converter connected to the DC collection grid in the offshore wind park. The DC collection grid is modelled as a DC voltage source with a resistance and a large capacitor in parallel. As can be seen from Fig. 9 the system also consists of a wind generator, bidirectional converter, high frequency transformer and a DC/AC converter (H-bridge).

The wind generator in the model is a squirrel cage induction machine. The machine parameters are from Vestas 750 kVA (660 kW) wind generator found in [29]. The transformer in the model is a single phase two winding transformer with a rated power of 0.75 MVA. The frequency is 10 kHz because that is the switching frequency of the converters which leads to the frequency of the square wave voltage in the transformer. The rated voltage is 1.3 kV for both windings which is the calculated output of the bidirectional converter. Every high frequency high power transformer is designed for a specific system. Therefore it is not easy to find parameters to use for the simulation model. PSCAD suggests some parameters which are used in the model for the rest of the parameters

needed to do the simulation. A detailed design of the high frequency transformer will be part of subsequent investigation.

The 3-phase AC-1-phase AC converter in Fig. 9 on the previous page is a bidirectional converter consisting of three legs with two switches, Fig. 6 on page 3. The switching frequency is 10 kHz and the bidirectional switches are made of two IGBTs of the new type described in II-B1 on page 3. The parameters for the IGBTs are the standard PSCAD values for semiconductor devices. The P and N connection points in Fig. 6 on page 3 are connected to the transformer side and there is always a square wave voltage input from the transformer. Each leg in the converter is connected to one phase on the generator side. The switches are controlled by using a dedicated switching pattern. A triangular carrier signal (10 kHz) is compared to the 3-phase sinusoidal 50 Hz reference signal. The sinusoidal reference signal is inverted for half of the carrier signal period. There is one reference signal for each leg controlling the switching of the two switches in the leg. The reference signals are generated by a control box. The switches in the same leg will never be ON at the same time, but there will always be three switches ON, one from each leg.

The full-bridge converter, also called H-bridge, has two legs with two switches, Fig. 5 on page 3. The switches consist of one IGBT and one diode in anti parallel. The parameters used for the diodes and the IGBTs in the converter are the standard one suggested by PSCAD. Each switch gets a control signal from the control system, 1 for ON and 0 for OFF.

B. New switching pattern

The bidirectional converter uses a dedicated switching pattern for the switching of the RB-IGBT switches. Considering the switching of the two switches in one leg the upper and the lower switch will never be ON at the same time. When the upper one is ON, i.e. the control signal to the switch is 1, the lower one will be OFF, control signal 0, and vice versa. The violet curve, number three from the top in Fig. 10, shows when the upper switch is ON and OFF with a DC input into the converter. This switching control can be obtained by using a switching technique called Pulse Width Modulation (PWM) [30]. This technique can be explained by looking at the second graph from the top in Fig. 10 and only considering the upper one of the two blue lines (made up of dark and light blue pieces). This blue line is actually a sinusoidal reference signal for one leg or phase (50 Hz) and will decide the frequency of the output. The green triangular signal is called a carrier and it decides the frequency with which the switches are switched. Since this carrier has a frequency of 10 kHz, the sinusoidal reference signal can be considered as a straight line for the small time intervals as in Fig. 10. When the sinusoidal reference signal is higher than the carrier signal the upper switch of the phase leg will be turned ON and the lower switch will be turned OFF. They will remain ON and OFF until the reference signal is lower than the carrier signal. At that moment the upper switch turns OFF and the lower one turns ON, until the reference signal again is higher than the carrier signal. This leads to a positive output of the leg when the upper one is ON and a negative output when the lower one is ON, as the yellow curve, fourth one from the top, in Fig. 10 shows.

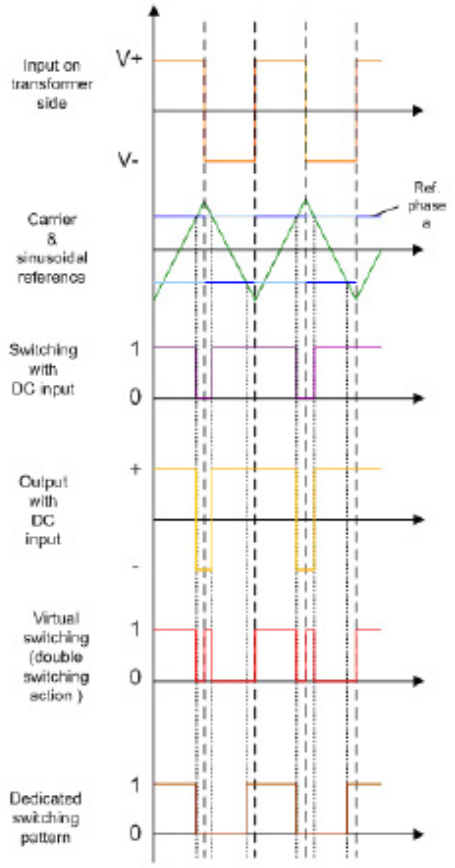

Fig. 10. Dedicated switching pattern for the RB-IGBTs [9]

The orange curve at the top of Fig. 10 shows the square wave voltage input to the converter from the transformer. To obtain the sinusoidal output as required for the converter the switches need to be switch oppositely for the negative period of the square wave input as for the positive period. Considering the upper switch S1 in the a-phase leg the red curve, second one from the bottom in Fig. 10 shows how the switch is switched. In the beginning the upper connection point P in Fig. 6 on page 3 is positive and the lower connection point N is negative. S1 is ON connecting the a-phase to the positive P-pole. Then after a while S1 is turned OFF and the lower one S4 is turned ON.

The lower switch then connects the a-phase to the negative N-pole. Since the voltage between P and N is a square wave

the polarity of P becomes negative after a while, and the polarity of N becomes positive. Phase a still has to be negative so S1 is turned ON and S4 OFF since P now is negative and N is positive. To get a positive output on phase a in this period, the lower switch S4 will have to be turned ON and the upper switch OFF. The square wave will then enter a period where P again becomes positive and N negative. This switching pattern is the pattern that would have given the desired output.

With the dedicated switching pattern, a sinusoidal output can be achieved with less number of switching sequences. The sinusoidal reference signal is inverted for half of the carrier period, the dark blue curve, second from the top in Fig. 10 on the previous page. Using this blue reference signal and the green carrier for the PWM switching technique, the upper switch will be ON and OFF as shown in the brown curve at the bottom in Fig. 10 on the preceding page. In the beginning the switch is ON because the blue reference signal is above the green carrier signal. Almost at the end of the first half period, the positive one of the input, the switch is turned OFF due to higher carrier than reference signal. For the negative half of the input period, the reference is inverted and remains below the carrier for a longer time than if it where not inverted. The switch will be turned ON before the second positive half period of the input begins. The reference signal in this positive half period is not inverted and the switch will remain ON until the reference signal again is below the carrier signal and so forth.

C. Simulation results

With the dedicated switching pattern the number of times switched each period is reduced. The red and brown patterns, the second one and the one at the bottom in Fig. 10 on the previous page, gives the switching sequence of one switch with the virtual pattern and the dedicated pattern. Considering these patterns, the brown one shows that the number of times switched per switch is halved, from four times to two. This is important at high voltage levels because of slower devices, due to longer delay time. By reducing the number of times switched, the switching losses are reduced and this results in less converter losses. A detailed investigation of losses will be included in the final paper.

In the simulation model the dedicated switching pattern is used for the bidirectional converter. The triangular carrier signal (10 kHz) and a sinusoidal reference signal for one phase (50 Hz) is shown in the top of Fig. 11. As can be seen from the figure, the sinusoidal reference signal is inverted for half of the carrier signal period which is 100 s. There is one sinusoidal reference signal for each phase just delayed with 120° and 240°. By using this technique there will always be three switches on at any instant of time. The square wave voltage, U_{out} in Fig. 11, is the input to the converter on the transformer side. Fig. 12 shows the output phase-to-phase voltage V_{ab} from the converter. This voltage is the voltage between the a-phase leg and the b-phase leg in the converter in Fig. 12. By using filters this will result in a sinusoidal output voltage.

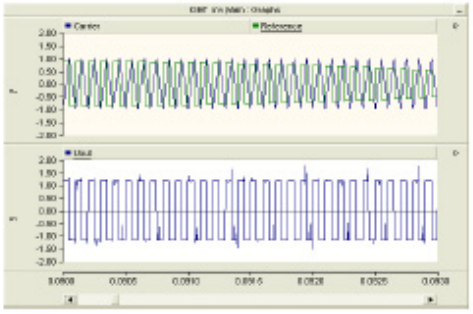

Fig. 11. Switching pattern, top: sinusoudal reference for one phase, bottom: output voltage on transformer side

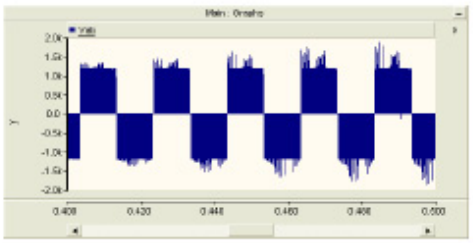

Fig. 12. Phase-to-phase voltage output on generator side

IV. Discussion

A series connected wind farm is to prefer due to no transformer substation, but the reliability at faults in the cables or turbines can be lower than with parallel or radial connected turbines [31]. When the turbines are connected in series the economical consequences of a cable fault is much larger than if they were connected in parallel. In parallel only the single turbine which is connected to the cable with a fault needs to be disconnected. If the fault is on the cable from the cluster to the connecting point, only this cluster needs to be disconnected. Therefore there will always be some wind turbines producing, even though there are faulty cables in the park. For the series connected wind turbines in Fig. 3 on page 2, there need to be some extra cables connecting different parts of the series connected turbines together to prevent the whole park from being disconnected during cable faults. If a fault arises, the current will need another path to flow, so the extra cable connections have to be connected to keep the park running. Where and how many of these extra cables to install in the offshore grid, will be a trade off between installation costs of the cables and the lost revenue due to lost production during fault and post-fault period [31]. This will also be a subject for further investigation.

By connecting a few wind turbines in series in clusters and the clusters in parallel the reliability increases. Now only the faulty cluster needs to be disconnected and the park can still produce some power. With a radial network the loss of production due to turbine disconnection depends on where the

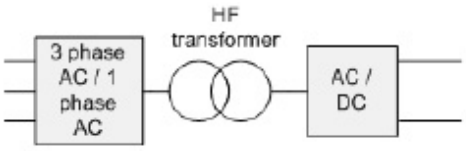

Fig. 13. Proposed converter topology

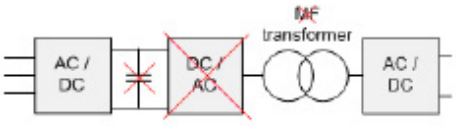

Fig. 14. Conventional converter topology

fault on the cable is located. If it is located near the connection to the substation, all of the turbines connected to the cable will be disconnected. If it is located between some of the turbines, the turbines between the substation and the fault will still be able to continue production.

If a turbine fault arises in a series connected wind park, i.e. a turbine must be disconnected, there should be switchgears disconnecting the turbine, but allowing the rest of the turbines to produce power. To obtain the same voltage across the turbines, the remaining turbines have to increase their production accordingly. There should also be switchgears allowing turbine disconnection in a radial park so the rest of the turbines in the radial can continue production. For the parallel connected turbines, there is only one turbine connected to one cable, so the other turbines are not affected by the faulty line. If there is a fault in the main transmission cables to shore, the whole park will be shut down independent of the layout. The only possibility to still deliver power to shore during such faults is to install extra cables to shore. Independent of the layout, a cable fault always leads to a decrease in revenue due to lower production.

Considering the converter topologies, i.e. the conventional one and the proposed one, some important differences are worth noticing. In the proposed one in Fig. 13 there will be three steps of conversion, 3-phase AC-1-phase AC, transformer (AC-AC) and AC-DC. As seen from Fig. 14, there will be four steps in the conventional converter topology, AC-DC, DC-AC, transformer (AC-AC) and AC-DC. One converter less in the proposed topology leads to fewer switches. Fewer switches give less switching losses. This is a great advantage since the converter losses contribute a lot to the total losses. The conventional topology also has a capacitor to smoothen the DC output of the rectifier before it enters the DC-DC converter. A capacitor is normally a heavy component, which is a disadvantage for a wind turbine. For wind turbines, especially floating ones, the weight of the components should be minimized to minimize the counterbalance of the foundation. For the same reason, the new topology has a high frequency (HF) transformer in stead of a medium frequency transformer. Transformers' size and weight is reduced with increasing frequency. Both the reduction in weight and the reduction in switching and ON-state losses are great advantage of the proposed topology.

V. Conclusion/Further work

In this paper a new converter topology for large offshore wind parks has been presented, explained and compared with a conventional one. A PSCAD model of the converter topology is explained and results described. The turbines are connected in series and directly connected to shore without any transformer stages. Since the voltage across the series connected wind turbines are high enough to be transmitted directly, offshore transformer substations are unnecessary. The risk of such a series connected park has to be considered and a trade off between extra cable installations and lost revenue at cable faults is unavoidable. The new topology with a 3-phase AC to 1-phase AC converter, a HF transformer and a full-bridge converter, consists of fewer converter stages than the conventional topology. With one converter less the converter system has fewer switches and less switching and ON-state losses come in to being. This is important because the converter losses are a great contributor to the total losses in the entire wind park. The proposed converter topology does not include a heavy capacitor and the transformer is smaller due to higher frequency. This is a weight reduction which is important to achieve for floating wind turbines.

The switches used for the AC-AC converter are a new type of reverse-blocking IGBT. This switch replaces the series connected IGBTs with anti parallel diodes. By using this new reverse-blocking IGBT without the anti parallel diode, the on-state losses are reduced due to fewer devices for the current to pass through.By introducing the dedicated switching pattern the number of switching actions is reduced. Compared to the virtual pattern the number of times is halved.

On the basis of the mentioned weight reduction and the no offshore substation, the proposed topology might be better suited for the large offshore wind parks. The reduction of switches, reduction of times switched with the new pattern and the new RB-IGBT reduce the converter losses which is the great contributor to the total losses in the electrical system.

The study of this offshore wind park topology has just started. The converter topology and its work in the whole system need to be further investigated. The switching pattern and the switch need to be tested and simulated to document good results. Some further tasks to prove the results of this report:

- Simulations in PSCAD of a model with a generator with the characteristics of a real wind turbine
- Design of the high frequency transformer
- Loss calculations and simulations in PSCAD for the switches and the total converter system
- Development of prototype, implementation of switching pattern and loss measurements

- Simulations of the whole wind park and its connection to the onshore grid during operation and faults, especially when one turbine is disconnected.

REFERENCES

[1] OffshoreCenterDanmark, "Offshore wind farms," Online, available: http://www.offshorecenter.dk/OffshoreWindFarms/.

[2] P. Bresesti, W. L. Kling, R. L. Hendriks, and R. Vailati, "HVDC connection of Offshore Wind Farms to the Transmission System," *IEEE Transactions of Energy Conversion*, vol. 22, no. 1, pp. 37–43, 2007.

[3] N. B. Negra, J. Todorovic, and T. Ackermann, "Loss evaluation of HVAC and HVDC transmission solutions for large offshore wind farms," *ELSEVIER Electric Power System Research, Science Direct*, no. 76, pp. 916–927, 2005.

[4] L. Xu and B. Andersen, "Grid Connection of Large Offshore Wind Farms Using HVDC," *Wind Energy*, no. 9, pp. 371–383, 2006.

[5] T. Ackermann, "Transmission Systems for offshore Wind Farms," *IEEE Power Engineering Review*, pp. 23–27, 2002.

[6] M. Takei, T. Naito, and K. Ueno, "The Reverse Blocking IGBT for Matrix Converter With Ultra-Thin Wafer Technology," *IEEE 15th International Symposium on Power Semiconductor Devices and ICs*, pp. 156 – 159, 2003.

[7] S. Lundberg, "Evaluation of wind farm layouts," *NORPIE*, 2004.

[8] L. Max., "Energy Evaluation for DC/DC Converters in DC based Wind Farms," Ph.D. dissertation, Chalmers University of Technology, Sweden, 2007.

[9] A. B. Mogstad, "New switching pattern for AC/AC converters with RB-IGBTs for offshore wind parks," Norwegian University of Science and Technology (NTNU), Tech. Rep., 2007.

[10] S. Meier and P. Kjr, "Benchmark of Annual Energy Production for Different Wind Farm Topologies," *IEEE 0-7803-9033-4*, pp. 2073–2080, 2005.

[11] M. J. Bland, P. W. Wheeler, J. C. Clare, and L. Empringham, "Comparison of Bi–directional Switch Components for Direct AC–AC Converters," *35th Annual IEEE Power Electronics Specialists Conference*, pp. 2905–2909, 2004.

[12] C. Klumpner and F. Blaabjerg, "Using Reverse–Blocking IGBTs in Power Converters for Adjustable–Speed Drives," *IEEE Transactions on Industry Applications*, vol. 42, no. 3, pp. 807–816, 2006.

[13] J. ichi Itoh, T. Iida, and A. Odaka, "Realization of High Efficiency AC link Converter System based on AC/AC Direct Conversion Techniques with RB-IGBT," *IEEE*, pp. 1703–1708, 2006.

[14] A. Lindemann, "A New IGBT with Reverse Blocking Capability," *EPE 2001, Graz*, 2001.

[15] H. Kapels and D. Drücke, "Optimized device concepts for reverse blocking IGBTs," *ISPSD*, pp. 148–151, 2003.

[16] M. Takei, Y. Harada, and K. Ueno, "600V–IGBT with Reverse Blocking Capability," *International Symposium on Power Semiconductor Devices and ICs*, pp. 413–416, 2001.

[17] T. Naito, M. Takei, M. Nemoto, T. Hayashi, and K. Ueno, "1200V Reverse Blocking IGBT with low losses for Matrix Converter," *International Symposium on Power Semiconductor Devices and ICs*, pp. 125–128, 2004.

[18] "Harakosan," http://www.harakosan.nl/, 2008.

[19] "Multibrid," http://www.multibrid.com/, 2008.

[20] "Vestas develops replacement for damaged offshore wind turbines," http://www.forbes.com/markets/feeds/afx/2007/09/25/afx4152963.html, 2007.

[21] Y. Chen, P. Pillay, and A. Khan, "Pm wind generator topologies," *IEEE Transaction on Industry Applications*, vol. 41, no. 6, 2005.

[22] A. Binder and T. Schneider, "Permanent magnet synchronous generators for regenerative energy conversion - a survey," *IEEE*, 2004.

[23] Neeltran, "High frequency transformer," Online, available: http://www.neeltran.com/hf_trns.htm.

[24] L. Heinemann, "An Actively Cooled High Power, High Frequency Transformer with High Insulation Capability," *IEEE*, 2002.

[25] M. Kheraluwala, D. Novotny, and D. Divan, "Coaxially Wound Transformers for High-Power High-Frequency Applications," *IEEE Transactions on Power Electronics*, vol. 7, no. 1, pp. 54–62, 1992.

[26] W. G. Hurley, W. H. Wölfle, and J. G. Breslin, "Optimized Transformer Design: Inclusive of High-Frequency Effects," *IEEE Transactions on Power Electronics*, vol. 13, no. 4, pp. 651–659, 1998.

[27] Epcos, "Ufi cores," Online, available: http://www.epcos.com.

[28] C. Meyer, "Key Components for Future Offshore DC Grids," Ph.D. dissertation, Rheinisch-Westfällischen Technischen Hochschule Aachen, Germany, 2007.

[29] J. A. Suul, "Use of standard frequency converters in power plants and Wind power and preproject to master thesis: Pumped-storage power plant with variable rotational speed(in norwegian)." Norwegian University of Science and Technology (NTNU), Tech. Rep., 2004.

[30] N. Mohan, T. M. Undeland, and W. P. Robbins, *Power Electronics – Converters, Application and Design*. John Wiley & Sons, INC. 3rd ed., 2003.

[31] J. Pechey, P. Taylor, R. Dixon, M. Lawson, and A. Dinning, "The Role of Medium Voltage Electrical System Design in Risk Management for Offshore Wind farms," *Wind Engineering*, vol. 28, no. 5, pp. 489–502, 2004.